Dissertation zur Erlangung des Doktorgrades

der Fakultät für Chemie und Pharmazie

der Ludwig-Maximilians-Universität München

Studies on the Physicochemical Stability of Antibody Conjugates

Corinna Valerie Dürr

aus

Tübingen, Deutschland

2018

Erklärung

Diese Dissertation wurde im Sinne von §7 der Promotionsordnung vom 28. November 2011 von Herrn Prof. Dr. Wolfgang Frieß betreut.

Eidesstattliche Versicherung

Diese Dissertation wurde eigenständig und ohne unerlaubte Hilfe erarbeitet.

Köln, den 10.03.2018

_____

Corinna Dürr

Dissertation eingereicht am:	16.03.2018
1. Gutachter:	Prof. Dr. Wolfgang Frieß
2. Gutachter:	Prof. Dr. Gerhard Winter
Mündliche Prüfung am:	19.04.2018

For my family

ACKNOWLEDGMENTS

This thesis was prepared between November 2013 and April 2017 at the Department of Pharmacy, Pharmaceutical Technology and Biopharmaceutics at the Ludwig-Maximilians-Universität München under the supervision of Prof. Dr. Wolfgang Frieß.

Foremost, I would like to express my gratitude to my supervisor Prof. Dr. Wolfgang Frieß. Thank you for all the scientific input, encouragement and professional but also personal guidance during the preparation of this thesis. I am very grateful for the opportunity to join his research group and work on this exciting research field. I also enjoyed the possibility to present my work at various conferences.

I would also like to thank the leader of the chair, Prof. Dr. Gerhard Winter, for kindly taking over the co-referee of this thesis and for establishing excellent working conditions. I appreciate the advice and discussions during the Thursday's seminar between all three groups of the chair. Moreover, I really enjoyed the numerous social activities our groups did together. Many thanks also go to Prof. Dr. Olivia Merkel, Dr. Julia Engert, Dr. Gerhard Simon, Imke Leitner and Sabine Kohler.

I also would like to express my gratitude to Coriolis Pharma GmbH for the possibility to use the Zetasizer APS plate reader and MicroCal autosampler. Special thanks go to Dr. Frank Schaubhut and Dr. Tim Menzen for their support and help. Thank you, Tim, also for the supervision of my Master's thesis, the insights I obtained then helped me throughout my PhD. From the TU Munich, I thank Prof. Dr. Thomas Letzel and Sylvia Große of the Chair of Urban Water Systems Engineering for the peptide map measurements.

I thank Prof. Dr. Marco van de Weert and Fabrice Rose from the University of Copenhagen for helping me out to finish all experiments at the end of my thesis. The time in Copenhagen was short, but very productive. Wyatt Technologies is appreciated for the possibility to use the DynaPro Reader. I also thank Prof. Dr. Ernst Wagner and Philipp Klein for the help with the ADC synthesis in the beginning of my PhD. Although we were not completely successful in the end, we had valuable ideas and I enjoyed the time in your lab.

This thesis would not have been possible without the excellent help of all the students involved: Michaela Neuhauser and Nicole Popp (both: Master's thesis, TUM), Ivonne Seifert (Master B), Kathrin Aftahy, Mariem Quraeschi, Karina Krois and Johannes Tanner (StEx WPF). I enjoyed working with all of you. Especially, I would like to highlight the work of Nicole and Ivi, who contributed significantly with their results.

I would like to thank all my former colleagues from the LMU for the great working atmosphere and for making my PhD time so enjoyable. Thank you so much for our weekly basketball, skiing trips, coffee

breaks and numerous other events. Particularly, I wish to address a special thanks to my long-time lab mate and friend Jacqueline for the support, the fun times and discussions we had together. I also want to thank Kerstin, Ellen, Ivi, Laura, Ben and Bifeng for their friendship.

Finally, I would like to thank my family for their ongoing confidence and support. I am very thankful to my parents, who have made so much possible for me and have always believed in me. Michi, thank you so much for your motivation, support and love during these past years.

TABLE OF CONTENTS

PUBLICATIONS ARISING FROM THIS THESIS

Poster presentations

C. Duerr, N. Popp, C. Soennichsen, W. Friess; Characterization of physicochemical properties of antibody conjugates; 3rd European Workshop on Protein Aggregation and Immunogenicity, Innsbruck, Austria, January 30-31, 2017.

C. Duerr, I. Seifert, W. Friess; Characterization of adsorption phenomena of antibody conjugates; Annual Meeting of the German Pharmaceutical Society- DPhG, Munich, Germany, October 4-7, 2016.

C. Duerr, W. Friess; How physically stable are antibody conjugates?; 10th World Meeting on Pharmaceutics, Biopharmaceutics and Pharmaceutical Technology, Glasgow, United Kingdom; April 4-7, 2016.

C. Duerr, W. Friess; Analysis of the physical stability of antibody conjugates; Bioanalytical & Formulation Congress, Berlin, Germany; September 15-16, 2015.
awarded as best poster presentation

Oral presentations

C. Duerr, T. Menzen, W. Friess; Analyse der thermischen Stabilität in Proteinformulierungen mittels DSF, 3. Life Science Conference, Jena, Germany, May 14-15, 2014.

LIST OF ABBREVIATIONS

A_2^*	apparent osmotic second virial coefficient
ADC	antibody-drug conjugate
ATR	attenuated total reflectance
AUC	area under the curve
a.u.	arbitrary units
CE	capillary electrophoresis
CF	correlation factor
D	diffusion coefficient
DAD	diode-array detector
CHO	chinese hamster ovary
D	dissipation
D_0	diffusion coefficient at infinite dilution
Da	Dalton
DAC	Deutscher Arzneimittel Codex
DAR	drug antibody ratio
DEAC	7-diethylaminocoumarin-3-carboxylic acid succinimidyl ester
DMF	dimethylformamide
DMSO	dimethyl sulfoxide
DOL	degree of labeling
DLS	dynamic light scattering
DTT	dithiothreitol
ε	extinction coefficient
EGFR	epidermal growth factor receptor
EIC	extracted ion chromatogram
Em	emission (wavelength)
EMA	European Medicines Agency
Eo	Eosin-5-isothiocyanate (Eosin-ITC)
Ex	excitation (wavelength)
f	frequency
FDA	U.S. Food and Drug Administration

Fl	5/6-carboxfluorescein succinimidyl ester
FTIR	Fourier transformed infrared spectroscopy
HCl	hydrochloric acid
HIC	hydrophobic interaction chromatography
HILIC	hydrophilic interaction liquid chromatography
His	histidine
HN	histidine sodium chloride buffer
HMWS	high molecular weight species
H_2O_2	hydrogen peroxide
HPLC	high performance liquid chromatography
HP-SEC	high performance - size exclusion chromatography
HS	histidine sucrose buffer
H_2SO_4	sulfuric acid
IEF	isoelectric focusing
IEP	isoelectric point
IgG	immunoglobulin class G
ITC	isothermal titration calorimetry
k_D	diffusion interaction parameter
LMWS	low molecular weight species
LO	light obscuration
M	molar
mAb	monoclonal antibody
mAb	naïve mAb
mAb DEAC	mAb DEAC conjugate
mAb Eo	mAb Eosin conjugate
mAb Fl	mAb Fluorescein conjugate
MCA	multiple cuvette array
MFI	micro-flow imaging
MS	mass spectrometry
MW	molecular weight
MWCO	molecular weight cut-off
NA	sample not analyzed
NaCl	sodium chloride
NaOH	sodium hydroxide
NHS	N-hydroxysuccinimide

PAGE	polyacrylamide gel electrophoresis
PBS	phosphate buffered saline buffer
PES	polyethersulfone
Ph. Eur.	European Pharmacopoeia
Phos	phosphate buffer
pI	isoelectric point
PN	phosphate sodium chloride buffer
PS	phosphate sucrose buffer
PTFE	polytetrafluoroethylene
PVDF	polyvinylidene fluoride
QCM	quartz crystal microbalance
r.h.	relative humidity
RPLC	reversed-phase liquid chromatography
rpm	revolutions per minute
RSD	relative standard deviation
r.h.	relative humidity
r_h	hydrodynamic radius
r.t.	room temperature
s	standard deviation
SDS	sodium dodecyl sulfate
SDS-PAGE	sodium dodecyl sulfate polyacrylamide gel electrophoresis
SE	standard error
SEC	size exclusion chromatography
SLS	static light scattering
t	time
t0	sample measured after preparation before stress
T_{agg}	temperature of aggregation
TEAoAc	triethylammonium acetate buffer
TFF	tangential flow filtration
TIC	total ion current
T_m	protein melting temperature
TRIS	tris(hydroxymethyl)aminomethane
USP	United States Pharmacopeia
UV	ultraviolet spectroscopy

UV-Vis	ultraviolet-visible light
w	weeks
wv	wavelength
w/v	weight per volume
π	surface pressure

CHAPTER I:

INTRODUCTION: ANTIBODY-DRUG CONJUGATES-STABILITY AND FORMULATION

1 WHAT ARE ANTIBODY-DRUG CONJUGATES?

The use of antibodies in cancer treatment has led to a tremendous increase in therapeutic possibilities [1-3]. Antibodies demonstrate little off-targeted toxicity due to their selective binding of the antigen or antigen-positive cells, respectively. However, antibodies are often not potent enough to efficiently combat a tumor [4]. Antibody-drug conjugates (ADCs) combine the benefits of an antibody and a cytotoxic agent, which enhances the efficacy and selectivity for tumor cell killing [5]. Once the antibody specifically binds to the target receptor of a cell, the ADC may be internalized and the cytotoxic agent released, leading to cell death (Figure I- 1) [6-8]. ADCs can thus be considered as advanced drug delivery systems [9]. This concept had already been discussed in the 1970s, but initial trials in the 1980s had a lack of success [4, 10] with b96-doxorubicin [11] and desacetylvinblastine [12] as payloads.

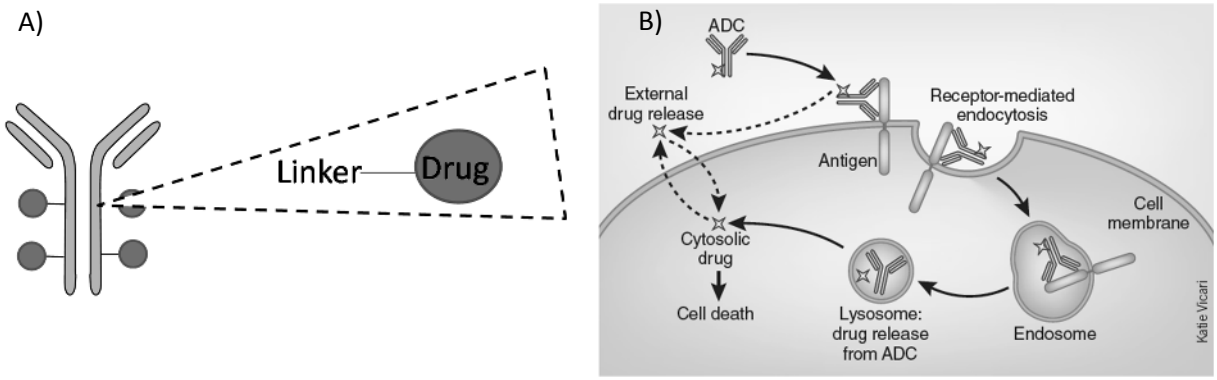

Figure I- 1: A) Basic concept of an ADC, adapted from [13]. B) Primary mechanism of action [6]. Solid lines depict cell death through receptor-mediated endocytosis and dashed lines through external drug release.

Since the approval of Mylotarg® (Gemtuzumab ozogamicin) in 2000 and later Adcetris® (brentuximab vedotin), Kadcyla® (trastuzumab emtansine), and most recently Bespona® (inotuzumab ozogamicin), research has flourished [4, 14, 15]. Sales are expected to multiply, as the market was valued at USD 1.3 Bn in 2015 and is predicted to increase up to USD 29.3 Bn by 2022 [16, 17]. Yet, of the more than 50 ADCs in clinical development, most are still in the pilot stages [18-20]. Different factors challenge the success of this payload delivery system, e.g. payload internalization, expression of the target antigen on tumor tissue, extra- as well as intracellular linker stability and the correct payload for the tumor to be addressed [21, 22].

With respect to antigen binding, the ADC should act like the parent antibody [9]. Conjugation may change the pharmacological properties of the antibodies, for example the mean half-life of trastuzumab is reduced from 28.5 to 6 days upon conjugation with emtansine [2, 23]. Bender et al. have demonstrated faster ADC clearance compared to mAb clearance because of deconjugation which involves antibody degradation [24]. Only 1.56 % of the administered payload reaches the target cells if each step in the ADC mechanism is 50 % efficient [13]. The actual uptake is assumed to be even lower [25]. A compromise for the number of drugs per antibody is typically needed for the highest possible cytotoxicity and the highest possible stability of the antibody [9]. A number of two to four drugs per antibody is considered to generate the best therapeutic window [9, 26, 27]. Moreover, larger drug payloads (e.g. bacterial exotoxins) may interfere with antigen/Fc receptor binding [28].

2 SPECIFIC COMPONENTS OF THE ADC

During the development of a clinically efficient monoclonal antibody (mAb) or ADC to a market product, a stable formulation needs to be developed. Proteins are susceptible to chemical and physical degradation [29-31]. Drug conjugation introduces more complexity and instability aspects to the antibody. In the following, stability considerations for each component and the whole ADC molecule will be discussed.

2.1 Antibody Component

MAbs can be characterized quite extensively, although Rituxan® as the first commercially available mAb was only approved in 1997 [32-38]. So far, only full IgG molecules have been utilized in ADC development because of their accumulation at the tumor and long circulatory half-life [13, 39]. Other antibody formats are conceivable for ADCs, but have not been tested in the clinics [39]. For solid tumors for example, the use of diabodies and minibodies might increase tumor penetration [40]. Following the general trend for mAbs, most ADCs are based on humanized or fully human sequences [41]. Moreover, the antibodies used in ADCs should typically be internalized upon target binding as most payloads are devised to be released intracellularly [42, 43].

For ADCs, the modification of the primary structure of the antibody caused by conjugation must be considered. It is vital for the product that the high immunoaffinity of the parent mAb is retained after conjugation [9]. For conjugation, various functional groups of the antibody have been used. These are the interchain cysteine residues (thiols), amines (lysines), alcohols, aldehydes and azides [44]. Free sulfhydryls may decrease mAb stability, but the reduction of interchain cysteines does not negatively affect antibody stability and is a commonly used conjugation method [44, 45]. Cysteine-linked ADCs

are heterogeneous in terms of drug load and conjugation site, as zero to eight drugs per antibody are possible [46]. In order to improve homogeneity, reactive thiol groups that do not alter IgG functions have been introduced through cysteine substitutions in the primary structure, which have been termed ThioMabs [23, 47, 48].

Modification of the surface lysine residues by addition of the linker neutralizes positive charge on these residues [49]. Up to eight conjugated drugs per antibody have been reported to result from lysine conjugation, although theoretically a higher number is possible [46]. In a lysine-conjugated ADC, almost 50 % of the lysines were partially modified, especially in regions of high flexibility and solvent accessibility [49, 50]. Hence, lysine-linked ADCs are more heterogeneous, but deviate less from the naïve mAb compared to the cysteine-linked ADCs [51]. In order to enable a better control of drug load and specificity for lysine-coupled ADCs, research is conducted to only target the lysines that are most solvent-accessible and reactive [52]. Further techniques such as enzymatic conjugation, conjugation by using non-natural amino acids [53-55], e.g. p-acetylphenylalanine [56] and site-specific conjugation via additional glycans [57] are under development [58].

2.2 Linker Component

The stability of the linker in the context of process chemistry, plasma circulation and product storage is of crucial importance for the ADC [9, 51, 59, 60]. Furthermore, the payload must be inert against endogenous reactive molecules and has to be released at the target [28]. The choice of linker also affects antigen and Fc receptor binding as well as thermal stability [61].

The different linkers have been nicely reviewed in literature [9, 44, 59, 62, 63]. In short, the linkers can be divided into chemically-labile, enzyme-labile and non-cleavable. The chemically labile linkers are cleaved through pH-dependent mechanisms, implying that they are susceptible to the acidic pH of the lysosome. An example is the hydrazone linker used in Mylotarg® and Besponsa® (Figure I- 2) [64, 65]. At pH 7.2, the linker is relatively stable ($t_{1/2}$> 60 h) compared to pH 5.0 ($t_{1/2}$ 3 h) [43]. As acidic conditions can also be found in the body outside of the lysosome, nonspecific drug release can occur [64]. One of the reasons for the temporary withdrawal of Mylotarg® was its instability in plasma [64]. Linker stability is increased using enzyme-labile linkers, which are cleaved by lysosomal proteases. This linkage has been successfully implemented for Adcetris® using a valine-citrulline dipeptide linker [43]. ADCs with non-cleavable linkers are internalized, upon which the antibody is degraded. For non-cleavable linkers, the non-targeted release of the free drug is reduced, which decreases systemic toxicity [66]. An example for an effective usage is Kadcyla® with the succinimidyl 4-(N-maleimidomethyl)cyclohexan-1-carboxylate (SMCC) linker. The drug and linker together act as the potent cytotoxic [9, 42, 67]. The optimal choice of linker also depends on the target antigen, which

should be located close to the cell-surface to enable binding of the ADC [46]. New forms of less hydrophobic linkers, which enable conjugation of a higher number of hydrophobic payloads per antibody are also discussed in literature [68].

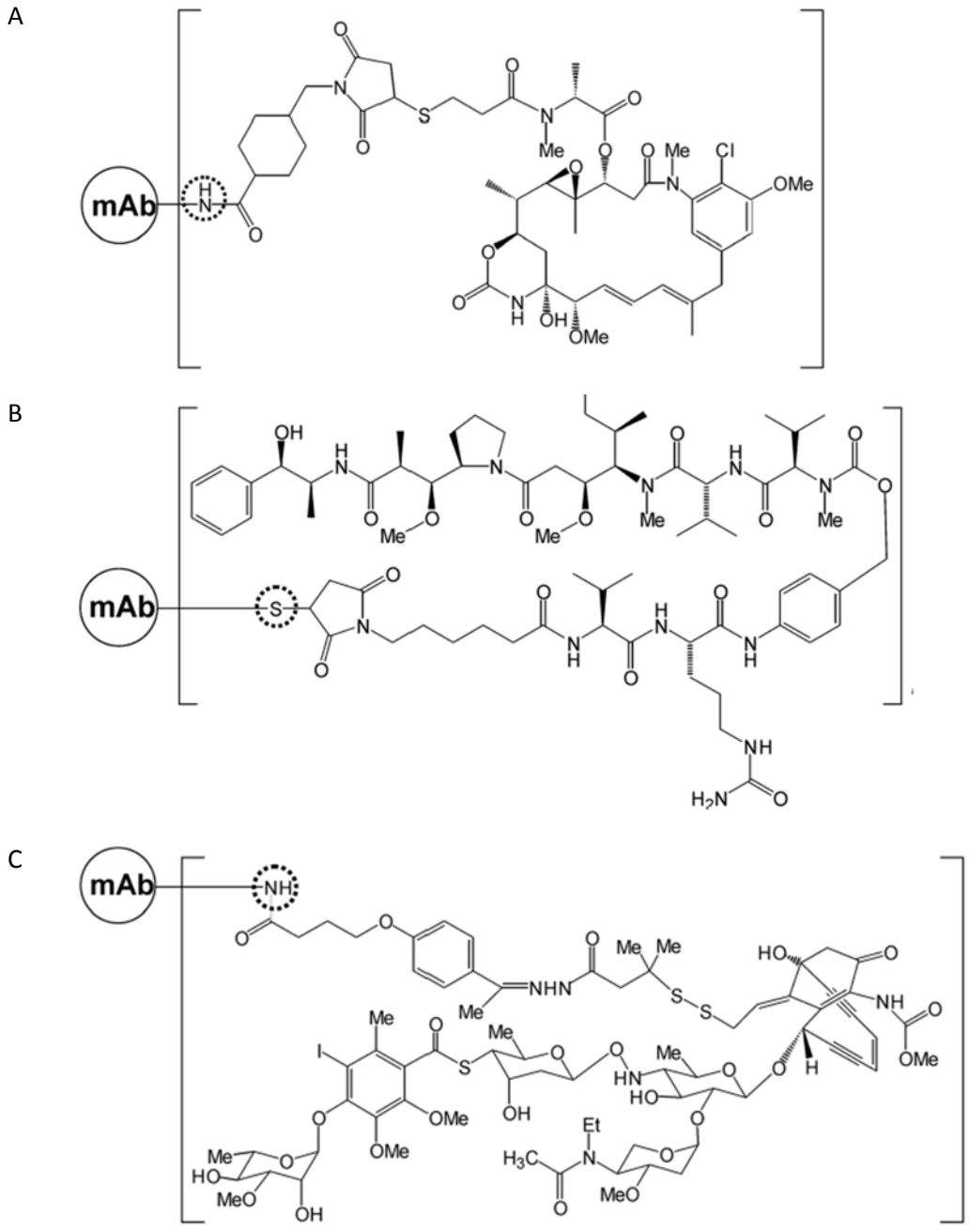

Figure I- 2: Chemical structures of the three linkages and payloads on the market: SMCC linked emtansine (A), valine-citrulline linked vedotin (B) and hydrazone linked ozogamicin (C), [14].

The choice of linker defines the drug antibody ratio (DAR), drug load distribution and stability of the linkage, which are vital to product quality [69]. Further, the analysis of residual or dissociated free drug is important for toxicity and safety assessment. [70]. As an example, the frequently used

thio-succinimide linker can undergo retro and exchange reactions at physiological pH and temperature if other thiols are in the vicinity and its hydrophobicity may increase protein aggregation [69, 71-73].

2.3 Payload Component

Drugs that are chosen as payloads for ADCs are highly cell toxic and are released from the ADC in their potent forms [63]. The payload and this final metabolite form determine the toxicity of an ADC molecule [74]. In the first era of ADCs, the released payload molecule differed from the free drug, which led to a reduced potency of the ADC [11, 60].

The payloads are typically too toxic for traditional chemotherapy and often have little selectivity for tumor cells [9, 15, 44, 75, 76]. For example, DNA alkylating agents such as duocarmycins [77] and pyrrolobenzodiazepines [78-80] have been reintroduced into research and development and new highly potent drugs are currently evaluated [75, 81, 82]. Typical physicochemical properties of payloads based on emtansine and vedotin (Figure I- 2) are a molecular weight of about 700 to 750 Da, an H donor and acceptor sum of about 15 and a log P of approx. four.

2.4 ADC Considerations

ADC characteristics are influenced by the DAR, as it determines the efficacy and stability of the ADC [70]. If the chosen DAR is too low, cytotoxicity is insufficient. If it is selected too high, the ADC might be recognized by the immune system and it is also more prone to aggregate [9]. A DAR of four is considered to be optimal [26]. Coupling itself may induce structural changes of the antibody molecule, which in turn could affect other biophysical characteristics [83]. Conformational and colloidal instability can induce protein aggregation, which may lead to a loss of efficiency and immunogenicity [38, 84].

Ross and Wolfe recently reviewed the physical and chemical stability of ADCs [85]. Upon cysteine linking of payloads, protein conformation is not considerably altered, but the conformational energy of unfolding is decreased, and a more hydrophobic local surface is created. Correspondingly, the melting temperatures can be decreased and aggregate formation is triggered [86-88]. Molecules with higher DARs are more prone for aggregation [28, 86] and a higher DAR species in a mixture determines the stability of the ADC as a whole [87]. The thermal stability of a cysteine-linked ADC was considerably decreased with a higher DAR and also with an increasing ionic strength [88]. The melting temperature of the C_H2 region was more influenced by conjugation compared to the Fab/C_H3 domain, even if the antibody was solely conjugated in the Fab region [86, 88].

Less literature is available on the stability of lysine-linked ADCs. Upon conjugation, the positive charge of a lysine is removed, and multiple isoforms are generated [89]. The melting temperatures of an ADC and its antibody-linker intermediate were decreased, and the percentages of higher molecular weight species were increased after seven days of storage at 40 °C. Wakankar et al. also showed that conjugation influenced the C_H2 domain the most, which can be explained by the high flexibility of the C_H2 domain and increased likeliness of conjugation [49]. Interestingly, the addition of the linker alone increased aggregation more than the addition of both linker and payload. The unconjugated linker may react with side chains of nucleophilic amino acids, leading to aggregation [49]. The hydrophobic payload and uneven charge distributions increase the aggregation propensity of lysine-linked ADCs [90]. The Fab domain was less sensitive to conjugation for lysine compared to thiol conjugates [61]. The effect of pH, temperature, agitation and freeze/thaw cycles on the stability of trastuzumab and the corresponding lysine-linked ADC (T-DM1) was recently compared by Mohamed et al. [91]. Degradation of T-DM1 was increased compared to the parent mAb upon thermal and mechanical stressing, as well as pH stress [91]. The comparison of Kadcyla® and a biosimilar candidate displayed a comparable thermal stability and aggregation behavior although the DARs slightly differed [92].

The chemical stability of ADCs depends on the parent mAb, the linker-payload instabilities and the site of conjugation on the antibody [28]. For example, the thioether succinimide linkage can be oxidized in a mild aqueous environment followed by sulfoxide elimination [28, 93].

For the conjugation process, the different physical and chemical properties of the antibody, linker and payload must be considered. For example, antibodies are more stable in buffered, aqueous solutions whereas the payloads often have limited aqueous solubility [94, 95]. The necessary use of organic solvents during conjugation can destabilize the antibody [96, 97]. Furthermore, the mAb should be supplied in a buffer at a pH that is compatible with the conjugation step. Side reactions during coupling may destabilize the antibody, e.g. succinimidyl esters that react not only with lysines but also cysteine and tyrosine [98, 99]. Moreover, buffers with primary amines, e.g. histidine, cannot be used for lysine-based coupling. For the patient's safety, the clearance of unconjugated drug and residual organic solvent is also indispensable [100].

3 FORMULATION CONSIDERATIONS FOR ADCS

The structural diversity of proteins calls for the development of a unique and specific formulation for each product, which can be very time-consuming [101-103]. For ADCs, the optimal formulation does not only depend on mAb stability, but must also consider the chemical stability of the linker and payload [28, 100]. A compilation of the formulations used for ADCs and immunoconjugates on the market in September 2017 is given in Table I- 1 and Table I- 2, respectively. The current ADC market was used as a basis for the formulation considerations below.

3.1 Key Factors for the Product

The concentration of the marketed ADCs is below 20 mg/mL (Table I- 1). This is in marked contrast to the concentrations above 50 mg/mL that are broadly discussed in literature for traditional mAb therapeutics [104-107]. The high selectivity and efficacy of ADCs for tumor cell killing as well as the i.v. application mitigates the necessity to use these concentrations [5]. At higher concentration, the risk of aggregation may be increased especially for a mAb carrying a hydrophobic payload. Furthermore, the solubility of an ADC may be decreased compared to the parent mAb because of a reduced net surface charge [89].

The ADCs on the market are given as infusions. In the infusion bag the ADC concentration is low, increasing the risk of drug loss due to adsorption onto plastic, which might by enhanced by the hydrophobic payload [51]. Dilution of the drug also decreases the level of stabilizer, which may induce aggregation and particle formation [108, 109]. In 0.9 % NaCl solution, electrostatic charge shielding may enhance attractive protein-protein interactions, leading to a possibly reduced solubility of high DAR species or an increased aggregation tendency [51].

Formulations with low ionic strength have shown to decrease aggregation and fragmentation for ADCs [88]. Especially for lysine-linked ADCs, surface charges are unevenly distributed. In traditional mAbs, molecules with an inconsistent charge distribution are expected to be more prone for intermolecular attractions [110]. The DAR distribution and high DAR species strongly influence the stability and formulation composition of the ADC [28, 87]. Furthermore, the choice of the appropriate pH is not only influenced by the IEP of the ADC but also by the linker e.g. hydrolysis of the thiol-succinimide linker is stimulated by an increasing pH [69]. The hydrolytic degradation of the linker during storage may be decreased with a freeze-dried formulation [69].

For biopharmaceuticals, liquid formulations are preferred and about 2/3 of the marketed products in Japan and the US in 2013 were solutions [111]. Reasons for the preference of liquid solutions are the lower costs and the higher convenience comparable to lyophilizates [112, 113]. However, the product

might face stability problems [30, 114]. Hitherto, all approved ADCs are lyophilized and formulated in a buffer with sugar and surfactant (Table I- 1). Only the immunoconjugates come as liquid or frozen solution (Table I- 2). So far, no publication has focused on the stability of ADCs in the liquid compared to the lyophilized state. Clearly, chemical degradation and especially the risk for free drug formation is strongly reduced by lyophilization [51, 115]. For example, the thio-succinimide linkage in Adcetris® and Kadcyla® can be degraded by succinimide hydrolysis or a retro-Michael reaction [69, 71-73]. The hydrazone linkage employed in Besponsa® and Mylotarg® is very labile [116] and is slowly hydrolyzed in plasma [72]. Interestingly, in contrast to traditional mAb therapeutics, ADCs can be light sensitive, and Mylotarg® and Besponsa® come in amber glass vials [117, 118].

Table I- 1: Formulations of approved ADCs.

Antibody product	Company	Generic name; description	Delivery route	Pharmaceutical form; storage	Formulation concentration	Dilution media	Diluted concentration*	Buffer components	Excipients	Stage°	Source
Mylotarg®	Pfizer	Gemtuzumab ozogamicin; humanized IgG4; anti-CD33	IV, infusion	lyophilized, 2-8 °C	1 mg/mL	NaCl	0.065 mg/mL	Na phosphate	NaCl, sucrose, dextran 40	A	EMA
Kadcyla®	Roche	trastuzumab emtansine; humanized IgG1; anti-HER2	IV, infusion	lyophilized, 2-8 °C	20 mg/mL	NaCl	1.008 mg/mL	succinic acid	NaOH, sucrose, polysorbate 20	A	EMA
Adcetris®	Takeda	brentuximab vedotin; recombinant chimerized IgG1, anti-CD30	IV, infusion	lyophilized, 2-8 °C	5 mg/mL	NaCl, dextrose, Ringer-Lactate	0.84 mg/mL	citrate	a,a-trehalose dihydrate, polysorbate 80	A	EMA
Besponsa®	Pfizer	inotuzumab ozogamicin, humanized IgG4; anti-CD22	IV, infusion	lyophilized, 2-8 °C	0.25 mg/mL	NaCl	0.009 mg/mL	TRIS	sucrose, polysorbate 80, sodium chloride	A	EMA

* calculations based on 70 kg, 175 m patient with the highest applicable dose and dilution into infusion bag with the lowest volume allowed.

° A: approved, DA: disapproved

Table I- 2: Formulations of immunoconjugates.

Antibody product	Company	Generic name; description	Delivery route	Pharmaceutical form; storage	Formulation concentration	Dilution media	Diluted concentration*	Buffer components	Excipients	Stage°	Source
Bexxar®	GSK	Tositumomab + Iodine 131	IV, injection	frozen solution	14 mg/mL	NaCl	0.7 mg/mL	ascorbic acid	maltose, povidone, sodium chloride, pH 7.0	DA	FDA
Zevalin®	Spectrum	Ibritumomab tiuxetan	IV, infusion	solution, 2-8 °C	1.6 mg/mL	-	0.2 mg/mL	-	sodium chloride	A	FDA
								added later: sodium acetate	albumin, sodium chloride, sodium phosphate, pentetic acid, potassium phosphate, potassium chloride		
Ontak®	Seragen	denileukin diftitox	IV, infusion	frozen solution	150 mcg/mL	NaCl	15 mcg/mL	citric acid	EDTA, polysorbate 20, pH 6.9-7.2	A	FDA

* calculations based on 70 kg, 175 m patient with the highest applicable dose and dilution into infusion bag with the lowest volume allowed.

° A: approved, DA: disapproved

3.2 ADC Formulation Components

ADC formulations are based on the same excipients as a mAb formulation [28, 69]. The choice of buffer depends on the target pH, the instability profile of the ADC and whether a liquid or lyophilized form is of interest. For highly concentrated mAb solutions, buffer-free formulations are recently discussed [119-121], but this might not be an option for the labile ADCs. As ADCs are admixed to infusions for applications, e.g. 0.9 % sodium chloride or 5 % dextrose solutions (Table I- 1), isotonicity of the ADC formulation is unnecessary. Still, tonicity agents such as sodium chloride, mannitol or sucrose are added to the ADC formulations. Sugars, specifically sucrose and trehalose, function as cryo- and lyoprotectants for the lyophilized ADCs [51, 112, 122, 123]. The concentration of sugar may need to be up to 5 % (w/v) during freezing, whereas a weight ratio of sugar to protein of at least 1:1 is necessary for the dried state [115]. Surfactants, specifically polysorbate 20 or 80, are used in mAb as well as in ADC formulations. Polysorbates may degrade, contain impurities, are an inhomogeneous mixture and are challenging to characterize [124-126]. But their positive effects prevail, as the surfactants stabilize the protein against accumulation and aggregation at interfaces and additionally may increase wettability during reconstitution [127]. Higher polysorbate concentrations may be required for ADCs compared to mAbs due to the heterogeneity and hydrophobicity of the drug substance [69]. To reduce the hydrophobic influence of the payload, the use of a low ionic strength buffer with a surfactant is suggested [51, 87, 88, 90]. ADCs show more pronounced aggregate formation and a lower T_m at higher ionic strength and independent of the type of salt [88].

4 Analytics for ADCs

The market approval for an ADC relies on a proven stability and maintained biological activity during long-term storage and possible stresses the protein may encounter [102]. The analytical toolbox employed for traditional mAbs also applies to ADCs (Figure I- 3) [70, 128]. However, not all methods can be transferred to an ADC without modifications, e.g. if the payload shows UV absorbance or the sample is highly heterogeneous. More distinct ADC analytics are still scarce and under development [90, 129, 130]. In the following, some of the analytics with special considerations for ADCs will be shortly described.

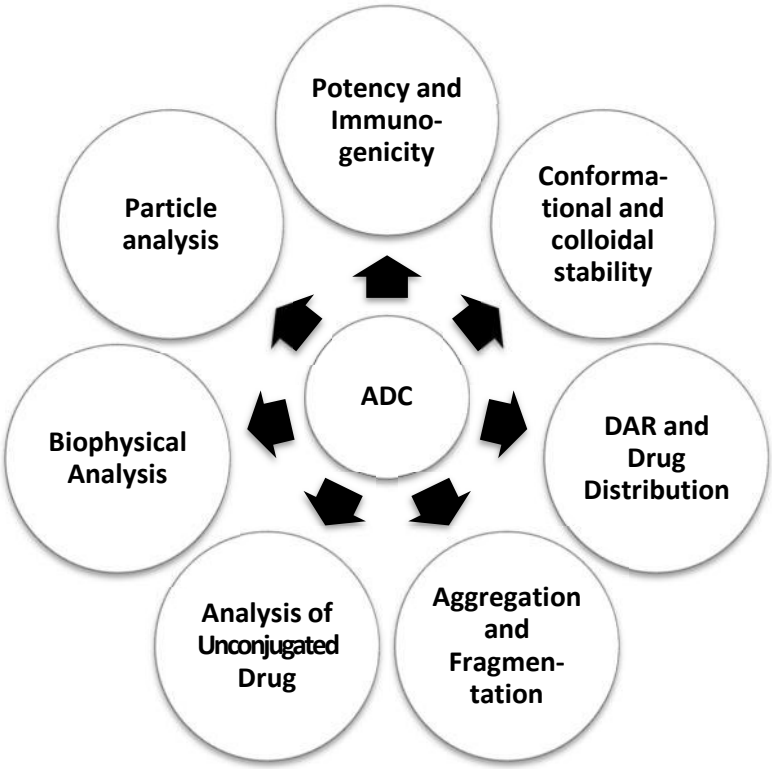

Figure I- 3: Analytical methods necessary to characterize an ADC.

The DAR can be measured by UV/Vis spectroscopy, but only if the absorption maxima differ between payload and antibody. Other methods to determine the DAR, as well as the drug load distribution and free drug, are hydrophobic interaction chromatography and LC-ESI-MS [131, 132]. Peptide mapping can be used to identify specific protein modifications that may result from conjugation and degradation [70, 129]. Unbound drug is traditionally determined using RP-HPLC, but CE and ELISA have also been used. Some characterization techniques require adaptions for ADCs, e.g. in SEC, stronger interactions with the column due to the hydrophobic payload may have to be reduced by the addition of an organic solvent [133]. Moreover, the extrinsic fluorescent dye SYPRO® Orange, used to determine the T_m in dynamic scanning fluorimetry [134], can interact with the hydrophobic payloads, preventing its applicability for ADCs.

5 REFERENCES

[1] D. M. Ecker, S. D. Jones, and H. L. Levine, "The therapeutic monoclonal antibody market," *MAbs,* vol. 7, no. 1, pp. 9-14, 2015.

[2] D. AlDeghaither, B. G. Smaglo, and L. M. Weiner, "Beyond peptides and mAbs--current status and future perspectives for biotherapeutics with novel constructs," *J Clin Pharmacol,* vol. 55 Suppl 3, pp. S4-20, 2015.

[3] I. B. Weinstein, "Cancer. Addiction to Oncogenes -- the Achilles Heal of Cancer," *Science,* vol. 297, no. 5578, pp. 63-64, 2002.

[4] I. Sassoon and V. Blanc, "Antibody–Drug Conjugate (ADC) Clinical Pipeline: A Review," in *Antibody-Drug Conjugates*. vol. 1045, L. Ducry, Ed., ed: Humana Press, pp. 1-27, 2013.

[5] J. M. Lambert, "Antibody-Drug Conjugates (ADCs): Magic Bullets at Last!," *Mol Pharm,* vol. 12, no. 6, pp. 1701-2, 2015.

[6] P. D. Senter and E. L. Sievers, "The discovery and development of brentuximab vedotin for use in relapsed Hodgkin lymphoma and systemic anaplastic large cell lymphoma," *Nat Biotechnol,* vol. 30, no. 7, pp. 631-7, 2012.

[7] G. J. Bernardes, G. Casi, S. Trussel, I. Hartmann, K. Schwager, J. Scheuermann, and D. Neri, "A traceless vascular-targeting antibody-drug conjugate for cancer therapy- Supporting Information," *Angew Chem Int Ed Engl,* vol. 51, no. 4, 2012.

[8] A. M. Wu and P. D. Senter, "Arming antibodies: prospects and challenges for immunoconjugates," *Nat Biotechnol,* vol. 23, no. 9, pp. 1137-46, 2005.

[9] L. Ducry and B. Stump, "Antibody-Drug Conjugates: Linking Cytotoxic Payloads to Monoclonal Antibodies," *Bioconjugate Chemistry,* vol. 21, pp. 5-13, 2010.

[10] T. Ghose and A. H. Blair, "Antibody-Linked Cytotoxic Agents in the Treatment of Cancer: Current Status and Future Prospects," *J Natl Cancer Inst,* vol. 61, no. 3, pp. 657-676, 1978.

[11] D. W. PA Trail, SJ Lasch, AJ Henderson, S Hofstead, AM Casazza, RA Firestone, I Hellstrom, KE Hellstrom, "Cure of xenografted human carcinomas by BR96-doxorubicin immunoconjugates," *Science,* vol. 261, no. 5518, pp. 212-215, 1993.

[12] Bruce H. Petersen, Sonja V. DeHerdt, Dennis W. Schneck, and T. F. Bumol, "The Human Immune Response to KS1/4-Desacetylvinblastine (LY256787) and KS1/4-Desacetylvinblastine Hydrazide (LY203728) in Single and Multiple Dose Clinical Studies," *Cancer Res,* vol. 51, pp. 2286-2290, 1991.

[13] B. A. Teicher and R. V. Chari, "Antibody conjugate therapeutics: challenges and potential," *Clin Cancer Res,* vol. 17, no. 20, pp. 6389-97, 2011.

[14] R. J. Ho and J. Chien, "Trends in translational medicine and drug targeting and delivery: new insights on an old concept-targeted drug delivery with antibody-drug conjugates for cancers," *J Pharm Sci,* vol. 103, no. 1, pp. 71-7, 2014.

[15] R. V. Chari, M. L. Miller, and W. C. Widdison, "Antibody-drug conjugates: an emerging concept in cancer therapy," *Angew Chem Int Ed Engl,* vol. 53, no. 15, pp. 3796-827, 2014.

[16] *Antibody Drug Conjugate Market: Global Industry Size, Share, Growth, Opportunities, Outlook, Analysis and Forecast 2016 to 2024*. Available: http://technorati.com/antibody-drug-conjugate-market-global-industry-size-share-growth-opportunities-outlook-analysis-and-forecast-2016-to-2024/

[17] C. Research, "Global Antibody Drug Conjugate Market By Drug (Kadcyla, Adcetris, Pipeline Analysis Of Antibody Drug Conjugate) - Growth, Future Prospects And Competitive Analysis, 2016 - 2024," 2017.

[18] A. M. Thayer, "Building Antibody-Drug Conjugates," *Chemical & Enginnering News,* vol. 92, no. 3, pp. 13-21, 2014.

[19] S. Sau, H. O. Alsaab, S. K. Kashaw, K. Tatiparti, and A. K. Iyer, "Advances in antibody-drug conjugates: A new era of targeted cancer therapy," *Drug Discov Today,* vol. 22, no. 10, pp. 1547-1556, 2017.

[20] Roots Analysis, "Antibody Drug Conjugates Market (3rd Edition)," 2015.

[21] H. Bouchard, C. Viskov, and C. Garcia-Echeverria, "Antibody-drug conjugates-a new wave of cancer drugs," *Bioorg Med Chem Lett,* vol. 24, no. 23, pp. 5357-63, 2014.

[22] A. W. Tolcher, "Antibody drug conjugates: lessons from 20 years of clinical experience," *Ann Oncol,* vol. 27, no. 12, pp. 2168-2172, 2016.

[23] B. Q. Shen, K. Xu, L. Liu, H. Raab, S. Bhakta, M. Kenrick, et al. and J. R. Junutula, "Conjugation site modulates the in vivo stability and therapeutic activity of antibody-drug conjugates," *Nat Biotechnol,* vol. 30, no. 2, pp. 184-9, 2012.

[24] B. Bender, D. D. Leipold, K. Xu, B. Q. Shen, J. Tibbitts, and L. E. Friberg, "A mechanistic pharmacokinetic model elucidating the disposition of trastuzumab emtansine (T-DM1), an antibody-drug conjugate (ADC) for treatment of metastatic breast cancer," *AAPS J,* vol. 16, no. 5, pp. 994-1008, 2014.

[25] K. Tsuchikama and Z. An, "Antibody-drug conjugates: recent advances in conjugation and linker chemistries," *Protein Cell,* vol. 9, no. 1, pp. 33-46, 2018.

[26] P. D. S. Kevin J. Hamblett, Dana F. Chace, Michael M. C. Sun, Joel Lenox, Charles G. Cerveny, Kim M. Kissler, Starr X. Bernhardt, Anastasia K. Kopcha, Roger F. Zabinski, Damon L. Meyer, Joseph A. Francisco, "Effects of Drug Loading on the Antitumor Activity of a Monoclonal Antibody Drug Conjugate," *Clin Cancer Res,* vol. 10, no. 20, pp. 7063-7070, 2004.

[27] C. F. McDonagh, E. Turcott, L. Westendorf, J. B. Webster, S. C. Alley, K. Kim, et al. and P. Carter, "Engineered antibody-drug conjugates with defined sites and stoichiometries of drug attachment," *Protein Eng Des Sel,* vol. 19, no. 7, pp. 299-307, 2006.

[28] K. Tsumoto, A. Young, and S. Ohtake, "Formulation and Stability," in *Antibody-Drug Conjugates*, ed: John Wiley & Sons, Inc., 2016, pp. 105-129.

[29] W. Wang, S. Singh, D. L. Zeng, K. King, and S. Nema, "Antibody structure, instability, and formulation," *J Pharm Sci,* vol. 96, no. 1, pp. 1-26, 2007.

[30] M. C. Manning, D. K. Chou, B. M. Murphy, R. W. Payne, and D. S. Katayama, "Stability of protein pharmaceuticals: an update," *Pharm Res,* vol. 27, no. 4, pp. 544-75, 2010.

[31] E. Y. Chi, S. Krishnan, T. W. Randolph, and J. F. Carpenter, "Physical stability of proteins in aqueous solution: Mechanism and driving forces in nonnative protein aggregation," *Pharmaceutical Research,* vol. 20, no. 9, pp. 1325-1336, 2003.

[32] U. Iyer and V. J. Kadambi, "Antibody drug conjugates - Trojan horses in the war on cancer," *J Pharmacol Toxicol Methods,* vol. 64, no. 3, pp. 207-12, 2011.

[33] G. Thiagarajan, A. Semple, J. K. James, J. K. Cheung, and M. Shameem, "A comparison of biophysical characterization techniques in predicting monoclonal antibody stability," *MAbs,* vol. 8, no. 6, pp. 1088-97, 2016.

[34] S. N. Telikepalli, O. S. Kumru, C. Kalonia, R. Esfandiary, S. B. Joshi, C. R. Middaugh, and D. B. Volkin, "Structural characterization of IgG1 mAb aggregates and particles generated under various stress conditions," *J Pharm Sci,* vol. 103, no. 3, pp. 796-809, 2014.

[35] D. B. Temel, P. Landsman, and M. L. Brader, "Orthogonal Methods for Characterizing the Unfolding of Therapeutic Monoclonal Antibodies: Differential Scanning Calorimetry, Isothermal Chemical Denaturation, and Intrinsic Fluorescence with Concomitant Static Light Scattering," *Methods Enzymol,* vol. 567, pp. 359-89, 2016.

[36] C. Kalonia, V. Toprani, R. Toth, N. Wahome, I. Gabel, C. R. Middaugh, and D. B. Volkin, "Effects of Protein Conformation, Apparent Solubility, and Protein-Protein Interactions on the Rates and Mechanisms of Aggregation for an IgG1Monoclonal Antibody," *J Phys Chem B,* vol. 120, no. 29, pp. 7062-75, 2016.

[37] A. Hawe, J. C. Kasper, W. Friess, and W. Jiskoot, "Structural properties of monoclonal antibody aggregates induced by freeze-thawing and thermal stress," *Eur J Pharm Sci,* vol. 38, no. 2, pp. 79-87, 2009.

[38] H. C. Mahler, W. Friess, U. Grauschopf, and S. Kiese, "Protein aggregation: pathways, induction factors and analysis," *J Pharm Sci,* vol. 98, no. 9, pp. 2909-34, 2009.

[39] R. Gebleux and G. Casi, "Antibody-drug conjugates: Current status and future perspectives," *Pharmacol Ther,* vol. 167, pp. 48-59, 2016.

[40] C. Peters and S. Brown, "Antibody-drug conjugates as novel anti-cancer chemotherapeutics," *Biosci Rep,* vol. 35, no. 4, 2015.

[41] J. M. Lambert, "Typical Antibody–Drug Conjugates," in *Antibody-Drug Conjugates*, ed: John Wiley & Sons, Inc., pp. 1-32, 2016.

[42] H. K. Erickson, P. U. Park, W. C. Widdison, Y. V. Kovtun, L. M. Garrett, K. Hoffman, et al. and W. A. Blattler, "Antibody-maytansinoid conjugates are activated in targeted cancer cells by lysosomal degradation and linker-dependent intracellular processing," *Cancer Res,* vol. 66, no. 8, pp. 4426-33, 2006.

[43] T. B. Doronina SO, Torgov MY, Mendelsohn BA, Cerveny CG, Chace DF, DeBlanc RL, Gearing RP, Bovee TD, Siegall CB, Francisco JA, Wahl AF, Meyer DL, Senter PD, "Development of potent monoclonal antibody auristatin conjugates for cancer therapy," *Nat Biotechnol,* vol. 21, no. 7, pp. 778-784, 2003.

[44] H. Yao, F. Jiang, A. Lu, and G. Zhang, "Methods to Design and Synthesize Antibody-Drug Conjugates (ADCs)," *Int J Mol Sci,* vol. 17, no. 2, 2016.

[45] H. Liu and K. May, "Disulfide bond structures of IgG molecules: structural variations, chemical modifications and possible impacts to stability and biological function," *MAbs,* vol. 4, no. 1, pp. 17-23, 2012.

[46] S. Panowksi, S. Bhakta, H. Raab, P. Polakis, and J. R. Junutula, "Site-specific antibody drug conjugates for cancer therapy," *MAbs,* vol. 6, no. 1, pp. 34-45, 2014.

[47] J. R. Junutula, H. Raab, S. Clark, S. Bhakta, D. D. Leipold, S. Weir, et al. and W. Mallet, "Site-specific conjugation of a cytotoxic drug to an antibody improves the therapeutic index," *Nat Biotechnol,* vol. 26, no. 8, pp. 925-32, 2008.

[48] S. Sukumaran, K. Gadkar, C. Zhang, S. Bhakta, L. Liu, K. Xu, et al. and K. Lin, "Mechanism-Based Pharmacokinetic/Pharmacodynamic Model for THIOMAB™ Drug Conjugates," *Pharm Res,* vol. 32, pp. 1884-1893, 2015.

[49] Aditya A. Wakankar, Maria B. Feeney, Javier Rivera, Yan Chen, Michael Kim, Vikas K. Sharma, and Y. J. Wang, "Physicochemical Stability of the Antibody-Drug Conjugate Trastuzumab-DM1: Changes due to Modification and Conjugation Processes," *Bioconjugate Chemistry,* vol. 21, no. 9, pp. 1588-1595, 2010.

[50] L. Wang, G. Amphlett, W. A. Blattler, J. M. Lambert, and W. Zhang, "Structural characterization of the maytansinoid-monoclonal antibody immunoconjugate, huN901-DM1, by mass spectrometry," *Protein Sci,* vol. 14, no. 9, pp. 2436-46, 2005.

[51] S. K. Singh, D. L. Luisi, and R. H. Pak, "Antibody-Drug Conjugates: Design, Formulation and Physicochemical Stability," *Pharm Res,* vol. 32, no. 11, pp. 3541-71, 2015.

[52] V. Gautier, A. J. Boumeester, P. Lossl, and A. J. Heck, "Lysine conjugation properties in human IgGs studied by integrating high-resolution native mass spectrometry and bottom-up proteomics," *Proteomics,* vol. 15, no. 16, pp. 2756-65, 2015.

[53] T. J. Hallam, E. Wold, A. Wahl, and V. V. Smider, "Antibody conjugates with unnatural amino acids," *Mol Pharm,* vol. 12, no. 6, pp. 1848-62, 2015.

[54] D. Y. Jackson, "Processes for Constructing Homogeneous Antibody Drug Conjugates," *Organic Process Research & Development,* vol. 20, no. 5, pp. 852-866, 2016.

[55] F. Tian, Y. Lu, A. Manibusan, A. Sellers, H. Tran, Y. Sun, et al. and P. Sapra, "A general approach to site-specific antibody drug conjugates," *Proc Natl Acad Sci U S A,* vol. 111, no. 5, pp. 1766-71, 2014.

[56] B. M. Hutchins, S. A. Kazane, K. Staflin, J. S. Forsyth, B. Felding-Habermann, V. V. Smider, and P. G. Schultz, "Selective formation of covalent protein heterodimers with an unnatural amino acid," *Chem Biol,* vol. 18, no. 3, pp. 299-303, 2011.

[57] F. L. van Delft, R. Van Geel, and M. A. Wijdeven, "Modified antibody, antibody-conjugate and process for the preparation thereof," ed: Google Patents, 2015.

[58] T. Kline, A. R. Steiner, K. Penta, A. K. Sato, T. J. Hallam, and G. Yin, "Methods to Make Homogenous Antibody Drug Conjugates," *Pharm Res,* vol. 32, no. 11, pp. 3480-93, 2015.

[59] B. Nolting, "Linker Technologies for Antibody–Drug Conjugates," in *Antibody-Drug Conjugates*. vol. 1045, L. Ducry, Ed., ed: Humana Press, pp. 71-100, 2013.

[60] M. R. Gordon, M. Canakci, L. Li, J. Zhuang, B. Osborne, and S. Thayumanavan, "Field Guide to Challenges and Opportunities in Antibody-Drug Conjugates for Chemists," *Bioconjug Chem,* vol. 26, no. 11, pp. 2198-215, 2015.

[61] M. Acchione, H. Kwon, C. M. Jochheim, and W. M. Atkins, "Impact of linker and conjugation chemistry on antigen binding, Fc receptor binding and thermal stability of model antibody-drug conjugates," *mAbs,* vol. 4, no. 3, pp. 362-372, 2012.

[62] F. Dosio, P. Brusa, and L. Cattel, "Immunotoxins and anticancer drug conjugate assemblies: the role of the linkage between components," *Toxins (Basel),* vol. 3, no. 7, pp. 848-83, 2011.

[63] J. Lu, F. Jiang, A. Lu, and G. Zhang, "Linkers Having a Crucial Role in Antibody-Drug Conjugates," *Int J Mol Sci,* vol. 17, no. 4, p. 561, 2016.

[64] J. R. McCombs and S. C. Owen, "Antibody drug conjugates: design and selection of linker, payload and conjugation chemistry," *AAPS J,* vol. 17, no. 2, pp. 339-51, 2015.

[65] P. R. Hamann, L. M. Hinman, I. Hollander, C. F. Beyer, D. Lindh, R. Holcomb, et al. and I. Bernstein, "Gemtuzumab Ozogamicin, A Potent and Selective Anti-CD33 Antibody-Calicheamicin Conjugate for Treatment of Acute Myeloid Leukemia," *Bioconj Chem,* vol. 13, pp. 47-58, 2002.

[66] A. E. Albers, A. W. Garofalo, P. M. Drake, R. Kudirka, G. W. de Hart, R. M. Barfield, et al. and D. Rabuka, "Exploring the effects of linker composition on site-specifically modified antibody-drug conjugates," *Eur J Med Chem,* vol. 88, pp. 3-9, 2014.

[67] S. O. Doronina, B. A. Mendelsohn, T. D. Bovee, C. G. Cerveny, S. C. Alley, D. L. Meyer, et al. and P. D. Senter, "Enhanced Activity of Monomethylauristatin F through Monoclonal Antibody Delivery: Effects of Linker Technology on Efficacy and Toxicity," *Bioconjugate Chemistry,* vol. 17, no. 1, pp. 114-124, 2006.

[68] R. Y. Zhao, S. D. Wilhelm, C. Audette, G. Jones, B. A. Leece, A. C. Lazar, et al. and R. V. Chari, "Synthesis and evaluation of hydrophilic linkers for antibody-maytansinoid conjugates," *J Med Chem,* vol. 54, no. 10, pp. 3606-23, 2011.

[69] J. A. Ji, J. Liu, and Y. J. Wang, "Formulation Development for Antibody-Drug Conjugates," in *Antibody-Drug Conjugates - The 21st Century Magic Bullets for Cancer*, J. Wang, W.-C. Shen, and J. Zaro, Eds., ed AAPS, pp. 79-95, 2015.

[70] A. Wakankar, Y. Chen, Y. Gokarn, and F. S. Jacobson, "Analytical methods for physicochemical characterization of antibody drug conjugates," *mAbs,* vol. 3, no. 2, pp. 161-172, 2011.

[71] P. L. Ross and J. Wolfe, "Antibody-Drug Conjugates: An Overview of the CMC and Characterization Process," in *Antibody-Drug Conjugates: Fundamentals, Drug Development, and Clinical Outcomes to Target Cancer*, J. O. J. Kenneth and S. A. Hurvitz, Eds., ed Wiley, pp. 59-83, 2016.

[72] L. N. Tumey, M. Charati, T. He, E. Sousa, D. Ma, X. Han, et al. and E. I. Graziani, "Mild Method for Succinimide Hydrolysis on ADCs: Impact on ADC Potency, Stability, Exposure, and Efficacy," *Bioconjugate Chemistry,* vol. 25, no. 10, pp. 1871-1880, 2014.

[73] A. D. Baldwin and K. L. Kiick, "Tunable degradation of maleimide-thiol adducts in reducing environments," *Bioconjug Chem,* vol. 22, no. 10, pp. 1946-53, 2011.

[74] H. Donaghy, "Effects of antibody, drug and linker on the preclinical and clinical toxicities of antibody-drug conjugates," *MAbs,* vol. 8, no. 4, pp. 659-71, 2016.

[75] H. L. Perez, P. M. Cardarelli, S. Deshpande, S. Gangwar, G. M. Schroeder, G. D. Vite, and R. M. Borzilleri, "Antibody-drug conjugates: current status and future directions," *Drug Discov Today,* vol. 19, no. 7, pp. 869-81, 2014.

[76] G. Casi and D. Neri, "Antibody-drug conjugates: basic concepts, examples and future perspectives," *J Control Release,* vol. 161, no. 2, pp. 422-8, 2012.

[77] D. L. Boger and D. S. Johnson, "CC-1065 and the duocarmycins: Unraveling the keys to a new class of naturally derived DNA alkylating agents," *Proc. Natl. Acad. Sci. USA,* vol. 92, pp. 3642-3649, 1995.

[78] K. M. Rahman, P. J. Jackson, C. H. James, B. P. Basu, J. A. Hartley, M. de la Fuente, et al. and D. E. Thurston, "GC-targeted C8-linked pyrrolobenzodiazepine-biaryl conjugates with femtomolar in vitro cytotoxicity and in vivo antitumor activity in mouse models," *J Med Chem,* vol. 56, no. 7, pp. 2911-35, 2013.

[79] K. M. Rahman, C. H. James, and D. E. Thurston, "Effect of base sequence on the DNA cross-linking properties of pyrrolobenzodiazepine (PBD) dimers," *Nucleic Acids Res,* vol. 39, no. 13, pp. 5800-12, 2011.

[80] J. A. Hartley, A. Hamaguchi, M. Coffils, C. R. Martin, M. Suggitt, Z. Chen, et al. and P. W. Howard, "SG2285, a novel C2-aryl-substituted pyrrolobenzodiazepine dimer prodrug that cross-links DNA and exerts highly potent antitumor activity," *Cancer Res,* vol. 70, no. 17, pp. 6849-58, 2010.

[81] G. Moldenhauer, A. V. Salnikov, S. Lüttgau, I. Herr, J. Anderl, and H. Faulstich, "Therapeutic Potential of Amanitin-Conjugated Anti-Epithelial Cell Adhesion Molecule Monoclonal Antibody Against Pancreatic Carcinoma," *JNCI: Journal of the National Cancer Institute,* vol. 104, no. 8, pp. 622-634, 2012.

[82] K. C. Lai, A. Muvaffak, M. Li, M. Themeles, S. Sikka, K. Donahue, et al. and T. Chittenden, "Abstract 45: In vitro&; in vivo activity of a novel c-Met-targeting antibody-drug conjugate using a DNA-alkylating, indolinobenzodiazepine payload," *Cancer Research,* vol. 77, no. 13 Supplement, p. 45, 2017.

[83] Y. Adem, K. Schwarz, E. Duenas, T. Patapoff, W. Galush, and O. Esue, "Auristatin Antibody Drug Conjugate Physical Instability and the Role of Drug Payload," *Bioconjug Chem,* vol. 25, no. 4, pp. 656-64, 2014.

[84] M. Ahmadi, C. J. Bryson, E. A. Cloake, K. Welch, V. Filipe, S. Romeijn, et al. and M. H. Fogg, "Small amounts of sub-visible aggregates enhance the immunogenic potential of monoclonal antibody therapeutics," *Pharm Res,* vol. 32, no. 4, pp. 1383-94, 2015.

[85] P. L. Ross and J. L. Wolfe, "Physical and Chemical Stability of Antibody Drug Conjugates: Current Status," *Journal of Pharmaceutical Sciences,* vol. 105, no. 2, pp. 391-397, 2016.

[86] N. S. Beckley, K. P. Lazzareschi, H. W. Chih, V. K. Sharma, and H. L. Flores, "Investigation into temperature-induced aggregation of an antibody drug conjugate," *Bioconjug Chem,* vol. 24, no. 10, pp. 1674-83, 2013.

[87] J. Guo, S. Kumar, A. Prashad, J. Starkey, and S. K. Singh, "Assessment of physical stability of an antibody drug conjugate by higher order structure analysis: impact of thiol- maleimide chemistry," *Pharm Res,* vol. 31, no. 7, pp. 1710-23, 2014.

[88] Y. T. Adem, K. A. Schwarz, E. Duenas, T. W. Patapoff, W. J. Galush, and O. Esue, "Auristatin antibody drug conjugate physical instability and the role of drug payload," *Bioconjug Chem,* vol. 25, no. 4, pp. 656-64, 2014.

[89] N. J. Boylan, W. Zhou, R. J. Proos, T. J. Tolbert, J. L. Wolfe, and J. S. Laurence, "Conjugation site heterogeneity causes variable electrostatic properties in Fc conjugates," *Bioconjug Chem,* vol. 24, no. 6, pp. 1008-16, 2013.

[90] B. Frka-Petesic, D. Zanchi, N. Martin, S. Carayon, S. Huille, and C. Tribet, "Aggregation of Antibody Drug Conjugates at Room Temperature: SAXS and Light Scattering Evidence for Colloidal Instability of a Specific Subpopulation," *Langmuir,* vol. 32, no. 19, pp. 4848-61, 2016.

[91] H. E. Mohamed, A. A. Mohamed, M. A. Al-Ghobashy, F. A. Fathalla, and S. S. Abbas, "Stabilty assessment of antibody-drug conjugate Trastuzumab emtansine in comparison to parent monoclonal antibody using orthogonal testing protocol," *Journal of Pharmaceutical and Biomedical Analysis,* vol. 150, pp. 268-277, 2018.

[92] L. Chen, L. Wang, H. Shion, C. Yu, Y. Q. Yu, L. Zhu, et al. and K. Gao, "In-depth structural characterization of Kadcyla(R) (ado-trastuzumab emtansine) and its biosimilar candidate," *MAbs,* vol. 8, no. 7, pp. 1210-1223, 2016.

[93] N. Fishkin, E. K. Maloney, R. V. Chari, and R. Singh, "A novel pathway for maytansinoid release from thioether linked antibody-drug conjugates (ADCs) under oxidative conditions," *Chem Commun (Camb),* vol. 47, no. 38, pp. 10752-4, 2011.

[94] I. Hollander, A. Kunz, and P. R. Hamann, "Selection of Reaction Additives Used in the Preparation of Monomeric Antibody-Calicheamicin Conjugates," *Bioconjugate Chemistry,* vol. 19, pp. 358-361, 2008.

[95] A. G. Myers, S. B. Cohen, and B. M. Kwon, "A Study of the Reaction of Calicheamycin γ1 with Glutathione in the Presence of Double-Stranded DNA," *J. Am. Chem. Soc.,* vol. 116, pp. 1255-1271, 1994.

[96] C. N. Pace, S. Trevino, E. Prabhakaran, and J. M. Scholtz, "Protein structure, stability and solubility in water and other solvents," *Philos Trans R Soc Lond B Biol Sci,* vol. 359, no. 1448, pp. 1225-34; discussion 1234-5, 2004.

[97] A. Tjernberg, N. Markova, W. J. Griffiths, and D. Hallen, "DMSO-related effects in protein characterization," *J Biomol Screen,* vol. 11, no. 2, pp. 131-7, 2006.

[98] H. W. Chih, B. Gikanga, Y. Yang, and B. Zhang, "Identification of amino acid residues responsible for the release of free drug from an antibody-drug conjugate utilizing lysine-succinimidyl ester chemistry," *J Pharm Sci,* vol. 100, no. 7, pp. 2518-25, 2011.

[99] C. Y. Lim, N. A. Owens, R. D. Wampler, Y. Ying, J. H. Granger, M. D. Porter, et al. and K. Shimazu, "Succinimidyl ester surface chemistry: implications of the competition between aminolysis and hydrolysis on covalent protein immobilization," *Langmuir,* vol. 30, no. 43, pp. 12868-78, 2014.

[100] W. Galush and A. Wakankar, "Formulation Development of Antibody–Drug Conjugates," in *Antibody-Drug Conjugates*. vol. 1045, L. Ducry, Ed., ed: Humana Press, pp. 217-233, 2013.

[101] N. Chennamsetty, V. Voynov, V. Kayser, B. Helk, and B. L. Trout, "Design of therapeutic proteins with enhanced stability," *Proc Natl Acad Sci U S A,* vol. 106, no. 29, pp. 11937-42, 2009.

[102] A. Fincke, J. Winter, T. Bunte, and C. Olbrich, "Thermally induced degradation pathways of three different antibody-based drug development candidates," *Eur J Pharm Sci,* vol. 62, pp. 148-60, 2014.

[103] E. Maggio, "Use of excipients to control aggregation in peptide and protein formulations," *Journal of Excipients and Food Chemicals,* vol. 1, no. 1, pp. 40-49, 2010.

[104] P. Garidel, A. B. Kuhn, L. V. Schafer, A. R. Karow-Zwick, and M. Blech, "High-concentration protein formulations: How high is high?," *Eur J Pharm Biopharm,* vol. 119, pp. 353-360, 2017.

[105] M. Zidar, A. Susteric, M. Ravnik, and D. Kuzman, "High Throughput Prediction Approach for Monoclonal Antibody Aggregation at High Concentration," *Pharm Res,* vol. 34, no. 9, pp. 1831-1839, 2017.

[106] E. Binabaji, J. Ma, and A. L. Zydney, "Intermolecular Interactions and the Viscosity of Highly Concentrated Monoclonal Antibody Solutions," *Pharm Res,* vol. 32, no. 9, pp. 3102-9, 2015.

[107] N. Whitaker, J. Xiong, S. E. Pace, V. Kumar, C. R. Middaugh, S. B. Joshi, and D. B. Volkin, "A Formulation Development Approach to Identify and Select Stable Ultra-High Concentration Monoclonal Antibody Formulations with Reduced Viscosities," *J Pharm Sci,* vol. 106, no. 11, pp. 3230-3241, 2017.

[108] O. S. Kumru, J. Liu, J. A. Ji, W. Cheng, Y. J. Wang, T. Wang, et al. and D. B. Volkin, "Compatibility, physical stability, and characterization of an IgG4 monoclonal antibody after dilution into different intravenous administration bags," *J Pharm Sci,* vol. 101, no. 10, pp. 3636-50, 2012.

[109] A. Sreedhara, Z. K. Glover, N. Piros, N. Xiao, A. Patel, and B. Kabakoff, "Stability of IgG1 monoclonal antibodies in intravenous infusion bags under clinical in-use conditions," *J Pharm Sci,* vol. 101, no. 1, pp. 21-30, 2012.

[110] S. Yadav, T. M. Laue, D. S. Kalonia, S. N. Singh, and S. J. Shire, "The influence of charge distribution on self-association and viscosity behavior of monoclonal antibody solutions," *Mol Pharm,* vol. 9, no. 4, pp. 791-802, 2012.

[111] S. Uchiyama, "Liquid formulation for antibody drugs," *Biochim Biophys Acta,* vol. 1844, no. 11, pp. 2041-2052, 2014.

[112] J. F. Carpenter, B. S. Chang, W. Garzon-Rodriguez, and T. W. Randolph, "Rational Design of Stable Lyophilized Protein Formulations: Theory and Practice," in *Rational Design of Stable Protein Formulations: Theory and Practice*, J. F. Carpenter and M. C. Manning, Eds., ed Boston, MA: Springer US, pp. 109-133, 2002.

[113] G. Chen, H. Shao, and X. Pan, "A randomized controlled trial to compare the effects of liquid versus powdered recombinant human growth hormone in treating patients with severe burns," *Biomed Rep,* vol. 4, no. 5, pp. 551-556, 2016.

[114] E. Köpf and W. Frieß, "Proteinformulierung: Vom Molekül zum Medikament," *Pharmakon,* vol. 4, pp. 125-133, 2016.

[115] J. F. Carpenter, M. J. Pikal, B. S. Chang, and T. W. Randolph, "Rational Design of Stable Lyophilized Protein Formulations: Some Practical Advice," *Pharmaceutical Research,* vol. 14, no. 8, pp. 969-975, 1997.

[116] N. Jain, S. W. Smith, S. Ghone, and B. Tomczuk, "Current ADC Linker Chemistry," *Pharm Res,* vol. 32, no. 11, pp. 3526-40, 2015.

[117] G. M. Cockrell, M. S. Wolfe, J. L. Wolfe, and C. Schöneich, "Photoinduced Aggregation of a Model Antibody–Drug Conjugate," *Molecular Pharmaceutics,* vol. 12, no. 6, pp. 1784-1797, 2015.

[118] B. A. Kerwin and R. L. Remmele, Jr., "Protect from light: photodegradation and protein biologics," *J Pharm Sci,* vol. 96, no. 6, pp. 1468-79, 2007.

[119] Y. R. Gokarn, E. Kras, C. Nodgaard, V. Dharmavaram, R. M. Fesinmeyer, H. Hultgen, et al. and S. Hershenson, "Self-buffering antibody formulations," *J Pharm Sci,* vol. 97, no. 8, pp. 3051-66, 2008.

[120] S. Bahrenburg, A. R. Karow, and P. Garidel, "Buffer-free therapeutic antibody preparations provide a viable alternative to conventionally buffered solutions: From protein buffer capacity prediction to bioprocess applications," *Biotechnology Journal,* vol. 10, no. 4, pp. 610-622, 2015.

[121] P. Garidel, B. Pevestorf, and S. Bahrenburg, "Stability of buffer-free freeze-dried formulations: A feasibility study of a monoclonal antibody at high protein concentrations," *Eur J Pharm Biopharm,* vol. 97, no. Pt A, pp. 125-39, 2015.

[122] K. Imamura, M. Ogawa, T. Sakiyama, and K. Nakanishi, "Effects of Types of Sugar on the Stabilization of Protein in the Dried State," *Journal of Pharmaceutical Sciences,* vol. 92, no. 2, pp. 266-274, 2003.

[123] W. Wang, "Lyophilization and development of solid protein pharmaceuticals," *International Journal of Pharmaceutics,* vol. 203, pp. 1-60, 2000.

[124] A. Martos, W. Koch, W. Jiskoot, K. Wuchner, G. Winter, W. Friess, and A. Hawe, "Trends on Analytical Characterization of Polysorbates and Their Degradation Products in Biopharmaceutical Formulations," *J Pharm Sci,* vol. 106, no. 7, pp. 1722-1735, 2017.

[125] R. S. Kishore, S. Kiese, S. Fischer, A. Pappenberger, U. Grauschopf, and H. C. Mahler, "The degradation of polysorbates 20 and 80 and its potential impact on the stability of biotherapeutics," *Pharm Res,* vol. 28, no. 5, pp. 1194-210, 2011.

[126] B. A. Kerwin, "Polysorbates 20 and 80 used in the formulation of protein biotherapeutics: structure and degradation pathways," *J Pharm Sci,* vol. 97, no. 8, pp. 2924-35, 2008.

[127] H. J. Lee, A. McAuley, K. F. Schilke, and J. McGuire, "Molecular origins of surfactant-mediated stabilization of protein drugs," *Adv Drug Deliv Rev,* vol. 63, no. 13, pp. 1160-71, 2011.

[128] S. C. Alley and K. E. Anderson, "Analytical and bioanalytical technologies for characterizing antibody-drug conjugates," *Curr Opin Chem Biol,* vol. 17, no. 3, pp. 406-11, 2013.

[129] R. Y. Huang and G. Chen, "Characterization of antibody-drug conjugates by mass spectrometry: advances and future trends," *Drug Discov Today,* vol. 21, no. 5, pp. 850-5, 2016.

[130] N. Spooner, M. Anderson, L. Dillen, L. Ferrari, M. Hilhorst, Z. Lam, et al. and D. Zimmer, "The changing world of bioanalysis: summary of panel discussions," *Bioanalysis,* vol. 9, no. 15, pp. 1175-1179, 2017.

[131] C. Xie and Z. Wang, "Bioanalytical Assay for Characterization of Antibody-Drug Conjugates (ADCs)," in *Antibody-Drug Conjugates: The 21st Century Magic Bullets for Cancer*, J. Wang, W.-C. Shen, and J. L. Zaro, Eds., ed Cham: Springer International Publishing, pp. 97-115, 2015.

[132] L. Basa, "Drug-to-Antibody Ratio (DAR) and Drug Load Distribution by LC-ESI-MS," in *Antibody-Drug Conjugates*, L. Ducry, Ed., ed Totowa, NJ: Humana Press, pp. 285-293, 2013.

[133] T. Chen, Y. Chen, C. Stella, C. D. Medley, J. A. Gruenhagen, and K. Zhang, "Antibody-drug conjugate characterization by chromatographic and electrophoretic techniques," *J Chromatogr B Analyt Technol Biomed Life Sci,* vol. 1032, pp. 39-50, 2016.

[134] T. Menzen and W. Friess, "High-throughput melting-temperature analysis of a monoclonal antibody by differential scanning fluorimetry in the presence of surfactants," *J Pharm Sci,* vol. 102, no. 2, pp. 415-28, 2013.

CHAPTER II:

AIMS OF THIS THESIS

The present thesis aims at a deeper understanding of the physicochemical characteristics of ADCs. A substantial number of ADCs is under development, for which an excellent drug product quality needs to be obtained. How the hydrophobicity of the payload and its coupling to the antibody alter the stability of the antibody in different formulations was to be investigated.

In the first part of this study, non-toxic model conjugates are established that carry similar characteristics as an ADC. Three different fluorescent dyes are selected and coupling procedures to the lysines of a mAb are developed. The colloidal and conformational stability in various formulations is to be tested. To correlate these results to long-term stability, the model conjugates are analyzed over 6 months at 2-8, 25 and 40 °C with focus on protein aggregation, particle formation and protein conformation.

The second part of the thesis focuses on the mechanical stability of model conjugates. Apart from a mechanical stress test, the effect of conjugation on antibody adsorption to the air-liquid and glass surfaces are shown. Moreover, the connection between mechanical stability and protein-protein-interactions is evaluated and discussed. Finally, the interactions of antibody conjugates with human plasma are investigated.

The results of this thesis are summarized in Chapter VI. It highlights the impact of the payload characteristics on the physicochemical stability of an ADC.

CHAPTER III:

UNFOLDING, AGGREGATION, AND INTERACTION OF ANTIBODY CONJUGATES

Abstract

Knowledge about the conformational and colloidal stability of a biotherapeutic is critical for formulation development. In this study, we analyzed the impact of three hydrophobic model payloads on mAb stability. Conformational stability was only slightly changed upon conjugation, but colloidal stability was significantly reduced. A long-term stability study for 6 months at 2-8, 25 and 40 °C demonstrated that more pronounced HMWS and to some extent particle formation were induced upon conjugation of the mAb. Destabilization was more affected by the change in charge state as compared to hydrophobicity coming with the payload. The mAb conjugates were more stable in sucrose containing histidine buffer compared to NaCl containing phosphate buffer, which was not evident for the naïve mAb. Charge and hydrophobicity influenced the colloidal stability more than conformational stability. These two factors, along with pH and ionic strength need to be carefully considered for formulation development.

The following chapter is intended for publication.

1 INTRODUCTION

Protein therapeutics are susceptible to both chemical and physical instability [1-3]. Conformational and colloidal instability can induce protein aggregation, which may lead to a loss of efficiency and enhanced immunogenicity [4, 5]. Excellent reviews of current methods for mAb characterization and analytics are given in literature [6-9]. Antibody-drug conjugates (ADCs), which combine the selectivity of antibodies and efficacy of potent cytotoxic drugs, have become increasingly important in the treatment of cancer [10-15]. ADCs constitute additional challenges to the formulation scientist due to the necessary stabilization of antibody, linker and payload [16-18]. The physical and chemical stability of ADCs have been explored to some extent, which was recently reviewed by Ross and Wolfe [19]. The payload of an ADC is typically of hydrophobic character, which alters the physicochemical characteristics of the naïve antibody, as can the linker moiety [16, 19-21]. Whereas an extensive study on a thiol-maleimide coupled ADC demonstrated lower stability and increased aggregation compared to the naïve mAb [16], only a higher aggregation propensity has been described for a lysine coupled ADC [20].

A more profound knowledge of the physical properties is essential for the future formulation development of ADCs. Hence, we have produced three distinct mAb conjugates with the fluorescent dyes NHS-Fluorescein (5/6-carboxyfluorescein, succinimidyl ester), Eosin-ITC (Eosin-5-isothiocyanate) and DEAC-SE (7-diethylamino-coumarin-3 carboxylic acid, succinimidyl ester) as payloads (Figure III- 1). Labeling of antibodies with a fluorescent molecule is routinely used, for example in molecular imaging [22-24] or flow cytometry [25-27]. These fluorescent dyes possess some of the properties of characteristic payloads of ADCs e.g. hydrophobicity and aromatic and/or heterocyclic rings (Table III- 1).

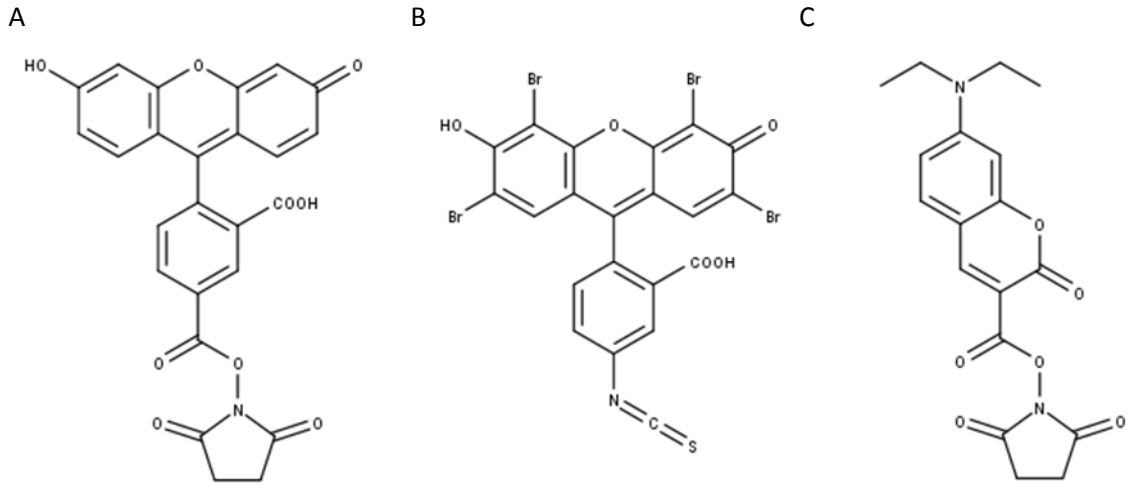

NHS-Fluorescein Eosin-ITC DEAC-SE

Figure III- 1: Structures of the fluorescent dyes: NHS-Fluorescein (A), Eosin-ITC (B) and DEAC-SE (C) used in this study.

Table III- 1: Properties of the fluorescent dyes NHS-Fluorescein, Eosin-ITC and DEAC-SE.

	NHS-Fluorescein	Eosin-ITC	DEAC-SE
Molecular Weight	473	701	358
cLogP	3.1	6.0	3.2
pkA	2.8, 3.5; 6.4	2.0, 3.3, 4.2	4.2
Ex wavelength	493 nm	530 nm	427 nm

Advantageously, none of these surrogate payloads poses a health risk to laboratory personnel. Eosin-ITC conjugates have already been studied previously with respect to photoinduced ADC degradation [28]. Both the NHS ester and the ITC react with primary amines, i.e. lysines and terminal amino groups of the mAb [29-31]. This conjugation site is used in Kadcyla®, Besponsa® and Mylotarg®, three of the four current ADCs on the market [32-34]. Depending on the mAb, 40 to 80 conjugation sites are possible, leading to heterogenous mixtures and potentially 10^6 different ADC species [35-37]. Hence, more selective coupling procedures continue to be a major area of research [38-40].

Cetuximab was used as the mAb in this work due to its widespread use in the treatment of metastatic colorectal cancer, metastatic non-small cell lung cancer and head and neck cancer as an epidermal growth factor receptor (EGFR) inhibitor [41]. It was originally approved by the U.S. Food and Drug Administration (FDA) in February 2004 and by the European Medicines Agency (EMA) in June 2004 under the trade name Erbitux® [42, 43]. In 2013 it achieved worldwide sales of US $2.3 billion [44]. As its basic patents have expired, cetuximab is also an interesting target for biosimilar developers [45]. In this study, we investigated the unfolding, aggregation and interaction of three model ADCs with an average degree of labeling (DOL) of 4-5, resembling the optimal ratio of mAb to drug for ADCs of about four [46]. To access whether conjugation influences the unfolding of cetuximab in various formulations, the temperature of unfolding was monitored. Moreover, the colloidal stability in terms of the aggregation temperature was evaluated. As addition of hydrophobic dyes to the antibody may alter the inter-protein interactions, the protein-protein interactions were studied via DLS. To access if differences seen in the protein-protein interactions correlate to stability data, the samples were stored for six months at 2-8, 25 and 40 °C and the impact of conjugation on particle formation and aggregation was monitored.

2 MATERIALS AND METHODS

2.1 MAb as Model Protein

Erbitux® (Merck KGaA, Darmstadt, Germany) was purchased at the local pharmacy as a 5 mg/mL Cetuximab formulation in citrate buffer pH 5.5 with glycine, polysorbate 80 and sodium chloride (NaCl) as stabilizers. Prior to further use, the antibody was purified from polysorbate 80 using protein A affinity chromatography on an ÄKTApurifier® 10 (GE Healthcare, Little Chalfront, Buckinghamshire, UK) at a UV detection of 280 nm, as described by Tim Menzen [47]. The samples were then buffer exchanged to 10 mM phosphate, 145 mM NaCl PBS buffer pH 7.2 or 100 mM bicarbonate buffer pH 9.0 using a Minimate™ TFF Capsule with Omega™ 30 K Membrane (PALL Life Sciences, Port Washington, NY, USA). The concentration was determined with ε_{280nm} of 1.49 mL g^{-1} cm^{-1}.

2.2 Preparation of Antibody Conjugates

For conjugation, the fluorescent dyes were dissolved in DMSO (VWR International, Radnor, PA, USA) at 10 mg/mL. 5/6-carboxfluorescein succinimidyl ester ((NHS)-Fluorescein) (Thermo Fisher Scientific, Waltham, MA, USA) was added in 20.0- fold molar excess to the mAb formulation in 10 mM phosphate, 145 mM NaCl PBS buffer. Similarly, 7-diethylaminocoumarin-3-carboxylic acid succinimidyl ester (DEAC-SE) (Sigma-Aldrich, St. Louis, MO, USA) was used in 10.0-fold molar excess. Eosin-5-isothiocyanate (Eosin-ITC) (Thermo Fisher Scientific) was added to the mAb formulation in 100 mM bicarbonate buffer pH 9.0. DMSO was added to all reaction mixtures to the same total percentage of 1.4 %. The labeling reaction was performed under gentle shaking conditions of 30 rpm for 1 h at room temperature. All steps were performed under light protection. The conjugated antibodies were separated from the unconjugated dye and organic solvent using a Minimate™ TFF Capsule with Omega™ 30 K Membrane. The samples were buffer exchanged into 10 mM phosphate buffer pH 7.2 and filtered with a 0.2 µm syringe filter (Pall, Port Washington, NY, USA). The naïve mAb was treated the same way without the addition of a dye. The sample names of the antibody and antibody conjugates used are described in Table III- 2.

Table III- 2: Antibody samples.

sample name	sample description
mAb	naïve mAb
mAb Fl	mAb Fluorescein conjugate
mAb DEAC	mAb DEAC conjugate
mAb Eo	mAb Eosin conjugate

The resulting concentration and degree of labeling were determined with the Nanodrop 2000 spectrophotometer (Thermo Fisher Scientific) using Equation III-1. The antibody conjugates were stored under light protection at 2 - 8 °C.

Equation III-1: Calculation of the protein concentration and the degree of labeling according to [30].

$$Protein\ conc\ (M) = \frac{A_{280} - (A_{max,fl} * Correction\ factor)}{\varepsilon_{protein}}$$

$$Degree\ of\ labeling = \frac{A_{max,fl}}{\varepsilon_{fl} * protein\ conc\ (M)}$$

At last, the samples were dialyzed with Vivaspin 20 or Vivaspin®2 tubes with a 30 kDa molecular weight cutoff polyethersulfone membrane (Sartorius Stedim Biotech, Göttingen, Germany) into the target formulation buffer (10 mM phosphate or histidine at pH 6.5, 7.2 or 8.5, with or without 145 mM NaCl or 7 % sucrose (m/V)). After adjustment of the pH, using 1 M hydrogen chloride or sodium hydroxide standard volumetric solutions (AppliChem GmbH, Darmstadt, Germany), filtration was performed using a 0.2 µm syringe filter and the protein concentration was determined again. A detailed description of the buffer systems used is presented in Table III- 3.

Table III- 3: Buffers used.

buffer name	buffer type	excipient	pH
HS 6.5	10 mM histidine	7 % sucrose (m/V)	6.5
HS 7.2	10 mM histidine	7 % sucrose (m/V)	7.2
HN 7.2	10 mM histidine	145 mM NaCl	7.2
PS 7.2	10 mM phosphate	7 % sucrose (m/V)	7.2
PN 6.5	10 mM phosphate	145 mM NaCl	6.5
PN 7.2	10 mM phosphate	145 mM NaCl	7.2
PN 8.5	10 mM phosphate	145 mM NaCl	8.5

2.3 Isoelectric Focusing (IEF)

Isoelectric focusing was performed according to the manufacturer instructions (Serva Electrophoresis GmbH, Heidelberg, Germany). The Servalyt™ Precotes™ gel 125 x125 x3 mm pH 6 – 9 (Serva Electrophoresis) was cooled at 5 °C on a Multiphor II electrophoresis system connected to a MultiTemp III water bath (GE Healthcare, Buckinghamshire, UK). The samples in 10 mM phosphate buffer with 145 mM NaCl were diluted with highly purified water to a concentration of 0.5 mg/mL in

order to reduce the salt concentration. 10 µL of the samples and 5 µL of the Serva marker mix 3 – 10 (Serva Electrophoresis) were applied across the gel 2 – 3 times. Protein separation was performed at 6 mA current, 2000 V and 5000 Vh with the power supply EPS 3501 XL (GE Healthcare, Buckinghamshire, UK). The gel was immediately fixed with 20 % (w/v) trichloroacetic acid, stained with Serva Blue W (Serva Electrophoresis), destained and neutralized using highly purified water. The wet gel was scanned with an Epson Perfection V750 PRO (Seiko Epson Corporation, Suwa, Japan). The isoelectric points (pI) of the protein bands were obtained by relating the positions to the marker bands. Each sample was analyzed at least on two separate gels.

2.4 Peptide Map

100 µL of 10 mg/mL of naïve mAb and mAb Fl in 10 mM phosphate 145 mM NaCl PBS buffer pH 7.2 were dried in 2 mL tubes (Eppendorf AG, Hamburg, Germany) using a flowtherm evaporator from Barkey GmbH & Co. KG (Leopoldshöhe, Germany). The bottom heater was set to 25 °C and the constant nitrogen gas stream (35 °C, 6 L/min) was guided through cut pipette tips into the sample tubes. The dried samples were redissolved in 6 M guanidine hydrochloride, 2 mM dithiothreitol (DTT) in 0.119 M tris(hydroymethyl)aminomethane buffer pH 8.0. After incubation at 37 °C for 1 h, samples were alkylated with 15 mM sodium iodoacetate at room temperature for 15 min. Subsequently, 20 mM triethylammonium acetate (TEAoAc) buffer pH 8.6 was added to a volume of 1.9 mL and trypsin from porcine pancreas (Sigma-Aldrich) was added (1:50 enzyme:protein w/w). The mixture was incubated at 37 °C for 2 h, after which the digestion was stopped by putting the samples at 80 °C for 10 min. The samples were dried using the flowtherm evaporator with both heaters off and a constant nitrogen gas stream of 1 L/min. The samples were redissolved in 1.9 mL of TEAoAc buffer, digested with trypsin again and were treated as described above.

For the LC/MS analysis, a serial coupling of a reversed-phase (RPLC) and hydrophilic interaction liquid chromatography (HILIC) was used as previously described [48]. In brief, 10 µL of the sample were injected onto a ZIC® -HILIC column (150 × 2.1 mm, 5 µm, 200Å) (Merck Sequant, Umeå, Sweden) and the second separation was performed on a Poroshell 120 EC-C18 (50.0×3.0 mm, 2.7 µm) (Agilent Technologies, Santa Clara, CA, USA) with two Agilent HPLC systems series 1260 Infinity. The detection was performed on an Agilent TOF-MS system series 6230 equipped with a Jet Stream ESI interface and a DAD detector. The following conditions were used on the ESI source: gas temperature 325 °C, gas flow 10 L/min, nebulizer pressure 45 psi, sheath gas flow 7.5 L/min, capillary voltage 2 kV and fragmentor voltage 250 V, in positive mode. The samples were analyzed between 65 and 3200 m/z. The UV signals of the DAD were recorded at 254, 280, 320 and 493 nm with the reference wavelength 360 nm. The RP mobile phase consisted of a mixture of ammonium acetate (NH_4Ac) and acetonitrile

(ACN). For the HILIC mobile phase, water and acetonitrile were added to the RP mobile phase (Table III- 4). Peaks were processed using the extracted ion chromatography (EIC) with the MassHunter Qualitative Analysis B.06.00 software (Agilent Technologies).

Table III- 4: Chromatographic conditions used for HILIC and RPLC.

		Pump 1				**Pump 2**	
Solvent A		ACN		Solvent C		10 mM NH_4Ac: ACN 90:10	
Solvent B		H_2O		Solvent D		10 mM NH_4Ac: ACN 10:90	
Column		HILIC		Column		RP	
Gradient	**Time (min)**	**B %**	**Flow (mL/min)**	**Gradient**	**Time (min)**	**D %**	**Flow (mL/min)**
	6	100	0.4		7	0	0.05
	13	60	0.4		12	50	0.05
	32	60	0.4		13	50	0.1
	33	100	0.8		22	100	0.1
	53	100	0.8		32	100	0.1
	54	100	0.4		33	0	0.1
	58	100	0.4		53	0	0.1
					54	0	0.05
					58	0	0.05

2.5 Intrinsic Fluorescence and Static Light Scattering (SLS) Measurements

Thermal scans of the intrinsic fluorescence and static light scattering (SLS) measurements were performed simultaneously using the OPTIM-1000 (Pall Corporation, Port Washington, NY, USA). 9 µL of 0.8 mg/mL samples were loaded in the cuvettes of the multiple cuvette array. A temperature ramp between 20 – 95 °C with a heat rate of 60 °C/h was used with recording steps of 1 °C or 2 °C. Onset and midpoint of the first derivative of each sigmoidal curve was classified using the OPTIM 1000 software Igor Pro 6. The static light scattering at 266 and 473 nm was employed to define the temperature of aggregation (T_{agg}). The melting temperature (T_m) was identified via the intrinsic ratio at 350/330°nm. The default secondary analysis methods given in the software were used. Samples were run in triplicates.

2.6 Temperature Ramps of Dynamic Light Scattering (DLS)

DLS temperature ramps of the samples were performed in 96-well plates (Corning® Costar®, Corning Inc., Corning, NY, US) with a Zetasizer APS (Malvern Instruments, Malvern, UK). A triplicate per well was measured for every sample with 20 acquisitions of 2 s per well. The temperature was recorded between 20 and 85 °C in 5 °C steps with a scan rate of about 60 °C/h and an equilibration time of 120 s. The diffusion coefficient (D) and the hydrodynamic radius (R_h) were taken as results. The refractive index (RI) of the buffers was measured using an Abbe refractometer from Carl Zeiss (Jena, Germany) at room temperature; the viscosity was checked using a mVROC viscosimeter from Rheosense Inc. (San Ramon, CA, USA) with an A-series chip, sample volumes of 250 µL and a flow rate of 150 µL/min at 20 °C (Table III- 5). As the effect of temperature was previously determined to be insignificant, the values were not temperature corrected [49].

Table III- 5: Refractive index and viscosity of the buffers used for DLS temperature ramps.

	Refractive index	Viscosity [mPa*s]
Phos NaCl	1.333	1.051
Phos Suc	1.339	1.639
His NaCl	1.335	1.154
His Suc	1.342	1.354

The diffusion coefficients D of seven samples with protein concentrations from 0.2 to 10 mg/mL were determined by DLS. A linear fit on D versus protein concentration was used to identify the diffusion coefficient at infinite dilution D_0 and to obtain the interaction parameter k_D [50], as well as ultimately the apparent osmotic second virial coefficient A_2* according to the TIM equation [49]. Below 60 °C, outliers were removed.

2.7 Isothermal Storage Stability Studies

Samples of 1 mg/mL mAb and mAb conjugates were formulated in PN 7.2 and HS 6.5. Aliquots of 1250 µL and 900 µL were filled in 2R glass vials using 50 mL Eppendorf advanced® Combitips (Eppendorf AG, Hamburg, Germany). The vials were stored upright at 5, 25 and 40 °C under light protection and without applying agitation for up to six months. Samples were prepared under aseptic conditions and were analyzed at the time points indicated in Table III- 6.

Table III- 6: Sampling points (x) of the isothermal storage stability study.

	0 M	1 M	3 M	6 M
5 °C	x		x	x
25 °C	x		x	x
40 °C	x	x	x	x

Visual inspection (2.7.1), turbidity (2.7.2), light obscuration (2.7.3), HP-SEC (2.7.4) were performed at all time points. For these, the 1250 µL samples were used. Additionally, MFI (2.7.5), SDS-PAGE (2.7.6), CE-SDS (2.7.7), DLS (2.7.8) and FTIR (2.7.9) were performed at t0 and after 6 months. The 900 µL samples were used for these analytics.

2.7.1 Visual Inspection

Images of the samples were taken with a Nikon D5300 camera (Nikon GmbH, Düsseldorf, Germany) in front of a black background. Moreover, each sample was analyzed according to the DAC-probe 5 (Table III- 7) [51]. The vial was gently shaken vertically and slowly rotated horizontally, whereby the sample was inspected for suspended particles for 5 s in front of black and white backgrounds. Each sample was evaluated according to the scores of the DAC.

Table III- 7: The evaluation method according to DAC for parenteral solutions [51].

Suspended particles	score
No particles visible within 5 s	0
Few particles visible within 5 s	1
Medium number of particles visible within 5 s	2
Large number of par particles directly visible	10

2.7.2 Optical Density at 700 nm

For turbidity analysis, 200 µL of the samples were analyzed in a 96-well quartz well plate (Hellma Analytics, Müllheim, Germany) for UV absorbance with a FLUOstar Omega well-plate reader and Omega software version 1.01 (BMG Labtech GmbH, Ortenberg, Germany). The absorbance at 280, 350, 429, 493, 530 and 700 nm was determined in triplicates with 20 flashes per well. The absorbance at 700 nm was used for turbidity characterization.

2.7.3 Light Obscuration (LO)

Subvisible particle analysis was conducted using a particle counter PAMAS SVSS-C (Partikelmess- und Analysesysteme GmbH, Rutesheim, Germany) equipped with a HCB-LD-25/25 optical sensor. Prior to each triplicate measurement, the system was rinsed with 10 mL of highly purified water until the cumulative particle concentration ≥ 1 µm was below 30 particles/mL. Measurements were performed according to USP 788 with a pre-run volume of 0.2 mL and four consecutive measurements of 0.2 mL with a pump rate of 10 mL/min [52]. Results of the particle counts were calculated as the mean value of the last three measurements for particles ≥1, ≥ 10 and ≥ 25 µm/mL, which were recorded with the PAMAS PMA V 2.1.2.0 software. The given particle numbers are for undiluted samples, samples labeled with 2 and 4 were measured after dilution (1:1 and 1:3 with corresponding buffer).

2.7.4 High Performance Size Exclusion Chromatography (HP-SEC)

HP-SEC analyses were conducted on an Agilent 1200 series system (Agilent Technologies, Santa Clara, CA, USA) equipped with a DAD detector set to 280, 427, 493 and 530 nm and a VWD detector at 280 nm. The temperature of the TSK-Gel® G3000SWXL (7.8 x 30 mm, 5 µm) column (TOSOH BioScience, Tokyo, Japan) and the autosampler was set to 20 °C and 4 °C, respectively. 40 µL samples were injected. The naïve mAb and mAb Fl were injected into a running buffer of 100 mM sodium phosphate, 100 mM sodium sulfate at pH 6.8 at 0.5 mL/min. mAb Eo was eluted with 50 mM sodium phosphate and 50 mM sodium chloride at pH 6.9 with a flow rate of 0.85 mL/min. mAb DEAC was analyzed with 80 % 0.1 M sodium phosphate, 0.2 M arginine pH 6.8 with 20 % acetonitrile at 0.85 mL/min on a YMC-Pack Diol-300 (500*8.0 I.D., 5.5 µm, 30 mm) column (YMC Co. Ltd., Kyoto, Japan). Chromatograms were analyzed using ChemStation® software Rev. B. 02.01 (Agilent Technologies).

2.7.5 Micro-Flow Imaging (MFI)

A MFI DPA4100 from Protein Simple (Santa Clara, CA, USA) was used for subvisible particle analysis. The system was equipped with a 470 nm LED light source and a high magnification (14 x) 100 µL flow cell and was controlled using MFI View Software Version 6.9. Prior to each measurement, the system was rinsed with highly purified water to provide a clean baseline and to optimize illumination. Each sample was investigated with a pre-run volume of 0.15 mL and a sample volume of 0.65 mL using a peristaltic pump at a flow rate of 0.1 mL/min. “Edge particle rejection” and “fill particle” options were activated. The particle numbers shown in the results are for undiluted samples, samples labeled with 2 and 5 were measured after dilution (1:1 and 1:4 with corresponding buffer).

2.7.6 Sodium Dodecyl-Sulfate Polyacrylamide Gel Electrophoresis (SDS-PAGE)

For non-reducing SDS-PAGE, the samples were diluted with NuPAGE® LDS Sample buffer to a starting concentration of 37.5 µg/mL, denatured for 5 min at 90 °C and analyzed on 3-8 % NuPAGE® Tris-Acetate Protein Gels (Life Technologies) according to the manufacturer manual. A protein amount of 0.45 µg was loaded into each well. Electrophoresis was performed at 150 V (Power Pac 200, Bio-Rad Laboratories, Hercules, CA, USA) using an XCell SureLock™ Mini-Cell Electrophoresis System (Novex by Life Technologies, Carlsbad, CA, USA). After 55 minutes, the electrophoresis was stopped and the gel was stained with SilverXpress® Silver Staining Kit according to the manufacturer manual (Invitrogen, Thermo Fisher Scientific). Stained gels were scanned using an Epson Perfection V750 Pro scanner and the molecular weights of bands was calculated using the molecular weight marker HiMark™ Pre-stained Protein Standard (Thermo Fisher Scientific).

2.7.7 Capillary Electrophoresis-Sodium Dodecyl Sulfate (CE-SDS)

The CE-SDS was realized on an Agilent 2100 Bioanalyzer (Agilent Technologies) using an Agilent Protein 230 protein chip under reducing conditions, following the manufacturer manual. 4 µL of sample were mixed with 2 µL of sample buffer containing 4.83 mM/µL DTT and denatured at 95°C for 5 minutes. After cooling, 84 µL of highly purified water were added and 6 µL were pipetted into each sample well. Gel-dye mix, destaining solution and molecular weight marker were added and the analysis was started immediately after preparation.

2.7.8 Dynamic Light Scattering (DLS)

The hydrodynamic radius of the samples was analyzed with a DynaPro Plate Reader from Wyatt Technologies (Dernbach, Germany) and Dynamics software version 7. 6 µL of each sample were pipetted into a 1536 well plate (Aurora Microplates, Edition Eight, LLC, East Whitefish, MT, USA), covered with silicone oil and centrifuged for 5 min at 2000 g. The measurements were performed at 830 nm, 150° and 25 °C with a set acquisition time at 5 s/well, 10 acquisitions/well and an auto-attenuation time limit of 60 s/well. The hydrodynamic radius was calculated by the software using a recorded autocorrelation function with a cumulants analysis via the Stokes-Einstein equation.

2.7.9 Fourier Transform Infrared Spectroscopy (FTIR)

FTIR measurements were performed using a Tensor 27 spectrophotometer (Bruker Optik GmbH, Ettlingen, Germany) with a BioATR cell™ II. 35 µL were measured at 25 °C. For each spectrum, a 120-scan interferogram was created at single beam mode with a 4 cm^{-1} resolution. Protein Dynamics for Opus 6.8 (Bruker Optik GmbH) was used to display the spectra as the vector-normalized second

derivative amide I-spectra, which were calculated with 25 smoothing points according to the Savitzky-Golay algorithms.

2.8 Software Drawings and Calculations

The structures of the fluorescent dyes were drawn with MarvinSketch 18.10.0 (ChemAxon Ltd, Budapest, Hungary). This software was also used to calculate the pkA and logP values. The pKa values were determined using macro mode, static acid/base prefix, a temperature of 298°K and tautomerization/resonance were considered. For the logP calculations, the NHS and ITC groups were replaced by a butyl residue. The consensus method was used with consideration of tautomerization / resonance and an electrolyte concentration of 0.1 mol/dm^3 of Cl^- and Na^+ and K^+, respectively.

3 RESULTS

3.1 Characterization of MAb Conjugates

For a conclusive analysis of the effect of conjugation on mAb stability, the mAb conjugates needed to be described in terms of their conjugation characteristics. The DOL was determined as described in 2.2 with the factors shown in Table III- 8. For NHS-Fluorescein, manufacturer information was used for the calculations [53]. The factors for Eosin-ITC were determined via fluorescence and UV spectroscopy measurements. For DEAC-SE, a shift of the excitation maximum from 442 to 427 nm was observed upon coupling. Hence, DOL calculation factors were determined using DEAC coupled to lysine.

Table III- 8: Properties of the fluorescent dyes NHS-Fluorescein (Fl), DEAC-SE (DEAC) and Eosin-ITC (Eo) necessary for the DOL calculation.

	excitation wavelength [nm]	correction factor ($\frac{A_{280}}{A_{ex.wv.dye}}$)	$\varepsilon_{\lambda,exc}$ dye [$M^{-1}*cm^{-1}$]
Fl	493	0.3	70,000
DEAC	427	0.2	38,790
Eo	530	0.41	83,000

We aimed to achieve antibody conjugates with a DOL of 4-5 to resemble the ADCs on the market [32, 46, 54]. Higher molar excess of fluorescent dye to mAb during coupling led to higher DOL (Figure III- 2 A-C). Moreover, the method of purification and the coupling volume influenced the DOL (Figure III- 2 D). For the final conjugation, purification was performed with TFF due to the high sample volumes and better reproducibility. For all three fluorescent dyes, we succeeded in finding the optimal conditions to achieve a DOL of 4-5.

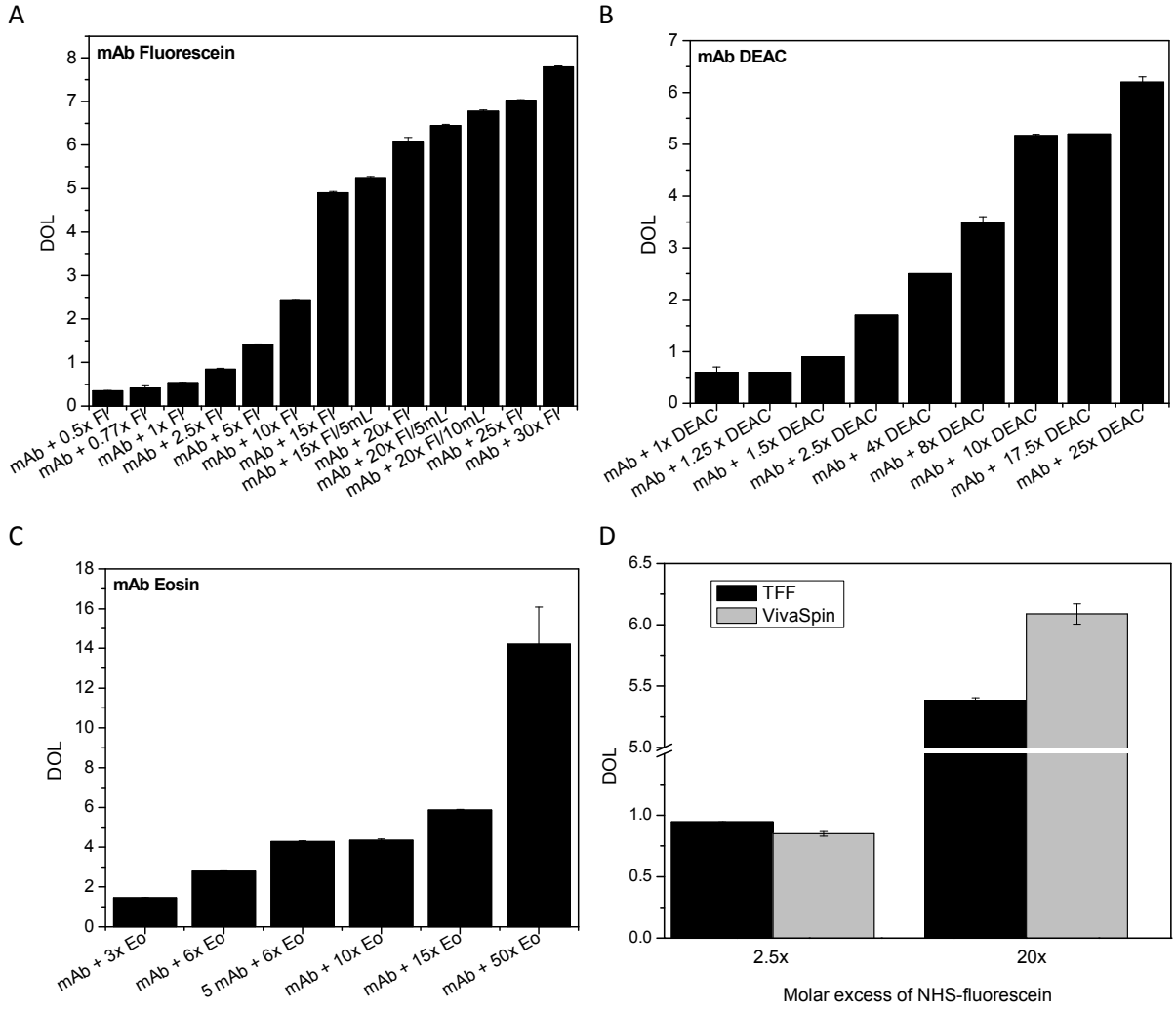

Figure III- 2: A)-C) DOL of mAb conjugates with different molar excess (0.5x to 50x) of activated fluorescent dyes upon coupling of 1 mL of 2 mg/mL mAb for 1 h at r.t.; A) mAb Fluorescein, B) mAb DEAC and C) mAb Eosin. D) DOL of mAb Fluorescein with 2.5x or 20x molar excess of NHS-fluorescein purified by TFF or VivaSpins units.

3.1.1 Determination of the Isoelectric Point of the MAb Conjugates

Isoelectric focusing (IEF) was performed to determine the isoelectric point (pI) of the antibody and the antibody conjugates (Table III- 9 and Figure SIII- 1). The naïve mAb displayed six characteristic isoforms between 7.6 and 8.0. At DOL 1, the mAb conjugates displayed a similar profile with no apparent change in the number of isoforms and a slight decrease of the pI to 7.4 – 8.0. The considerable number of solvent accessible lysine residues on the naïve mAb and the conjugation reaction resulted in a broad mixture of isoforms with higher molar excesses [55] and no distinct isoforms could be assigned for mAb conjugation with DOL 4. Whereas the pI of mAb DEAC decreased to 7.0 – 8.0, the pI decreased to 5.3 – 7.4 for mAb Fl and mAb Eo conjugates.

Table III- 9: pI values and appearance of isoforms of mAb and mAb conjugates.

Species	Appearance	pI value
Naïve mAb	6 isoforms	7.6 – 8.0
mAb Fl DOL 1	5 isoforms	7.4 - 8.0
mAb Fl DOL 4	broad distribution	5.3 - 7.4
mAb Eo DOL 1	5 isoforms	7.4 - 8.0
mAb Eo DOL 5	broad distribution	5.3 - 7.4
mAb DEAC DOL 1	6 isoforms	7.0 - 8.0
mAb DEAC DOL 3.5	broad distribution	7.4 – 7.8

3.1.2 Peptide Map

Figure III- 3 displays the total ion current chromatograms for mAb and mAb Fl obtained after tryptic digest. No significant changes in the extracted ion chromatograms (EIC) were observed between the naïve mAb and mAb Fl. Considerable differences were found in the adsorption at 493 nm, representative for fluorescein, which could not be related to Cetuximab peptides with m/z above 1000 m/z (Mascot search Results).

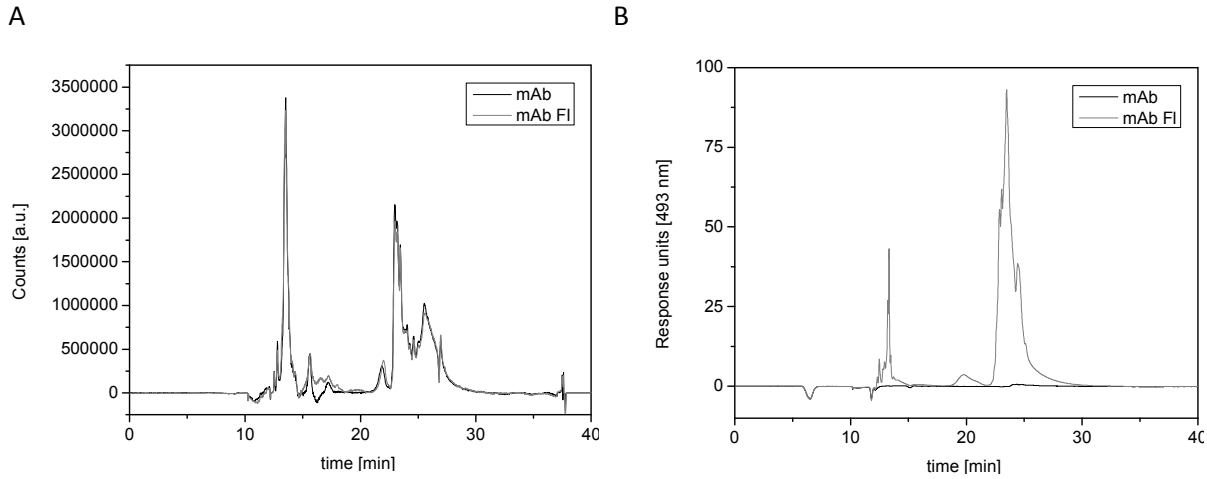

Figure III- 3: A) Total ion current chromatogram and B) Adsorption at 493 nm for trypsin digested mAb and mAb Fl.

3.2 Thermal Stability and Interactions of Antibody Conjugates

3.2.1 Unfolding and Aggregation of Antibody Conjugates in Various Buffer Systems

The protein melting temperature (T_m), the point at which 50 % of the protein are unfolded, is commonly associated with conformational stability, whereas the temperature of aggregation (T_{agg}) is an indicator for aggregation of the unfolding protein [49, 56, 57]. The T_m and T_{agg} values are shown in Table III- 10. The onset of the T_m ($T_{m,\ onset}$) was similar for all tested mAb and mAb conjugate formulations except for mAb Eo in HS 7.2, PS 7.2 and PN 8.5, which showed a statistically significantly lower $T_{m,\ onset}$ compared to the naïve mAb. The T_m was similar for all samples, only mAb Eo PN 7.2 displayed a statistically significantly lower T_m.

The aggregation behavior was characterized by SLS using two laser wavelengths. The light scattering at 266 nm is highly sensitive and portrays smaller particles the best, whereas the scattering at 473 nm has a higher dynamic range and represents larger particles [58]. Similar trends were observed at 266 nm and 473 nm for $T_{agg,\ onset}$ and $T_{agg,\ Trans}$. $T_{agg,\ onset}$ of the naïve mAb was generally higher compared to the conjugates, indicating a lower resistance of the mAb conjugates against aggregation. For mAb DEAC the differences were very small and statistically not significant. The destabilization of mAb Fl was statistically significant in HN 7.2, PN 6.5 and at 266 nm also for the PN 7.2 formulations. mAb Eo was significantly less stable compared to the naïve mAb for all formulations except HS 7.2 (only 266 nm) and PS 7.2. Moreover, the buffers containing sucrose had lower values compared to those with NaCl.

Table III- 10: Thermal stability of mAb, mAb Fl, mAb DEAC and mAb Eo in different formulations in histidine or phosphate buffer with sucrose or NaCl at pH 6.5 or 7.2, respectively. The onset and midpoint (Trans) of aggregation (T_{agg}) were determined with SLS at 266 and 473 nm, the melting temperatures (T_m) using the ratio of intrinsic fluorescence of 350 to 330 nm (* p ≤ 0.05, p ≤ 0.01, *** p ≤ 0.001).**

			T_{agg} 266 nm, onset		T_{agg} 266 nm Trans		T_{agg} 473 nm, onset		T_{agg} 473 nm Trans		T_m,onset		T_m	
mAb	His Suc	pH 6.5	67.50	± 1.00	76.81	± 0.86	72.17	± 1.30	78.36	± 5.10	57.59	± 2.08	68.85	± 0.79
		pH 7.2	65.64	± 2.14	71.80	± 0.79	70.31	± 1.25	73.32	± 0.84	56.77	± 2.58	69.57	± 0.31
	His NaCl	pH 7.2	69.20	± 0.54	72.42	± 0.12	70.72	± 0.01	76.17	± 4.73	51.60	± 6.11	69.35	± 0.41
	Phos Suc	pH 7.2	65.79	± 2.89	72.75	± 0.88	67.98	± 2.38	74.86	± 0.38	57.44	± 3.07	70.10	± 0.10
	Phos NaCl	pH 6.5	69.05	± 0.71	72.35	± 0.26	70.99	± 0.14	73.50	± 0.12	54.16	± 4.61	67.92	± 1.42
		pH 7.2	69.59	± 0.56	72.65	± 0.26	71.38	± 0.27	73.56	± 0.07	54.30	± 5.31	68.42	± 0.95
		pH 8.5	69.08	± 0.68	72.90	± 0.43	71.35	± 0.44	74.92	± 0.34	55.21	± 5.09	67.34	± 1.37
mAb Fl	His Suc	pH 6.5	66.12	± 1.40	72.73*	± 0.07	70.64	± 0.14	73.40***	± 0.25	56.31	± 1.59	69.53	± 0.89
		pH 7.2	63.37	± 3.08	69.44	± 2.14	67.41	± 3.70	72.51	± 0.63	57.21	± 2.95	68.33	± 1.07
	His NaCl	pH 7.2	65.01***	± 0.25	70.69***	± 0.10	68.94***	± 0.32	72.36	± 0.54	53.77	± 4.65	66.54	± 0.91
	Phos Suc	pH 7.2	63.03	± 0.46	68.85	± 0.99	67.15	± 1.05	72.14***	± 0.13	60.27	± 3.49	70.38	± 0.31
	Phos NaCl	pH 6.5	65.28**	± 0.75	71.41	± 0.62	69.21**	± 0.30	72.14**	± 0.33	50.66	± 4.96	67.50	± 0.65
		pH 7.2	67.16*	± 1.14	72.70	± 0.39	71.37	± 0.44	74.76**	± 0.39	50.64	± 1.93	66.81	± 1.73
		pH 8.5	66.91	± 2.31	72.93	± 0.83	71.22	± 0.59	76.75	± 1.10	47.22	± 5.16	65.49	± 0.40
mAb DEAC	His Suc	pH 6.5	67.53	± 0.27	74.29*	± 0.51	72.57	± 0.45	77.75***	± 0.39	58.54	± 9.15	69.67	± 0.69
		pH 7.2	65.21	± 1.08	70.97	± 0.33	68.95**	± 0.29	72.42	± 0.37	56.13	± 3.78	69.21	± 0.68
	His NaCl	pH 7.2	68.09	± 0.97	72.07	± 0.33	70.22*	± 0.26	73.19	± 0.19	57.26	± 1.15	69.49	± 1.04
	Phos Suc	pH 7.2	61.35	± 3.14	68.96	± 0.61	66.24	± 1.76	70.74***	± 0.19	56.82	± 1.86	68.91	± 0.38
	Phos NaCl	pH 6.5	68.00	± 0.76	71.59*	± 0.18	70.13*	± 0.34	72.85*	± 0.19	56.59	± 2.08	68.23	± 0.80
		pH 7.2	67.66	± 1.61	72.06	± 0.59	70.65	± 0.41	73.48	± 0.25	56.75	± 2.57	68.34	± 1.21
		pH 8.5	68.38	± 0.12	72.91	± 0.09	71.20	± 0.37	75.35	± 0.09	54.79	± 2.57	67.35	± 1.07
mAb Eo	His Suc	pH 6.5	61.00***	± 0.76	66.77***	± 0.86	62.28***	± 2.10	69.68***	± 1.72	53.82	± 1.35	68.28	± 1.24
		pH 7.2	62.25	± 0.44	67.55***	± 0.44	65.52**	± 0.30	69.46***	± 0.39	51.01*	± 2.20	69.13	± 1.75
	His NaCl	pH 7.2	63.35**	± 0.87	68.41**	± 0.60	66.21**	± 0.91	70.41	± 1.00	51.69	± 1.95	67.10	± 2.43
	Phos Suc	pH 7.2	60.39	± 0.80	65.84***	± 0.88	63.26	± 0.43	68.40***	± 0.77	49.71*	± 2.76	68.84	± 0.88
	Phos NaCl	pH 6.5	61.29*	± 2.53	67.40**	± 0.76	66.39**	± 1.46	68.62***	± 0.20	54.47	± 12.32	69.70	± 1.45
		pH 7.2	62.76***	± 0.43	69.33***	± 0.21	68.09***	± 0.30	71.14**	± 0.65	47.78	± 3.07	64.58**	± 2.56
		pH 8.5	63.46**	± 1.00	70.15***	± 0.18	68.64**	± 0.09	72.03***	± 0.17	43.81*	± 4.85	66.12	± 1.61

3.2.2 Interactions of the MAb Conjugates at Various Buffer Systems

To analyze the effect of conjugation on protein-protein interactions, the k_D of the conjugates and the naïve mAb as a function of a temperature ramp was analyzed via DLS [49, 59]. Exemplarily, the temperature ramps of the naïve mAb and mAb Fl in 10 mM histidine buffer with 145 mM NaCl at pH 7.2 are shown in Figure SIII- 2. The hydrodynamic radius r_h was constant between 20 and 65 °C and strongly increased at higher temperatures, demonstrating protein aggregation. From the diffusion coefficients of seven concentrations between 0.2 and 10 mg/mL, the D_0, the diffusion interaction parameter at infinite dilution, and k_D were calculated. The D_0 started at a value of 2.5 x 10^{-7} cm^2/s for the naïve mAb, increased up to 65 °C to values at about 7.0 x 10^{-7} cm^2/s, followed by a decrease. The k_D was rather constant up to 65 °C and then it sharply dropped. This is due to the aggregation of the mAb samples, upon which the k_D values are not calculated correctly. For the naïve mAb, the k_D began at slightly positive values at 20 °C, whereas the k_D of mAb Fl was at about -25 mL/g. Whereby k_D reflects both thermodynamic and hydrodynamic contributions, A_2^* consists of only the thermodynamic parameter [49]. After transfer of the k_D values to A_2^*, negative A_2^* values mark net attractive protein-protein interactions and positive values indicate net repulsive interactions [49, 60]. The A_2^* values were used to evaluate the thermodynamic stability of the naïve mAb and mAb conjugate formulations and are displayed in Figure III- 4.

For the naïve mAb, the samples generally depicted positive, repulsive interactions, up to 60 to 70 °C, depending on the formulations. Exceptions were the PS°7.2 and PN 6.5 buffers, in which the mAb samples showed attractive interaction already at 20 °C. The high error of the values at 70 °C and above reflect the inadequate fit upon aggregation and these values should not be used for further interpretation [49]. The A_2^* values for the mAb conjugates greatly differed, but showed more attractive values at 20 °C, which indicates a higher aggregation propensity and lower colloidal stability. For mAb Fluorescein, attractive interactions appeared at ambient temperatures for all buffers except PN 6.5 and PN 8.5. The A_2^* range was comparable to the naïve mAb. Similarly, negative, attractive values were found for most buffers for mAb Eosin. Only PS 7.2 and PN 6.5 showed repulsive interactions below 60 °C for mAb Eo. mAb DEAC revealed negative values at 20 °C in all buffers, but these turned positive at 40 °C for the buffers tested, except for HN 7.2 which remained negative.

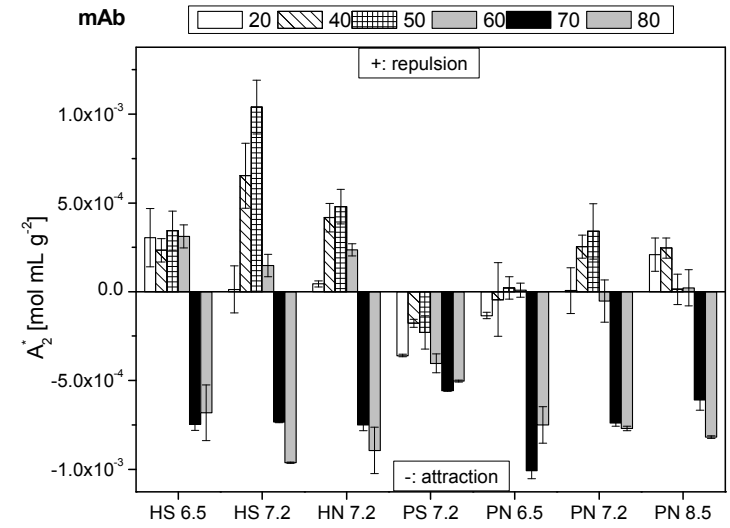
mAb
20 40 50 60 70 80
+: repulsion
-: attraction
A_2^* [mol mL g^{-2}]
1.0x10^{-3}
5.0x10^{-4}
0.0
-5.0x10^{-4}
-1.0x10^{-3}
HS 6.5
HS 7.2
HN 7.2
PS 7.2
PN 6.5
PN 7.2
PN 8.5

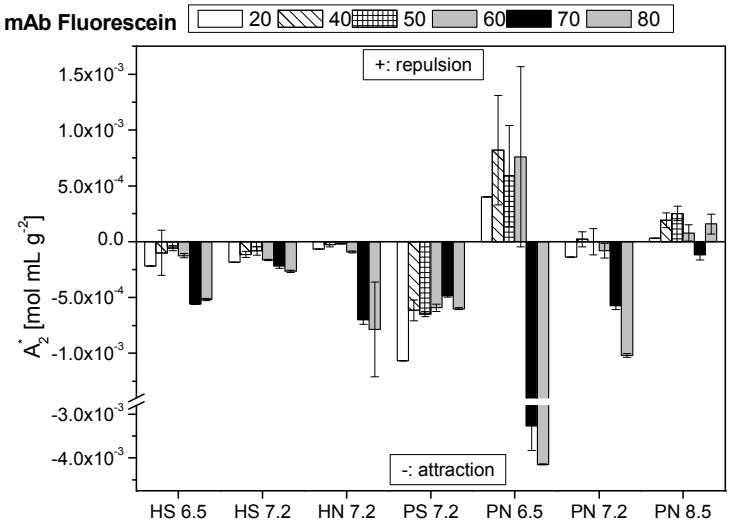
mAb Fluorescein
20 40 50 60 70 80
+: repulsion
-: attraction
A_2^* [mol mL g^{-2}]
1.5x10^{-3}
1.0x10^{-3}
5.0x10^{-4}
0.0
-5.0x10^{-4}
-1.0x10^{-3}
-3.0x10^{-3}
-4.0x10^{-3}
HS 6.5
HS 7.2
HN 7.2
PS 7.2
PN 6.5
PN 7.2
PN 8.5

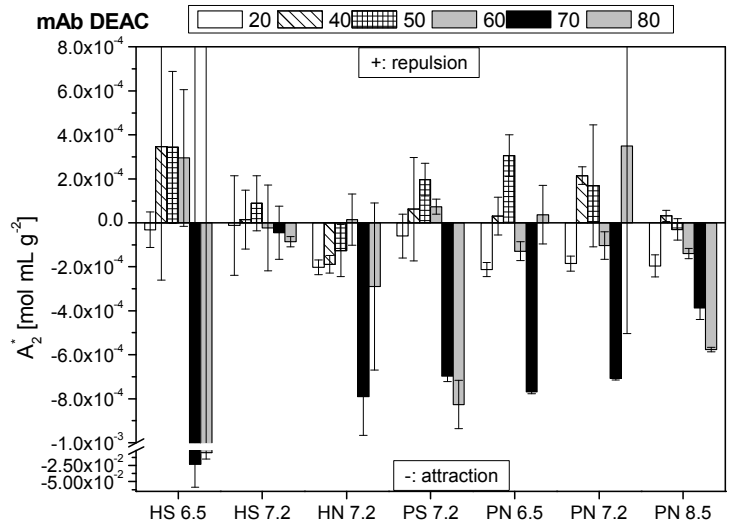
mAb DEAC
20 40 50 60 70 80
+: repulsion
-: attraction
A_2^* [mol mL g^{-2}]
8.0x10^{-4}
6.0x10^{-4}
4.0x10^{-4}
2.0x10^{-4}
0.0
-2.0x10^{-4}
-4.0x10^{-4}
-6.0x10^{-4}
-8.0x10^{-4}
-1.0x10^{-3}
-2.50x10^{-2}
-5.00x10^{-2}
HS 6.5
HS 7.2
HN 7.2
PS 7.2
PN 6.5
PN 7.2
PN 8.5

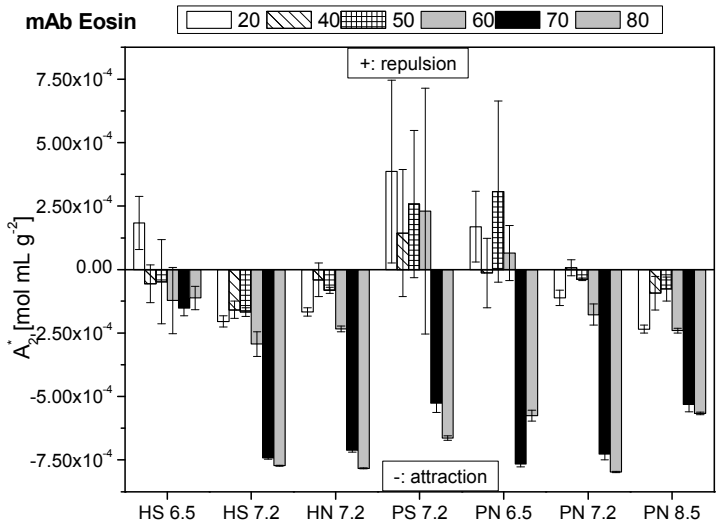

Figure III- 4: A_2^* of the naïve mAb and mAb conjugates in different buffer systems as a function of temperature.

3.3 Isothermal Storage Stability Studies of MAb Conjugates

To study whether the difference in colloidal stability between the naïve mAb and mAb conjugates translates into an effect upon storage, the samples were stored for 6 months at 2-8 °C, 25 °C and 40 °C in different formulations [61]. Samples were analyzed for aggregation, fragmentation and changes in secondary structure.

3.3.1 Formation of Visible Particles

The formation of visible particles of the mAb samples was accessed through photographs and visual inspection according to the evaluation scale of the Deutscher Arzneimittel Codex (DAC) probe 5 [51]. Visible particles could not be detected by photography (Figure SIII- 3 - Figure SIII- 5). Directly after conjugation, particles were observed in the mAb Eosin HS 6.5 formulation upon visual inspection and DAC evaluation, whereas all other formulations were free of visible particles (Table III- 11). For the naïve mAb, storage did not induce the formation of visible particles in the PN 7.2 buffer, but led to visible particles after 6 months at 5 and 25 °C in HS 6.5 (Table SIII- 1 and Table SIII- 2). For mAb Fl and mAb DEAC low numbers of visible particles were observed in PN 7.2 and HS 6.5 buffers. Whereas no substantial visible particles were seen for mAb DEAC in any condition, visible particles were detected after 6 months of mAb Fl storage in HS 6.5 at 25 °C. In contrast, mAb Eo samples showed visible particles at all storage time points in the HS 6.5 formulation. After 6 months at 25 and 40 °C, visible particles occurred for mAb Eo also in PN 7.2 (Table III- 11). The amount of visible particles increased during the long-term storage, whereby the particle formation can be ranked in the ascending order of 5 °C < 25 °C < 40 °C. An exception was the naïve mAb HS 6.5 sample, which showed high particle

numbers at 25 and 5 °C. In general, more particles were observed in the mAb HS 6.5 formulations compared to PN 7.2 formulations. MAb Eosin in HS 6.5 showed the most substantial visible particle formation. For the other mAb conjugates, visible particle formation was comparable to the naïve mAb.

Table III- 11: Visible particles according to the DAC-probe 5 scale for mAb stability samples after storage for 0, 1, 3 and 6 m at 40 °C.

40 °C	0 m			1 m			3 m			6 m		
mAb HS 6.5	0	0	1	0	0	1	2	2	2	2	2	2
mAb PN 7.2	0	0	0	1	0	1	2	1	2	1	1	2
mAb Fl HS 6.5	0	0	0	0	0	1	2	2	2	2	2	2
mAb Fl PN 7.2	0	0	0	1	2	2	1	1	1	1	1	1
mAb DEAC HS 6.5	0	0	0	2	0	0	2	1	2	2	2	2
mAb DEAC PN 7.2	0	0	0	1	2	1	1	1	1	1	1	1
mAb Eo HS 6.5	2	2	2	2	2	2	2	10	2	10	10	10
mAb Eo PN 7.2	0	0	0	2	2	2	2	2	2	10	2	10
buffer HS 6.5	0	0	0	0	0	0	0	0	0	0	0	0
buffer PN 7.2	0	0	0	0	0	0	0	0	0	0	0	0

3.3.2 Formation of Subvisible Particles

Results of the light scattering reflected in the absorbance values at 700 nm, as an indicator for particle formation, are reported in Figure SIII- 6. Light scattering measurements at 350 nm, the wavelength which is typically used, were unsuitable due to strong absorption of the conjugated fluorescent dyes. At t0, the absorbance values at 700 nm of the mAb samples were similar to the reference buffer between 0.03 for 0.04. Over storage at 5 °C, 25 °C and 40 °C, absorbance values of the naïve mAb and mAb conjugate samples fluctuated between 0.03 and 0.045, which was not significantly different from the reference buffers. Thus, no substantial formation of light scattering particles occurred, neither for the naïve mAb nor for the mAb conjugates.

Additionally, light obscuration (LO) and micro-flow imaging (MFI) measurements were performed. In the LO results, low particle numbers ≥ 1 µm/mL were obtained for the naïve mAb after the mock-conjugation (Figure III- 5). During storage, the particle numbers increased and after 6 months, the highest number of particles occurred in the HS 6.5 buffer at 25 °C. Storage at 5 °C also resulted in higher particle numbers in the HS 6.5 buffer. These trends for the naïve mAb also occurred for particles ≥ 10 µm/mL (Figure SIII- 7) and ≥ 25 µm/mL (Figure SIII- 8). For the mAb conjugates, particle numbers also increased upon storage. MAb Fl showed similar particles numbers as the naïve mAb and more particles were generated in the HS 6.5 compared to PN 7.2 buffer. However, more particles were formed after storage at 5 °C compared to 25 °C and 40 °C. Overall, mAb DEAC exhibited very low

particle numbers. MAb Eo showed high subvisible particle numbers already directly after conjugation and after storage at 40°C. Due to the formation of visible particles and precipitates (s. 3.3.1), the mAb Eo samples after 3 and 6 months of storage were diluted for LO and MFI analyses. For mAb DEAC and mAb Eo, stability in HS 6.5 and PN 7.2 did not differ. As the buffer controls showed low particles numbers at all time points, the generated subvisible particles did not originate from the container closure system. Furthermore, typical particle images obtained via MFI are shown in Figure SIII- 9. Heterogenous mixtures of protein particles (differing in intensity and structure) appeared, without evidence for foreign particles [62, 63]. MFI values were higher compared to LO due to the higher sensitivity of the MFI and showed large fluctuations, possibly also related to a change of the MFI cell during the 6 month storage period, so that no clear trends in particle formation could be seen (Figure III- 6) [63-66].

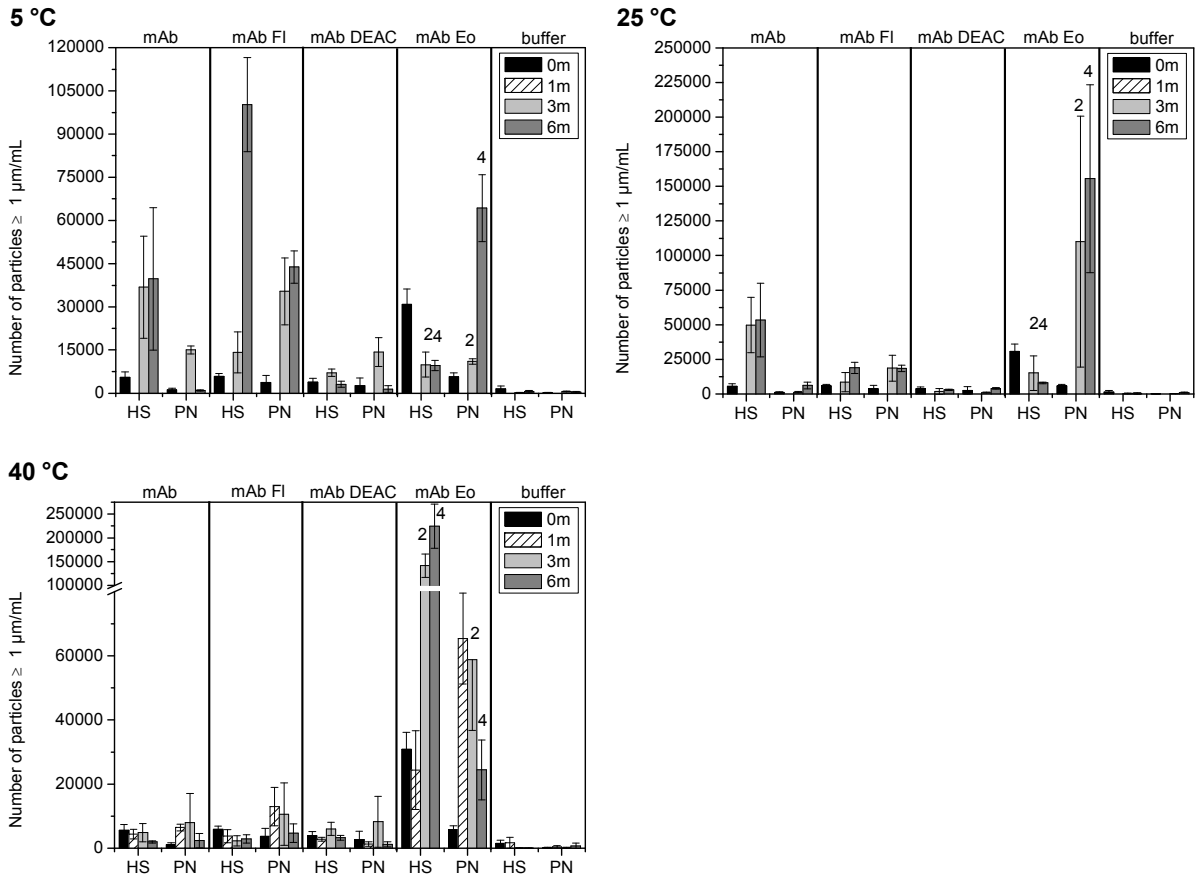

Figure III- 5: LO particle counts ≥ 1 µm/mL for naïve mAb and mAb conjugates stored for 0, 1, 3 and 6 months at 5, 25 and 40 °C.

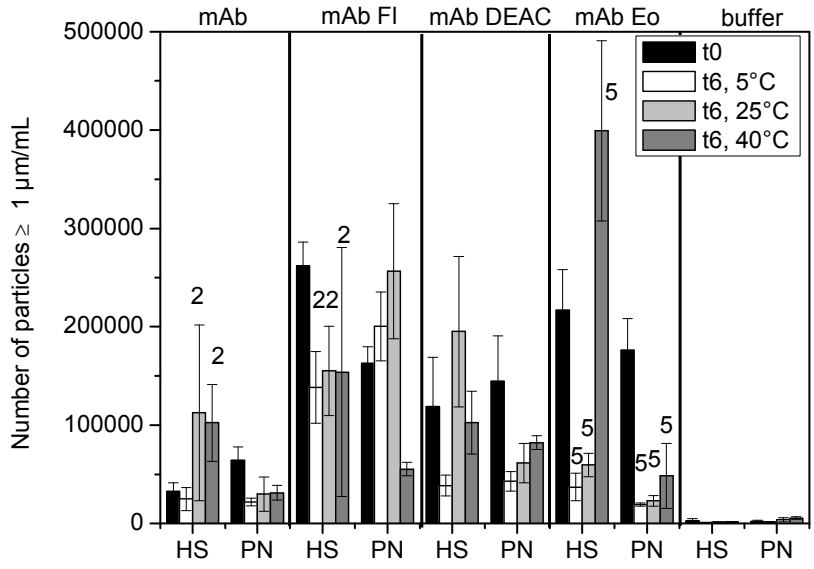

Figure III- 6: MFI particle counts ≥ 1 µm/mL after 0 m and 6 m storage at 5, 25 and 40 °C.

3.3.3 Formation of Soluble Aggregates and Fragments

The aggregation and fragmentation of the mAb samples were further analyzed using HP-SEC, SDS-PAGE, CE-SDS and DLS. For HP-SEC, the AUC at t0 was set at 100 % for each mAb and mAb conjugate formulation separately (Table SIII- 3). Three different mobile phases and two different columns were used because of different interactions between the naïve mAb and mAb conjugates and the column resin matrixes. For the naïve mAb, the AUC remained unchanged in the HS 6.5 formulation. After 6 months at 40 °C in PN 7.2 the AUC decreased, indicating a substantial formation of insoluble aggregates have formed, which were removed before or on the column. The AUC of mAb Fl also decreased upon storage for 6 months, whereas mAb DEAC showed comparable AUC levels for all time points. MAb Eo displayed the greatest change in AUC with decreases after 6 months at 40°C in both buffers. None of the tested mAb and mAb conjugates showed any differences in the AUC after storage at 5°C and 25 °C.

The distribution of the mAb and mAb conjugate samples in monomer, fragment and soluble aggregate shares is shown in Table III- 12 to Table III- 14. At t0, the naïve mAb exhibited approximately 97 % monomer, ≤ 3 % LMWS and ≤0.5 % HMWS. These percentages were similar for mAb DEAC and mAb Eo. MAb Fl showed approx. 4 % HMWS after conjugation. For the naïve mAb, the monomer content decreased during the 6 months. Correspondingly, the LMWS increased, e.g. up to 17 % for mAb PN 7.2 after 6 months at 40 °C. The monomer content for the mAb conjugates also decreased during storage. Whereas the amount of LMWS was comparable to the naïve mAb, HMWS increased during storage for mAb DEAC. Aggregate formation increased with higher temperatures; after 6 months at 40 °C 12 % of the sample was aggregated in the PN 7.2 formulation.

Temperature-dependent aggregation and fragmentation were also observed for mAb Fl and mAb Eo. Whereas mAb Fl had slightly higher HMWS than mAb DEAC, mAb Eo had the highest levels of aggregates and fragments. After storage at 40 °C, 21 % of mAb Eo in PN 7.2 were aggregated. In general, the monomer content of the mAb and mAb conjugate samples decreased more in PN 7.2 compared to the HS 6.5 buffer.

Table III- 12: Monomer (main peak), LMWS (lower molecular weight species) and HMWS (higher molecular weight species) content of mAb samples in HS 6.5 and PN 7.2 buffers stored at 5 °C as determined by HP-SEC.

5°C		t0						t3, 5°C						t6, 5°C					
		HMWS		Monomer		LMWS		HMWS		Monomer		LMWS		HMWS		Monomer		LMWS	
mAb	HS	**0.29**	± 0.04	**97.50**	± 0.09	**2.21**	± 0.05	**0.00**	± 0.00	**91.95**	± 0.38	**8.06**	± 0.38	**0.00**	± 0.00	**92.86**	± 0.29	**7.14**	± 0.29
	PN	**0.52**	± 0.05	**96.54**	± 0.05	**2.94**	± 0.09	**0.16**	± 0.01	**97.00**	± 0.27	**2.84**	± 0.28	**0.47**	± 0.43	**88.82**	± 1.53	**10.71**	± 1.13
mAb Fl	HS	**4.10**	± 0.03	**94.68**	± 0.51	**1.21**	± 0.52	**1.19**	± 0.27	**89.36**	± 1.82	**9.45**	± 1.64	**1.32**	± 0.15	**84.56**	± 0.04	**14.11**	± 0.15
	PN	**4.73**	± 0.40	**94.34**	± 0.42	**0.93**	± 0.11	**2.98**	± 0.13	**94.44**	± 0.16	**2.58**	± 0.13	**4.63**	± 0.08	**78.40**	± 2.17	**16.97**	± 2.10
mAb DEAC	HS	**0.11**	± 0.05	**96.69**	± 0.22	**3.20**	± 0.22	**0.00**	± 0.00	**96.57**	± 0.06	**3.43**	± 0.06	**0.02**	± 0.04	**96.63**	± 0.28	**3.35**	± 0.24
	PN	**0.80**	± 0.11	**95.77**	± 0.54	**3.42**	± 0.47	**0.50**	± 0.08	**94.84**	± 0.63	**4.66**	± 0.58	**1.20**	± 0.17	**89.39**	± 3.12	**9.42**	± 3.25
mAb Eo	HS	**0.97**	± 0.12	**96.35**	± 0.05	**2.68**	± 0.17	**1.13**	± 0.35	**91.04**	± 1.42	**7.83**	± 1.08	**1.50**	± 0.13	**72.20**	± 1.81	**26.30**	± 1.89
	PN	**1.55**	± 0.40	**95.90**	± 0.42	**2.56**	± 0.70	**1.85**	± 0.25	**95.11**	± 0.40	**3.04**	± 0.21	**2.40**	± 0.13	**64.45**	± 0.11	**33.16**	± 0.24

Table III- 13: Monomer (main peak), LMWS (lower molecular weight species) and HMWS (higher molecular weight species) content of mAb samples in HS 6.5 and PN 7.2 buffers stored at 25 °C as determined by HP-SEC.

25°C		t0						t3, 25°C						t6, 25°C					
		HMWS		Monomer		LMWS		HMWS		Monomer		LMWS		HMWS		Monomer		LMWS	
mAb	HS	**0.29**	± 0.04	**97.50**	± 0.09	**2.21**	± 0.05	**0.00**	± 0.00	**87.42**	± 0.74	**12.58**	± 0.74	**0.00**	± 0.00	**84.48**	± 0.61	**15.52**	± 0.61
	PN	**0.52**	± 0.05	**96.54**	± 0.05	**2.94**	± 0.09	**0.33**	± 0.10	**96.16**	± 0.44	**3.50**	± 0.41	**0.69**	± 0.24	**87.70**	± 1.47	**11.61**	± 1.24
mAb Fl	HS	**4.10**	± 0.03	**94.68**	± 0.51	**1.21**	± 0.52	**1.30**	± 0.09	**88.50**	± 0.15	**10.20**	± 0.08	**1.54**	± 0.35	**82.07**	± 1.34	**16.39**	± 1.56
	PN	**4.73**	± 0.40	**94.34**	± 0.42	**0.93**	± 0.11	**2.56**	± 0.13	**94.23**	± 0.05	**3.21**	± 0.12	**4.76**	± 0.08	**75.17**	± 2.80	**20.07**	± 2.76
mAb DEAC	HS	**0.11**	± 0.05	**96.69**	± 0.22	**3.20**	± 0.22	**0.29**	± 0.09	**94.40**	± 0.16	**5.31**	± 0.23	**0.35**	± 0.03	**93.50**	± 0.39	**6.14**	± 0.42
	PN	**0.80**	± 0.11	**95.77**	± 0.54	**3.42**	± 0.47	**1.18**	± 0.14	**94.10**	± 0.36	**4.72**	± 0.42	**2.14**	± 0.37	**86.16**	± 3.14	**11.71**	± 3.47
mAb Eo	HS	**0.97**	± 0.12	**96.35**	± 0.05	**2.68**	± 0.17	**1.36**	± 0.28	**90.61**	± 0.37	**8.03**	± 0.57	**2.49**	± 0.07	**68.72**	± 0.51	**28.79**	± 0.46
	PN	**1.55**	± 0.40	**95.90**	± 0.42	**2.56**	± 0.70	**2.28**	± 0.64	**93.67**	± 0.96	**4.05**	± 0.49	**3.36**	± 0.33	**64.44**	± 0.73	**32.21**	± 0.94

Table III- 14: Monomer (main peak), LMWS (lower molecular weight species) and HMWS (higher molecular weight species) content of mAb samples in HS 6.5 and PN 7.2 buffers stored at 40 °C as determined by HP-SEC.

40°C		t0						t1, 40°C					
		HMWS		Monomer		LMWS		HMWS		Monomer		LMWS	
mAb	HS	**0.29**	± 0.04	**97.50**	± 0.09	**2.21**	± 0.05	**0.09**	± 0.13	**95.02**	± 0.40	**4.89**	± 0.52
	PN	**0.52**	± 0.05	**96.54**	± 0.05	**2.94**	± 0.09	**1.36**	± 0.07	**93.26**	± 0.31	**5.38**	± 0.34
mAb Fl	HS	**4.10**	± 0.03	**94.68**	± 0.51	**1.21**	± 0.52	**2.36**	± 0.23	**86.92**	± 0.55	**10.72**	± 0.76
	PN	**4.73**	± 0.40	**94.34**	± 0.42	**0.93**	± 0.11	**6.32**	± 0.59	**89.03**	± 0.53	**4.66**	± 0.14
mAb DEAC	HS	**0.11**	± 0.05	**96.69**	± 0.22	**3.20**	± 0.22	**0.38**	± 0.28	**93.78**	± 0.28	**5.83**	± 0.50
	PN	**0.80**	± 0.11	**95.77**	± 0.54	**3.42**	± 0.47	**3.13**	± 0.19	**90.40**	± 0.40	**6.47**	± 0.45
mAb Eo	HS	**0.97**	± 0.12	**96.35**	± 0.05	**2.68**	± 0.17	**2.65**	± 0.32	**87.21**	± 0.63	**10.14**	± 0.93
	PN	**1.55**	± 0.40	**95.90**	± 0.42	**2.56**	± 0.70	**4.51**	± 0.43	**91.61**	± 0.53	**3.89**	± 0.80

		t3, 40°C						t6, 40°C					
		HMWS		Monomer		LMWS		HMWS		Monomer		LMWS	
mAb	HS	**0.04**	± 0.07	**93.10**	± 1.27	**7.34**	± 0.90	**0.32**	± 0.07	**86.59**	± 1.23	**13.08**	± 1.25
	PN	**2.88**	± 1.14	**88.65**	± 2.06	**8.47**	± 0.93	**1.30**	± 0.20	**81.43**	± 1.46	**17.27**	± 1.65
mAb F	HS	**2.14**	± 0.07	**82.97**	± 0.37	**14.89**	± 0.32	**4.28**	± 0.78	**72.76**	± 4.15	**22.96**	± 4.92
	PN	**13.74**	± 0.86	**80.84**	± 1.10	**5.42**	± 0.25	**13.51**	± 0.47	**67.06**	± 0.91	**19.43**	± 0.68
mAb DEAC	HS	**1.49**	± 0.66	**80.87**	± 3.79	**17.64**	± 4.40	**5.23**	± 0.52	**76.78**	± 0.73	**18.00**	± 0.22
	PN	**8.81**	± 0.97	**81.75**	± 1.09	**9.11**	± 1.00	**12.33**	± 0.09	**70.77**	± 0.17	**16.90**	± 0.08
mAb Eo	HS	**3.36**	± 0.20	**82.22**	± 0.84	**14.42**	± 0.66	**3.23**	± 0.36	**60.12**	± 1.30	**36.66**	± 1.45
	PN	**9.69**	± 0.23	**85.46**	± 0.37	**4.85**	± 0.27	**21.42**	± 0.41	**62.06**	± 0.84	**16.52**	± 1.20

Furthermore, SDS-PAGE was used to investigate the aggregation and fragmentation of the mAb samples. For the naïve mAb, clear bands for monomer and fragments in HS 6.5 and PN 7.2 were visible after silver staining (Figure SIII- 10). No additional bands were visible for the naïve mAb after storage for 6 months. For mAb Fl and mAb Eo, dimer formation with a molecular weight of about 300 kDa was seen independent of the buffer after conjugation. Storage for 6 months did not induce additional bands for these two mAb conjugates. MAb DEAC displayed a monomer band and fragment peaks after conjugation and storage at 5 °C for 6 months. Storage at 25 °C induced dimer formation for mAb DEAC PN 7.2 and at 40 °C for all buffers.

Possibly formed covalent, but non-reducible, bonds were identified using CE-SDS under reducing conditions. The gels are displayed in Figure SIII- 11 and the results are summarized in Table III- 15. For the naïve mAb, a substantial amount of LMWS and little HMWS were observed at t0. In contrast to the SEC and SDS-PAGE results, fragmentation as well as aggregation enhanced upon storage for 6 months. However, fragmentation did not increase as significantly as seen in the SEC results. The molecular weight doubled from 70 kDa to approx. 140 kDa, indicating that dimers may have formed. The temperature-dependent increase in aggregation and fragmentation seen in SEC was confirmed. The mAb and the mAb conjugates showed similar stability in both buffers. The comparable percentages of HMWS in SEC and CE-SDS indicate that the HMWS were not covalently bond.

Table III- 15: CE-SDS results under reducing conditions. Percentage of HMWS and LMWS as well as monomer (light+heavy chain) of naïve mAb (mAb), mAb Fluorescein (mAb Fl), mAb DEAC (mAb DEAC), mAb Eosin (mAb Eo) in histidine sucrose buffer (HS 6.5) and phosphate NaCl buffer (PN 7.2). NA: sample not analyzed.

		HMWS [%]	Monomer [%]	LMWS [%]
mAb HS 6.5	t0	0.7	93.7	5.6
	t6, 5°C	0.5	89.2	10.3
	t6, 25°C	3.3	93.6	3.1
	t6, 40°C	4	90.9	5.1
mAb PN 7.2	t0	0.7	98.1	1.2
	t6, 5°C	0.5	95.2	4.3
	t6, 25°C	3.2	95.5	1.3
	t6, 40°C	NA	NA	NA
mAb Fl HS 6.5	t0	5.3	93.0	1.7
	t6, 5°C	3.9	96.1	0.0
	t6, 25°C	2.6	94	3.4
	t6, 40°C	6.8	90.6	2.6
mAb Fl PN 7.2	t0	4.4	93.9	1.7
	t6, 5°C	3.7	94.7	1.6
	t6, 25°C	4.1	93.4	2.5
	t6, 40°C	6.8	86.6	6.6
mAb DEAC HS 6.5	t0	0.6	96.8	2.6
	t6, 5°C	0.9	98.1	1.0
	t6, 25°C	4.4	92.1	3.5
	t6, 40°C	4.1	91.7	4.2
mAb DEAC PN 7.2	t0	1.9	95.6	2.6
	t6, 5°C	1.3	98.7	0
	t6, 25°C	2	94.4	3.6
	t6, 40°C	8.6	83.3	8.1
mAb Eo HS 6.5	t0	2.6	94.3	3.2
	t6, 5°C	2.6	94.7	2.7
	t6, 25°C	6.3	91.5	2.2
	t6, 40°C	17.4	74.5	8.1
mAb Eo PN 7.2	t0	5.8	92.8	1.5
	t6, 5°C	8.2	88.9	2.9
	t6, 25°C	11	89	0
	t6, 40°C	11.2	80.5	8.3

The hydrodynamic radius of the naïve mAb and mAb conjugates, as measured by DLS, was about 6 nm and did not increase over 6-month storage at 5 °C and 25 °C (Figure III- 7). Whereas storage at 40 °C in HS 6.5 did not lead to a change, the hydrodynamic radii were significantly increased in the PN 7.2 buffer for the naïve mAb and mAb conjugates. The change in the hydrodynamic radius in HS 6.5 for mAb DEAC and mAb Eo is not statistically significant.

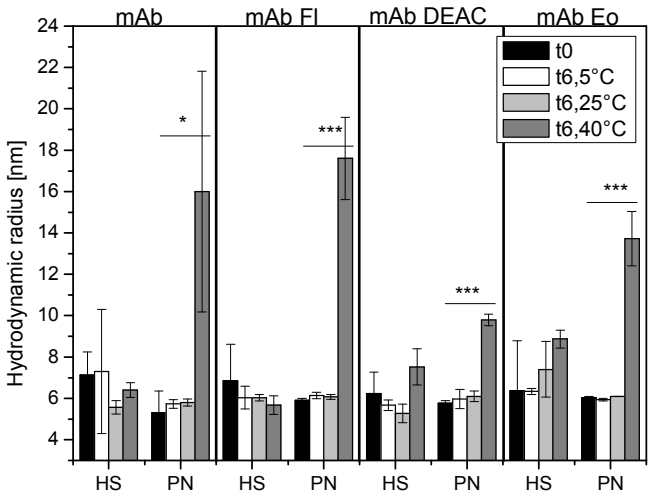

Figure III- 7: Hydrodynamic radii [nm] of naïve mAb (mAb), mAb Fluorescein (mAb Fl), mAb DEAC (mAb DEAC) and mAb Eosin (mAb Eo) in histidine sucrose (HS 6.5) and phosphate NaCl (PN 7.2) buffer, respectively (* p 0.05, p ≤ 0.01, *** p ≤ 0.001).**

3.3.4 Changes in Secondary Structure

Potential conformational changes due to conjugation as well as upon storage were analyzed by FTIR spectroscopy considering the amide I band [67-71]. The spectrum of the naïve mAb in HS 6.5 was dominated by the β-sheet elements at 1639 cm^{-1} (Figure SIII- 12). The small band at 1689 cm^{-1} can also be assigned to β-sheet structures, whereas the band at 1664 cm^{-1} can be attributed to turns. Either β-sheet structures or side-chain effects induced the band at 1616 cm^{-1} [67, 70]. No differences were seen between the naïve mAb and the mAb conjugates at t0. Minor differences were seen in the FTIR spectra between HS 6.5 and PN 7.2 buffers, but these were not significant for the assigned bands. Upon storage for 6 months, the secondary structure did not change significantly. Thus, the secondary structure was not influenced by the hydrophobic payloads or storage for up to 6 months.

4 DISCUSSION

Coupling of a hydrophobic payload to an antibody may negatively impact the physical stability and increase the aggregation propensity. In this study, three different mAb model conjugates of similar DOL were compared to the parent mAb with respect to conformational, colloidal and long-term storage stability.

All conjugates were generated through coupling of an activated fluorescent dye via primary amino groups on cetuximab. The pIs was markedly decreased for mAb Fl and mAb Eo. NHS-Fluorescein and Eosin-ITC introduce two negative charges to the mAb for each molecule attached at pH 6.5 and above and remove the positive charge of lysine. In contrast, the tertiary amino group of DEAC-SE has a theoretical pKa of 4.2, and the molecule is neutrally charged at the pH values tested. For mAb DEAC-SE, the pI was hardly affected, indicating that the low pI of mAb Fl and mAb Eo can essentially be attributed to the added charge. This relationship has been discussed in the literature for different fluorescent dyes [9, 55, 72]. The higher hydrophobicity of Eosin compared to Fluorescein did not have an influence on the pI. The high availability of primary amino groups from lysine side chains and the N-termini per mAb leads to heterogeneous mixtures of DOLs [73, 74]. This also poses challenges for MS analysis. Previous MS studies have identified 40 out of 86 lysines to be conjugated to DM1, with low abundances per site [35]. Although differences were found between mAb and mAb Fl in peptide map analysis, these changes could not be attributed to specific lysine residues.

4.1 Thermal Conformational Stability and Temperature Dependent Protein-Protein Interactions

Conjugation does not significantly change the conformational stability in terms of T_m. The T_m and $T_{m,onset}$ values were not changed for mAb conjugates compared to the naïve mAb except for mAb Eo in selected formulations. Several authors have described a T_m decrease for ADCs conjugated via the cysteines [16, 75, 76]. This destabilization for the cysteine linkage compared to our lysine linkage could result from a generalized destabilization of the antibody due to changes in the hinge region which typically stabilizes antibodies. Acchione et al., who coupled biotin to different mAb structures, also revealed that conjugation to the thiols in the hinge region decreased the thermal stability of the IgG1 scaffold more compared to amine and carbohydrate coupling [77]. For lysine-linked Kadcyla®, the T_m1 of the C_H2 region was decreased by 4.5 °C compared to its naïve mAb [20]. The authors explained this with the density of lysine residues present in the C_H2 region as well as their reaction propensity. For our antibody, cetuximab, the first DSC transition reflects a pre-transition of the Fab region and the

large second peak resembles the main transition of Fab and C_H2 [47]. Hence, the unfolding characteristics of our cetuximab conjugates may not have changed because the region most affected by coupling of a payload is not featured in the lowest T_m value. The decreased values for a few mAb Eo formulations could result from the stronger hydrophobicity of Eosin compared to Fluorescein. The in general close proximity of T_m and T_{agg} for mAb Eo points to almost simultaneous unfolding and aggregation.

Changes were seen in the T_{agg} as the resistance against aggregation can be ranked in the order of naïve mAb > mAb DEAC> mAb Fl > mAb Eo. As the pI values of mAb DEAC and the naïve mAb are comparable, the destabilization for mAb DEAC is most likely due to the added hydrophobicity, corresponding to literature values on ADCs [16]. In four of the tested seven buffers for mAb Fl and in six for mAb Eo showed a lower T_{agg} compared to the naïve mAb. At pH 6.5 and 7.2 these conjugates are close to their pI and exhibit low net charge. This correlation between T_{agg} and a pH close to pI was also described by Kheddo et al. [78]. mAb Eo is more hydrophobic than mAb Fl which explains the higher aggregation propensity at increasing temperature. Correspondingly, mAb Fl and mAb Eo are more stable in the lower ionic strength sucrose formulations [16], whereas in the presence of NaCl the stronger charge shielding reduces repulsive charge-based protein-protein interactions.

Thus, whereas conformational stability of cetuximab appears to be more or less unaffected by the conjugation, the results already point to an increased aggregation propensity and colloidal instability of the mAb conjugates in the context of unfolding. Analysis of the interaction parameter k_D upon unfolding conditions is not conclusive due to an inadequate fit and model. For long term stability of mAb conjugates at a storage temperature far below T_m, the interaction parameter correspondingly to the protein-protein-interactions should be of more importance.

Low ionic strength buffers at a pH near the pI of the mAb increase the propensity for self-association as no charge stabilizes it [79, 80]. For example, the naïve mAb showed net attraction at 20 to 80 °C in PS 7.2, which is close to cetuximab's pI. Moreover, this correlates to the results discussed above, as PS 7.2 had demonstrated the highest conformational, but lowest colloidal stability. Addition of the salt when the mAb is charged, e.g. PN 6.5, also destabilizes the mAb as the salt shields repulsive charges, leading to attraction. MAb DEAC, with almost identical pI, showed more net attraction compared to the naïve mAb, which must result from the added hydrophobic payload. The results obtained for mAb Fl and mAb Eo demonstrated more attractive protein-protein interactions, which can also be explained by electrostatic interactions and the hydrophobic payload. Aggregation and colloidal instability of the mAb conjugates may also be attributed to aggregation hot spots or a small unstable fraction of the conjugated sample [81, 82].

4.2 Isothermal Storage Stability Studies of MAb Conjugates

Storage stability over 6 months was tested at 5, 25 and 40 °C to access whether the differences, specifically in protein-protein-interactions between the mAb conjugates and the naïve mAb, translate into a different storage stability relevant for drug product development. The two formulation conditions tested were HS 6.5 and PN 7.2, which reflect a high and low ionic strength formulation at two pH values in the neutral and the slightly acidic region. For these two buffer systems, mAb DEAC shows a small decrease in colloidal stability compared to the naïve mAb, whereas mAb Fl was colloidally more instable and mAb Eo demonstrated slightly conformational and colloidal destabilization based on T_m and A_2^*.

Aggregate formation was assessed at different levels. Large particles were analyzed by visual inspection and photography, subvisible particles by LO and MFI, particles in the higher nm range via absorbance at 700 nm, small HMWS by SEC and DLS, and dimers and trimers by SDS-PAGE and CE-SDS.

After 6 months, the formation of visible particles was noted in HS formulations, specifically for mAb Eo stored at 40 °C and mAb and mAb Fl stored at 25 °C. Subvisible particles as determined with LO and MFI increased upon storage and elevated temperatures in correspondence to the results obtained from the visible particles. For example, cetuximab, which showed an increased number of visible particles particularly at 25 °C in HS 6.5, also displayed the highest number of subvisible particles greater than 10 and 25 µm/mL. The decreased colloidal and conformational stability of mAb Eo compared to the naïve mAb resulted in the most pronounced formation of subvisible particles ≥ 1 µm/mL. The morphology of the particles was translucent, implying that they are most likely protein particles [64, 66, 83]. For the other mAb conjugates, mAb DEAC and mAb Fl, particle formation was not enhanced. Thus, only the most hydrophobic payload, which also leads to a substantial negative charge, induced instability. Turbidity measured via absorbance at 700 nm was low and did not change upon storage for the naïve mAb ad mAb conjugates. Even smaller aggregates were accessed by DLS. The hydrodynamic radius of cetuximab and the conjugates obtained via DLS at t0 is comparable to literature [84-87], corresponding to the monomer. Upon storage at 40 °C in PN, the radii increased for both mAb and mAb conjugates. The greater hydrodynamic radii for the PN samples correlates to the higher amount of HMWS during HP-SEC analysis.

Aggregation and fragmentation were furthermore analyzed using the orthogonal methods HP-SEC, SDS-PAGE, and CE-SDS. Naïve mAb samples showed little HMWS formation upon storage. After 6 months at 40 °C, the mAb conjugates showed an increase in the HMWS fraction in the order of mAb DEAC < mAb Fl < mAb Eo. Already after conjugation, a slight dimer formation was visible with

unreduced SDS-PAGE and reduced CE-SDS. The aggregate percentages are comparable in the unreduced and reduced SDS methods, indicating that the aggregates formed are not covalently bond.

Aggregation is a common phenomenon for mAbs and ADCs. Cockrell et al. observed an enhanced aggregation for a mAb Eo conjugate upon exposure to light [28]. Wakankar et al. reported 15 % aggregate formation for Kadcyla® after 70 days at 40 °C [20]. Increased aggregation was shown for cysteine linked ADCs as well [16, 75, 76]. The aggregate formation of our mAb conjugates is less pronounced but correlates with the conjugate properties. At pH 6.5 and 7.2 mAb Fl and mAb Eo carry a net neutral charge due to their lower pI as compared to the naïve mAb, which promotes aggregation. Additionally, mAb Eo is more hydrophobic than mAb Fl, which triggers aggregation. For mAb DEAC and the naïve mAb with similarly high pI, aggregate formation is less pronounced. Still aggregation is stimulated for mAb DEAC due to the increased hydrophobicity and stronger attractive protein-protein-interactions. Potentially, free lysine residues increase mAb stability, as the exchange against arginine mutants has been shown to lead to a decreased mAb stability [88]. The aggregates were mainly not covalently bond as seen with CE-SDS. Aggregation was more pronounced in the PN buffer compared to HS for all formulations. This is due to the decreased electrostatic repulsion in PN with higher ionic strength [76] and the pH of 7.2 at which also the naïve mAb and mAb DEAC are neutrally charged. Independently, sucrose may reduce aggregation by stabilization based on preferential exclusion of water molecules [89].

The susceptibility of our mAb conjugates to fragmentation is mostly related to the mAb itself [20, 70, 74]. Fragmentation was increased substantially for all samples after 6 months as detected with SEC and CE-SDS. For the naïve mAb, the increase of aggregates was minimal, and the formation of fragments plays a significant role for cetuximab degradation. This correlates to 14 % fragment formation in PBS pH 6.0 after 26 weeks of storage at 40 °C / 75 % r.h. [90]. Non-enzymatic fragmentation of the protein backbone can occur due to the amino acid sequence, local flexibility, solvent conditions or metals and free radicals [91, 92]. As the percentage of fragments is similar for the naïve mAb and mAb conjugates in both buffers, fragmentation is independent of the conjugation process, added charge and added hydrophobicity.

No differences in the secondary structure were detectable for the mAb conjugates. The used concentration of 1 mg/mL is at the lower end of the instrument's sensitivity, which could explain inaccuracies of the overlays and limitations on the sensitivity to detect changes. The secondary structure was also unaltered in other ADC studies [16, 75, 82]. Beckley et al. showed that secondary structures of the HMWS fraction of DOL 6 species of a thiol-linked ADC were altered after applying thermal stress for 4 weeks at 40 °C [75]. The HMWS fraction tested is very small compared to the entire mAb formulation in our case and possible subtle changes are not detectable with FTIR.

Thus, a correlation between conformational and colloidal stability and our isothermal stability study is possible. The most pronounced aggregation formation upon storage occurs for mAb Eo, which demonstrates a markedly decreased colloidal and conformational instability. The Eosin payload induces negative charges, leading to a low pI and a high hydrophobicity (cLogP: 6.0). Aggregation rates are comparable for the other two mAb conjugates, but mAb Fl shows more pronounced particle formation. MAb Fl, with the same charge as mAb Eo but a lower hydrophobicity (clogP: 3.1), exhibits a decreased colloidal stability. MAb DEAC, which has the same hydrophobicity as mAb Fl and a neutral charge compared to the positively charged lysine of the naïve mAb demonstrates slightly decreased colloidal stability. Overall, we see a decrease in the long-term stability of mAb conjugates in the order of mAb Eo> mAb Fl> mAb DEAC. This effect we can specifically link to the colloidal instabilities reflected by the protein-protein interaction parameter A_2^* and to less extent to the conformational stability reflected by T_m. Contrary to Frka-Petesic et al. [82], we find that the prediction of stability based on interaction parameters is reasonable also for ADCs. We coupled the hydrophobic payload to the antibody via the primary amines. Since the linker has proven to be a critical aspect for ADC stability, pharmacokinetics and the therapeutic index [77, 93-95], future research could include different linker and spacer chemistry.

5 CONCLUSION

Overall, the results of this study have shown that the correlation between conformational and colloidal stability and long-term stability is also possible for mAbs with hydrophobic payloads. We have identified and explained divergences that occurred in the characterization for a mAb with three hydrophobic payloads with different properties compared to the naïve mAb. The three model conjugates were hydrophobic fluorescent dyes, which carried neutral or negative charge as the positively charged lysine to which they were covalently coupled to on the mAb. The isoelectric point was decreased significantly upon adding negative charges. Melting temperatures did not differ greatly compared to the naïve mAb. Colloidal stability in terms of aggregation temperatures and apparent osmotic second virial coefficient was strongly formulation dependent. Taken together, the hydrophobic payloads decreased the colloidal stability. Upon storage at 2 - 8, 25 and 40 °C, mAb conjugates displayed increased aggregation. In some cases, also particle formation was detectable. Charge effects with conjugation had a greater impact on mAb stability than increased hydrophobicity. As for the naked mAbs, we recommend performing orthogonal analytics to assess the specific challenges of ADC stability.

6 ACKNOWLEDGMENTS

The peptide map measurements were performed at the Chair of Urban Water Systems Engineering of the TU Munich, for which we are indebted to the expertise and experimental help of Sylvia Grosse and Thomas Letzel. We thank Coriolis Pharma (Martinsried, Germany) for the possibility to use the Zetasizer APS. We are grateful for the opportunity to perform some of the OPTIM measurements at the Section of Biologics, Department of Pharmacy at the University of Copenhagen with the help of Fabrice Rose and Marco van de Weert. We also appreciate the possibility given by Wyatt Technologies and Lorenzo Gentiluomo to use the DynaPro Reader. Furthermore, we thank Nicole Popp (TU Munich) for her experimental help.

7 REFERENCES

[1] W. Wang, S. Singh, D. L. Zeng, K. King, and S. Nema, "Antibody structure, instability, and formulation," *J Pharm Sci,* vol. 96, no. 1, pp. 1-26, 2007.

[2] M. C. Manning, D. K. Chou, B. M. Murphy, R. W. Payne, and D. S. Katayama, "Stability of protein pharmaceuticals: an update," *Pharm Res,* vol. 27, no. 4, pp. 544-75, 2010.

[3] E. Y. Chi, S. Krishnan, T. W. Randolph, and J. F. Carpenter, "Physical stability of proteins in aqueous solution: Mechanism and driving forces in nonnative protein aggregation," *Pharmaceutical Research,* vol. 20, no. 9, pp. 1325-1336, 2003.

[4] M. Ahmadi, C. J. Bryson, E. A. Cloake, K. Welch, V. Filipe, S. Romeijn, et al. and M. H. Fogg, "Small amounts of sub-visible aggregates enhance the immunogenic potential of monoclonal antibody therapeutics," *Pharm Res,* vol. 32, no. 4, pp. 1383-94, 2015.

[5] H. C. Mahler, W. Friess, U. Grauschopf, and S. Kiese, "Protein aggregation: pathways, induction factors and analysis," *J Pharm Sci,* vol. 98, no. 9, pp. 2909-34, 2009.

[6] H.-C. Mahler, W. Friess, U. Grauschopf, and S. Kiese, "Protein Aggregation: Pathways, Induction Factors and Analysis," *Journal of Pharmaceutical Sciences,* vol. 98, no. 9, pp. 2909-2934, 2009.

[7] S. Zölls, M. Wiggenhorn, R. Tantipolphan, G. Winter, W. Jiskoot, W. Friess, and A. Hawe, "Particles in Therapeutic Protein Formulations, Part 1: Overview of Analytical Methods," *Journal of Pharmaceutical Sciences,* vol. 101, no. 10, pp. 914-935, 2012.

[8] G. Thiagarajan, A. Semple, J. K. James, J. K. Cheung, and M. Shameem, "A comparison of biophysical characterization techniques in predicting monoclonal antibody stability," *MAbs,* vol. 8, no. 6, pp. 1088-97, 2016.

[9] T. Arakawa, Y. Kurosawa, M. Storms, T. Maruyama, C. J. Okumura, and N. K. Maluf, "Biophysical characterization of a model antibody drug conjugate," *Drug Discov Ther,* vol. 10, no. 4, pp. 211-7, 2016.

[10] G. Casi and D. Neri, "Antibody-drug conjugates: basic concepts, examples and future perspectives," *J Control Release,* vol. 161, no. 2, pp. 422-8, 2012.

[11] S. C. Alley, N. M. Okeley, and P. D. Senter, "Antibody–drug conjugates: targeted drug delivery for cancer," *Current Opinion in Chemical Biology,* vol. 14, no. 4, pp. 529-537, 2010.

[12] D. Jackson and D. Stover, "Using the Lessons Learned From the Clinic to Improve the Preclinical Development of Antibody Drug Conjugates," *Pharm Res,* vol. 32, no. 11, pp. 3458-69, 2015.

[13] J. M. Lambert, "Antibody-Drug Conjugates (ADCs): Magic Bullets at Last!," *Mol Pharm,* vol. 12, no. 6, pp. 1701-2, 2015.

[14] N. Diamantis and U. Banerji, "Antibody-drug conjugates--an emerging class of cancer treatment," *Br J Cancer,* vol. 114, no. 4, pp. 362-7, 2016.

[15] M. Leal, P. Sapra, S. A. Hurvitz, P. Senter, A. Wahl, M. Schutten, et al. and O. Kabbarah, "Antibody-drug conjugates: an emerging modality for the treatment of cancer," *Ann N Y Acad Sci,* vol. 1321, no. 1, pp. 41-54, 2014.

[16] J. Guo, S. Kumar, A. Prashad, J. Starkey, and S. K. Singh, "Assessment of physical stability of an antibody drug conjugate by higher order structure analysis: impact of thiol- maleimide chemistry," *Pharm Res,* vol. 31, no. 7, pp. 1710-23, 2014.

[17] W. Galush and A. Wakankar, "Formulation Development of Antibody–Drug Conjugates," in *Antibody-Drug Conjugates*. vol. 1045, L. Ducry, Ed., ed: Humana Press, pp. 217-233, 2013.

[18] K. Tsumoto, A. Young, and S. Ohtake, "Formulation and Stability," in *Antibody-Drug Conjugates*, ed: John Wiley & Sons, Inc., pp. 105-129, 2016.

[19] P. L. Ross and J. L. Wolfe, "Physical and Chemical Stability of Antibody Drug Conjugates: Current Status," *Journal of Pharmaceutical Sciences,* vol. 105, no. 2, pp. 391-397, 2016.

[20] Aditya A. Wakankar, Maria B. Feeney, Javier Rivera, Yan Chen, Michael Kim, Vikas K. Sharma, and Y. J. Wang, "Physicochemical Stability of the Antibody-Drug Conjugate Trastuzumab-DM1: Changes due to Modification and Conjugation Processes," *Bioconjugate Chemistry,* vol. 21,no. 9, pp. 1588-1595, 2010.

[21] S. K. Singh, D. L. Luisi, and R. H. Pak, "Antibody-Drug Conjugates: Design, Formulation and Physicochemical Stability," *Pharm Res,* vol. 32, no. 11, pp. 3541-71, 2015.

[22] J. Pauli, M. Grabolle, R. Brehm, M. Spieles, F. M. Hamann, M. Wenzel, et al. and U. Resch-Genger, "Suitable labels for molecular imaging--influence of dye structure and hydrophilicity on the spectroscopic properties of IgG conjugates," *Bioconjug Chem,* vol. 22, no. 7, pp. 1298-308, 2011.

[23] M. Ogawa, N. Kosaka, P. L. Choyke, and H. Kobayashi, "In vivo molecular imaging of cancer with a quenching near-infrared fluorescent probe using conjugates of monoclonal antibodies and indocyanine green," *Cancer Res,* vol. 69, no. 4, pp. 1268-72, 2009.

[24] J. Rao, A. Dragulescu-Andrasi, and H. Yao, "Fluorescence imaging in vivo: recent advances," *Curr Opin Biotechnol,* vol. 18, no. 1, pp. 17-25, 2007.

[25] P. O. Krutzik and G. P. Nolan, "Fluorescent cell barcoding in flow cytometry allows high-throughput drug screening and signaling profiling," *Nat Methods,* vol. 3, no. 5, pp. 361-8, 2006.

[26] S. A. Weston and C. R. Parish, "New fluorescent dyes for lymphocyte migration studies," *Journal of Immunological Methods,* vol. 133, pp. 87-97, 1990.

[27] D. W. Hedley, M. L. Friedlander, I. W. Taylor, C. A. Rugg, and E. A. Masgrove, "Method for Analysis of Cellular DNA Content of Paraffin-embedded Pathological Material Using Flow Cytometry," *The Journal of Histochemistry and Cytochemistry,* vol. 31, no. 11, pp. 1333-1335, 1983.

[28] G. M. Cockrell, M. S. Wolfe, J. L. Wolfe, and C. Schöneich, "Photoinduced Aggregation of a Model Antibody–Drug Conjugate," *Molecular Pharmaceutics,* vol. 12, no. 6, pp. 1784-1797, 2015.

[29] S. Kalkhof and A. Sinz, "Chances and pitfalls of chemical cross-linking with amine-reactive N-hydroxysuccinimide esters," *Analytical and Bioanalytical Chemistry,* vol. 392, no. 1-2, pp. 305-312, 2008.

[30] Molecular probes by life technologies, "Amine-Reactive Probes," MAN0001774, MP00143, 2013.

[31] G. T. Hermanson, "The Reactions of Bioconjugation," in *Bioconjugate Techniques*, vol. 3, G.T. Hermanson, Ed., ed Elsevier, pp. 229-258, 2013.

[32] M. T. Kim, Y. Chen, J. Marhoul, and F. Jacobson, "Statistical modeling of the drug load distribution on trastuzumab emtansine (kadcyla), a lysine-linked antibody drug conjugate," *Bioconjug Chem,* vol. 25, no. 7, pp. 1223-32, 2014.

[33] N. Jain, S. W. Smith, S. Ghone, and B. Tomczuk, "Current ADC Linker Chemistry," *Pharm Res,* vol. 32, no. 11, pp. 3526-40, 2015.

[34] J. Marcoux, T. Champion, O. Colas, E. Wagner-Rousset, N. Corvaia, A. Van Dorsselaer, et al. and S. Cianferani, "Native mass spectrometry and ion mobility characterization of trastuzumab emtansine, a lysine-linked antibody drug conjugate," *Protein Sci,* vol. 24, no. 8, pp. 1210-23, 2015.

[35] L. Wang, G. Amphlett, W. A. Blattler, J. M. Lambert, and W. Zhang, "Structural characterization of the maytansinoid-monoclonal antibody immunoconjugate, huN901-DM1, by mass spectrometry," *Protein Sci,* vol. 14, no. 9, pp. 2436-46, 2005.

[36] J. R. Junutula, H. Raab, S. Clark, S. Bhakta, D. D. Leipold, S. Weir, et al. and W. Mallet, "Site-specific conjugation of a cytotoxic drug to an antibody improves the therapeutic index," *Nat Biotechnol,* vol. 26, no. 8, pp. 925-32, 2008.

[37] S. Panowksi, S. Bhakta, H. Raab, P. Polakis, and J. R. Junutula, "Site-specific antibody drug conjugates for cancer therapy," *MAbs,* vol. 6, no. 1, pp. 34-45, 2014.

[38] K. Tsuchikama and Z. An, "Antibody-drug conjugates: recent advances in conjugation and linker chemistries," *Protein Cell,* vol. 9, no. 1, pp. 33-46, 2018.

[39] M. R. Gordon, M. Canakci, L. Li, J. Zhuang, B. Osborne, and S. Thayumanavan, "Field Guide to Challenges and Opportunities in Antibody-Drug Conjugates for Chemists," *Bioconjug Chem,* vol. 26, no. 11, pp. 2198-215, 2015.

[40] T. Kline, A. R. Steiner, K. Penta, A. K. Sato, T. J. Hallam, and G. Yin, "Methods to Make Homogenous Antibody Drug Conjugates," *Pharm Res,* 2014.

[41] M. L. Mierzwa, M. K. Nyati, M. A. Morgan, and T. S. Lawrence, "Recent advances in combined modality therapy," *Oncologist,* vol. 15, no. 4, pp. 372-81, 2010.

[42] EMA, "EMA/13275/2014 EPAR summary for the public. Erbitux," 2014.

[43] FDA, "BL 125084/0 Approval Letter for Cetuximab," 2004.

[44] WHO, "WHO/BS/2016.2296 Expert Committee on Biological Standardization," 2016.

[45] A. Beck, "Biosimilar, biobetter and next generation therapeutic antibodies," *mAbs,* vol. 3, no. 2, pp. 107-110, 2014.

[46] P. D. S. Kevin J. Hamblett, Dana F. Chace, Michael M. C. Sun, Joel Lenox, Charles G. Cerveny, Kim M. Kissler, Starr X. Bernhardt, Anastasia K. Kopcha, Roger F. Zabinski, Damon L. Meyer, Joseph A. Francisco, "Effects of Drug Loading on the Antitumor Activity of a Monoclonal Antibody Drug Conjugate," *Clin Cancer Res,* vol. 10, no. 20, pp. 7063-7070, 2004.

[47] T. A. Menzen, "Temperature-Induced Unfolding, Aggregation, and Interaction of Therapeutic Monoclonal Antibodies," Fakultät für Chemie und Pharmazie, Ludwig-Maximilians-Universität München, Dissertation, 2014.

[48] G. Greco, S. Grosse, and T. Letzel, "Serial coupling of reversed-phase and zwitterionic hydrophilic interaction LC/MS for the analysis of polar and nonpolar phenols in wine," *J Sep Sci,* vol. 36, no. 8, pp. 1379-88, 2013.

[49] T. Menzen and W. Friess, "Temperature-Ramped Studies on the Aggregation, Unfolding, and Interaction of a Therapeutic Monoclonal Antibody," *Journal of Pharmaceutical Sciences,* vol. 103, no. 2, pp. 445-455, 2014.

[50] J. Rubin, L. Linden, W. M. Coco, A. S. Bommarius, and S. H. Behrens, "Salt-induced aggregation of a monoclonal human immunoglobulin G1," *J Pharm Sci,* vol. 102, no. 2, pp. 377-86, 2013.

[51] Deutscher Arzneimittel Codex, "DAC-Probe 5," G. Verlag, Ed., ed, pp. 1-4, 2006.

[52] USP, "General Chapters: <787> Subvisible particulate matter in therapeutic protein injections," in *USP 37 - NF 32* vol. 28, ed: Pharmacopeial Forum, 2014.

[53] Thermo Scientific, "Instructions: NHS-Fluorescein," 2011.

[54] B. A. Teicher and R. V. Chari, "Antibody conjugate therapeutics: challenges and potential," *Clin Cancer Res,* vol. 17, no. 20, pp. 6389-97, 2011.

[55] N. J. Boylan, W. Zhou, R. J. Proos, T. J. Tolbert, J. L. Wolfe, and J. S. Laurence, "Conjugation site heterogeneity causes variable electrostatic properties in Fc conjugates," *Bioconjug Chem,* vol. 24, no. 6, pp. 1008-16, 2013.

[56] M. H. Chiu and E. J. Prenner, "Differential scanning calorimetry: An invaluable tool for a detailed thermodynamic characterization of macromolecules and their interactions," *Journal of Pharmacy and Bioallied Sciences,* vol. 3, no. 1, pp. 39-59, 2011.

[57] A. W. Vermeer and W. Norde, "The thermal stability of immunoglobulin: unfolding and aggregation of a multi-domain protein," *Biophysical Journal,* vol. 78, no. 1, pp. 394-404, 2000.

[58] Unchained Labs, *Application Note: Get the whole story: combine T_m and T_{agg} with sizing and polydispersity on Uncle,* 2016, last accessed 2017-05-22.

[59] I. Teraoka, *Polymer Solutions: An Introduction to Physical Properties*: John Wiley & Sons, Inc., 2002.

[60] S. Yadav, T. M. Scherer, S. J. Shire, and D. S. Kalonia, "Use of dynamic light scattering to determine second virial coefficient in a semidilute concentration regime," *Anal Biochem,* vol. 411, no. 2, pp. 292-6, 2011.

[61] International Conference on Harmonisation of Technical Requirements for Registration of Pharmaceuticals for Human Use (ICH), "Stability Testing of New Drug Substances and Products Q1A(R2)," 2003.

[62] M. K. Joubert, Q. Luo, Y. Nashed-Samuel, J. Wypych, and L. O. Narhi, "Classification and characterization of therapeutic antibody aggregates," *Journal of Biological Chemistry,* vol. 286, no. 28, pp. 25118-25133, 2011.

[63] S. Zolls, M. Gregoritza, R. Tantipolphan, M. Wiggenhorn, G. Winter, W. Friess, and A. Hawe, "How subvisible particles become invisible-relevance of the refractive index for protein particle analysis," *J Pharm Sci,* vol. 102, no. 5, pp. 1434-46, 2013.

[64] C. T. Huang, D. Sharma, P. Oma, and R. Krishnamurthy, "Quantitation of protein particles in parenteral solutions using micro-flow imaging," *J Pharm Sci,* vol. 98, no. 9, pp. 3058-71, 2009.

[65] B. Demeule, S. Messick, S. J. Shire, and J. Liu, "Characterization of particles in protein solutions: reaching the limits of current technologies," *AAPS J,* vol. 12, no. 4, pp. 708-15, 2010.

[66] K. Wuchner, J. Buchler, R. Spycher, P. Dalmonte, and D. B. Volkin, "Development of a microflow digital imaging assay to characterize protein particulates during storage of a high concentration IgG1 monoclonal antibody formulation," *J Pharm Sci,* vol. 99, no. 8, pp. 3343-61, 2010.

[67] S. Matheus, W. Friess, and H. C. Mahler, "FTIR and nDSC as analytical tools for high-concentration protein formulations," *Pharm Res,* vol. 23, no. 6, pp. 1350-63, 2006.

[68] H. Yang, S. Yang, J. Kong, A. Dong, and S. Yu, "Obtaining information about protein secondary structures in aqueous solution using Fourier transform IR spectroscopy," *Nat Protoc,* vol. 10, no. 3, pp. 382-96, 2015.

[69] Aichun Dong, Ping Huang, and W. S. Caughey, "Protein secondary structures in water from second-derivative amide I infrared spectra," *Biochemistry,* vol. 29, no. 13, pp. 3303-3308, 1990.

[70] J. T. Pelton and L. R. McLean, "Spectroscopic methods for analysis of protein secondary structure," *Anal Biochem,* vol. 277, no. 2, pp. 167-76, 2000.

[71] M. van de Weert, J. A. Hering, and P. I. Haris, "Fourier Transform Infrared Spectroscopy," in *Methods for Structural Analysis of Protein Pharmaceuticals*, Wim Jiskoot and D. Crommelin, Eds., ed AAPS, pp. 131-166, 2005.

[72] J. Pauli, M. Pochstein, A. Haase, J. Napp, A. Luch, and U. Resch-Genger, "Influence of Label and Charge Density on the Association of the Therapeutic Monoclonal Antibodies Trastuzumab and Cetuximab Conjugated to Anionic Fluorophores," *Chembiochem,* vol. 18, no. 1, pp. 101-110, 2017.

[73] F. Dosio, P. Brusa, and L. Cattel, "Immunotoxins and anticancer drug conjugate assemblies: the role of the linkage between components," *Toxins (Basel),* vol. 3, no. 7, pp. 848-83, 2011.

[74] J. Lin and A. C. Lazar, "Determination of Charge Heterogeneity and Level of Unconjugated Antibody by Imaged cIEF," in *Antibody-Drug Conjugates*, L. Ducry, Ed., ed Humira Press, pp. 295-302, 2013.

[75] N. S. Beckley, K. P. Lazzareschi, H. W. Chih, V. K. Sharma, and H. L. Flores, "Investigation into temperature-induced aggregation of an antibody drug conjugate," *Bioconjug Chem,* vol. 24, no. 10, pp. 1674-83, 2013.

[76] Y. T. Adem, K. A. Schwarz, E. Duenas, T. W. Patapoff, W. J. Galush, and O. Esue, "Auristatin Antibody Drug Conjugate Physical Instability and the Role of Drug Payload," *Bioconjug Chem,* vol. 25, no. 4, pp. 656-64, 2014.

[77] M. Acchione, H. Kwon, C. M. Jochheim, and W. M. Atkins, "Impact of linker and conjugation chemistry on antigen binding, Fc receptor binding and thermal stability of model antibody-drug conjugates," *mAbs,* vol. 4, no. 3, pp. 362-372, 2012.

[78] P. Kheddo, M. Tracka, J. Armer, R. J. Dearman, S. Uddin, C. F. van der Walle, and A. P. Golovanov, "The effect of arginine glutamate on the stability of monoclonal antibodies in solution," *Int J Pharm,* vol. 473, no. 1-2, pp. 126-33, 2014.

[79] S. V. Sule, J. K. Cheung, V. Antochshuk, A. S. Bhalla, C. Narasimhan, S. Blaisdell, et al. and P. M. Tessier, "Solution pH that minimizes self-association of three monoclonal antibodies is strongly dependent on ionic strength," *Mol Pharm,* vol. 9, no. 4, pp. 744-51, 2012.

[80] V. Le Brun, W. Friess, S. Bassarab, S. Muhlau, and P. Garidel, "A critical evaluation of self-interaction chromatography as a predictive tool for the assessment of protein-protein interactions in protein formulation development: a case study of a therapeutic monoclonal antibody," *Eur J Pharm Biopharm,* vol. 75, no. 1, pp. 16-25, 2010.

[81] C. J. Roberts, "Therapeutic protein aggregation: mechanisms, design, and control," *Trends Biotechnol,* vol. 32, no. 7, pp. 372-80, 2014.

[82] B. Frka-Petesic, D. Zanchi, N. Martin, S. Carayon, S. Huille, and C. Tribet, "Aggregation of Antibody Drug Conjugates at Room Temperature: SAXS and Light Scattering Evidence for Colloidal Instability of a Specific Subpopulation," *Langmuir,* vol. 32, no. 19, pp. 4848-61, 2016.

[83] D. K. Sharma, D. King, P. Oma, and C. Merchant, "Micro-flow imaging: flow microscopy applied to sub-visible particulate analysis in protein formulations," *AAPS J,* vol. 12, no. 3, pp. 455-64, 2010.

[84] C. B. Andersen, M. Manno, C. Rischel, M. Thorolfsson, and V. Martorana, "Aggregation of a multidomain protein: a coagulation mechanism governs aggregation of a model IgG1 antibody under weak thermal stress," *Protein Sci,* vol. 19, no. 2, pp. 279-90, 2010.

[85] Muppalla Sukumar, Brandon L. Doyle, Jessica L. Combs, and A. H. Pekar, "Opalescent Appearance of an IgG1 Antibody at High Concentrations and Its Relationship to Noncovalent Association," *Pharmaceutical Research,* vol. 21, no. 7, pp. 1087-1093, 2004.

[86] J. K. Armstrong, R. B. Wenby, H. J. Meiselman, and T. C. Fisher, "The hydrodynamic radii of macromolecules and their effect on red blood cell aggregation," *Biophys J,* vol. 87, no. 6, pp. 4259-70, 2004.

[87] A. Hawe, W. L. Hulse, W. Jiskoot, and R. T. Forbes, "Taylor dispersion analysis compared to dynamic light scattering for the size analysis of therapeutic peptides and proteins and their aggregates," *Pharm Res,* vol. 28, no. 9, pp. 2302-10, 2011.

[88] J. I. Austerberry, R. Dajani, S. Panova, D. Roberts, A. P. Golovanov, A. Pluen, et al. and R. Curtis, "The effect of charge mutations on the stability and aggregation of a human single chain Fv fragment," *Eur J Pharm Biopharm,* vol. 115, pp. 18-30, 2017.

[89] J. C. Lee and S. N. Timasheff, "The Stabilization of Proteins by Sucrsoe," *The Journal of Biological Chemistry,* vol. 256, no. 14, pp. 7193-7201, 1981.

[90] K. M. Ziegler, "Untersuchungen zur Stabilisierung und Interaktion von Cetuximab mit nicht-ionischen Tensiden," Dissertation, Fakultät für Chemie und Pharmazie, Ludwig-Maximilians-Universität München, Dissertation, 2013.

[91] J. Vlasak and R. Ionescu, "Fragmentation of monoclonal antibodies," *mAbs,* vol. 3, no. 3, pp. 253-263, 2014.

[92] A. J. Cordoba, B. J. Shyong, D. Breen, and R. J. Harris, "Non-enzymatic hinge region fragmentation of antibodies in solution," *Journal of Chromatography B: Analytical Technologies in the Biomedical and Life Sciences,* vol. 818, no. 2, pp. 115-121, 2005.

[93] A. E. Albers, A. W. Garofalo, P. M. Drake, R. Kudirka, G. W. de Hart, R. M. Barfield, et al. and D. Rabuka, "Exploring the effects of linker composition on site-specifically modified antibody-drug conjugates," *Eur J Med Chem,* vol. 88, pp. 3-9, 2014.

[94] E. E. Hong and R. Chari, "Linker Design for Antibody-Drug Conjugates," in *Antibody-Drug Conjugates*. vol. 17, J. Wang, Ed., ed AAPS, pp. 49-76, 2015.

[95] R. P. Lyon, T. D. Bovee, S. O. Doronina, P. J. Burke, J. H. Hunter, H. D. Neff-LaFord, et al. and P. D. Senter, "Reducing hydrophobicity of homogeneous antibody-drug conjugates improves pharmacokinetics and therapeutic index," *Nat Biotechnol,* vol. 33, no. 7, pp. 733-5, 2015.

8 SUPPLEMENTARY INFORMATION

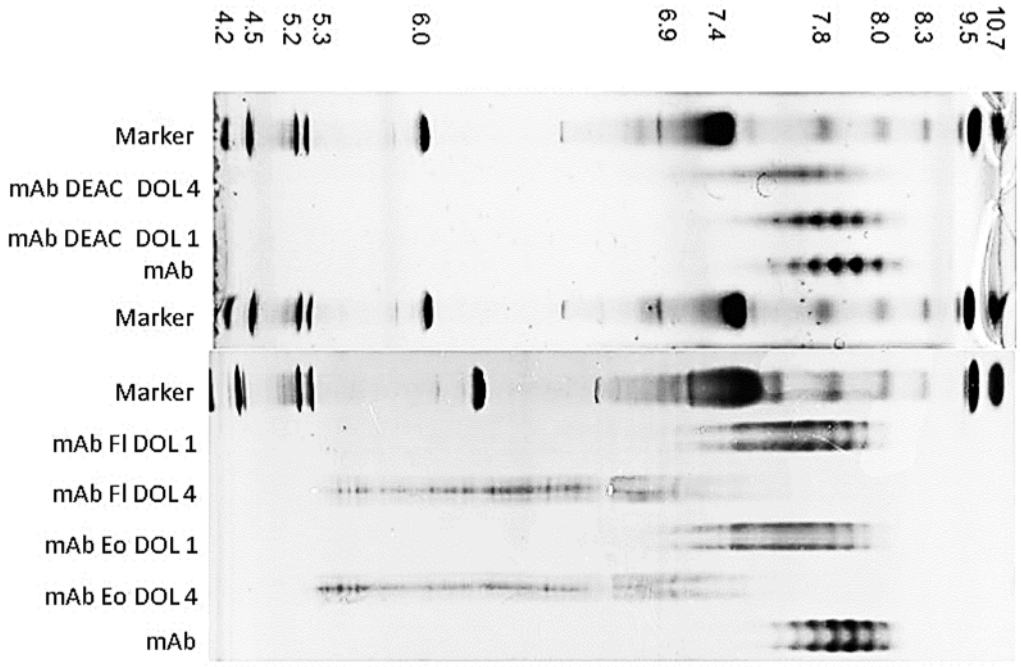

Figure SIII- 1: Decolorized scans of the IEF gels of the mAb samples after staining with Serva Blue. Cathode (-) and anode (+) were located at the right and left, respectively.

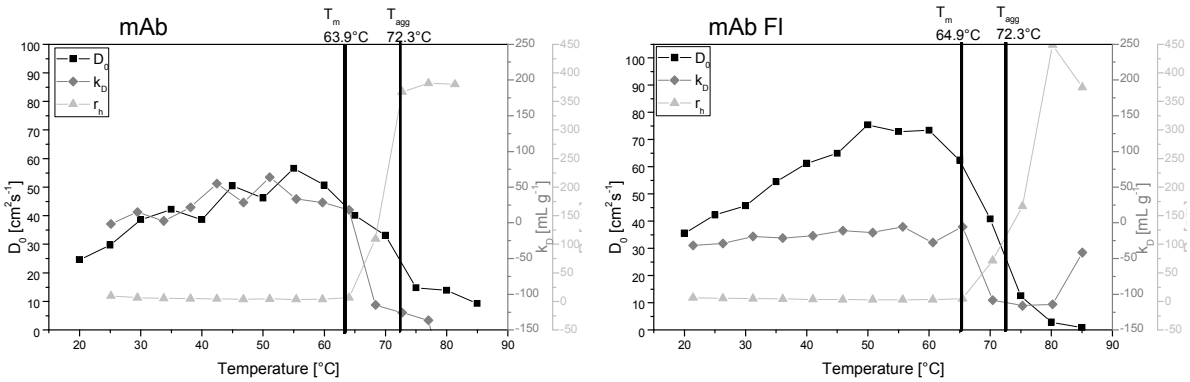

Figure SIII- 2: Hydrodynamic radius r_h (light grey triangles), interaction parameter k_D (dark grey diamonds) and diffusion coefficient at infinite dilution (D_0) (black squares) as a function of temperature. The melting temperature T_m and aggregation temperature T_{agg} are also filled in as black lines. A) mAb and B) mAb Fl in 10 mM histidine 145 mM NaCl pH 7.2 are shown as an example.

Table SIII- 1: Visible particles according to the DAC-probe 5 scale for mAb stability samples after storage for 0, 3 and 6 m at 25 °C.

25 °C	0 m			3 m			6 m		
mAb HS 6.5	0	0	1	2	2	2	10	10	10
mAb PN 7.2	0	0	0	1	1	1	1	1	2
mAb Fl HS 6.5	0	0	0	2	2	1	10	10	10
mAb Fl PN 7.2	0	0	0	0	0	1	1	1	0
mAb DEAC HS 6.5	0	0	0	0	0	1	1	1	1
mAb DEAC PN 7.2	0	0	0	1	1	1	1	0	1
mAb Eo HS 6.5	2	2	2	1	2	1	2	2	10
mAb Eo PN 7.2	0	0	0	1	1	1	2	2	2
buffer HS 6.5	0	0	0	0	0	0	0	0	0
buffer PN 7.2	0	0	0	0	0	0	0	0	0

Table SIII- 2: Visible particles according to the DAC-probe 5 scale for mAb stability samples after storage for 0, 3 and 6 m at 5 °C.

5 °C	0 m			3 m			6 m		
mAb HS 6.5	0	0	1	0	1	0	10	10	2
mAb PN 7.2	0	0	0	0	0	0	1	1	1
mAb Fl HS 6.5	0	0	0	2	2	2	2	2	2
mAb Fl PN 7.2	0	0	0	0	1	0	1	1	0
mAb DEAC HS 6.5	0	0	0	0	0	1	1	1	1
mAb DEAC PN 7.2	0	0	0	0	0	0	1	1	1
mAb Eo HS 6.5	2	2	2	1	1	1	1	2	2
mAb Eo PN 7.2	0	0	0	0	1	0	1	1	1
buffer HS 6.5	0	0	0	0	0	0	0	1	0
buffer PN 7.2	0	0	0	0	0	0	0	0	0

40 °C

sample	0 m	1 m	3 m	6 m
mAb HS 6.5	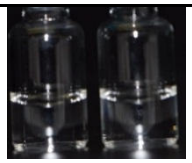	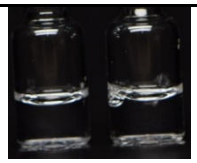		
mAb PN 7.2		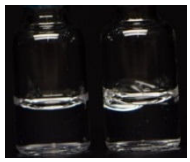	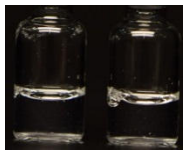	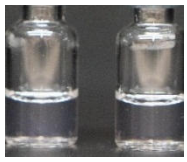
mAb Fl HS 6.5	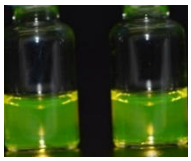	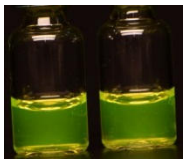		
mAb Fl PN 7.2	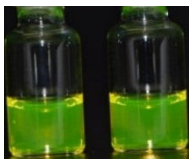		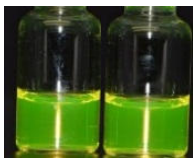	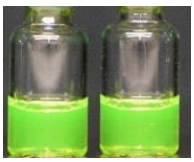
mAb DEAC HS 6.5	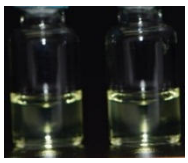			
mAb DEAC PN 7.2	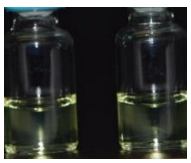		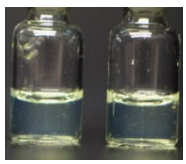	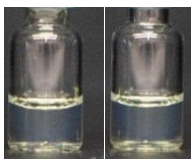
mAb Eo HS 6.5	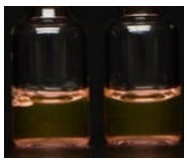	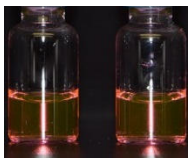		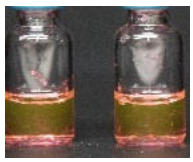
mAb Eo PN 7.2		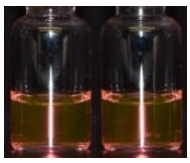		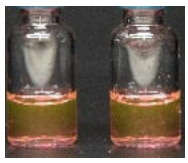
buffer HS 6.5		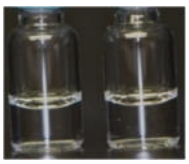		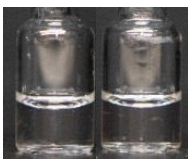
buffer PN 7.2	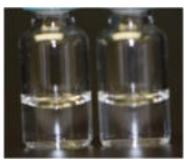	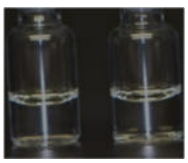	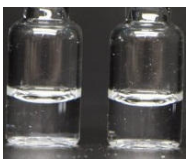	

Figure SIII- 3: Photographs of the mAb samples after storage for 0, 1, 3 and 6 months at 40 °C.

25 °C

sample	0 m	3 m	6m
mAb HS 6.5	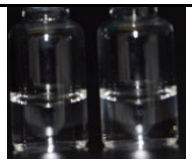	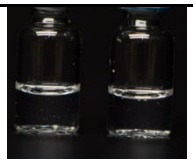	
mAb PN 7.2			
mAb Fl HS 6.5	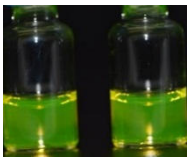	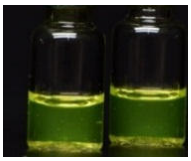	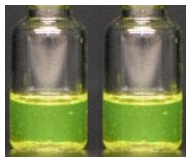
mAb Fl PN 7.2	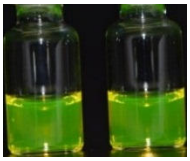	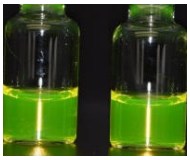	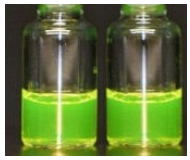
mAb DEAC HS 6.5	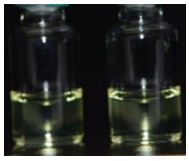	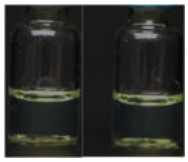	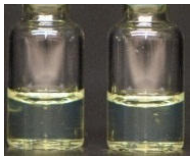
mAb DEAC PN 7.2	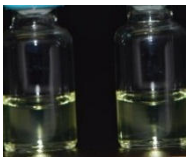		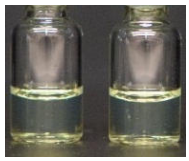
mAb Eo HS 6.5	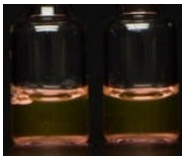	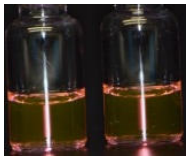	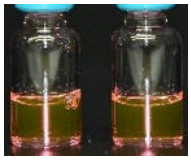
mAb Eo PN 7.2		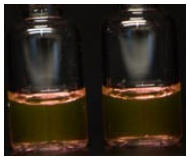	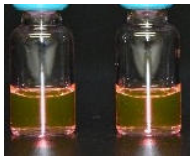
buffer HS 6.5		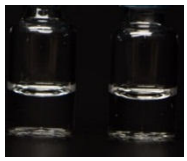	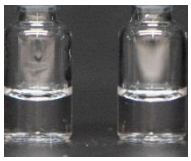
buffer PN 7.2	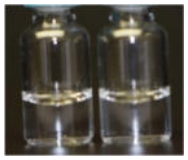	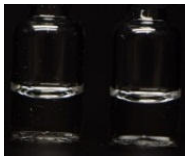	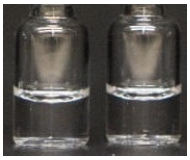

Figure SIII- 4: Photographs of the mAb samples after storage for 0, 3 and 6 months at 25 °C.

5 °C

sample	0 m	3 m	6m
mAb HS 6.5	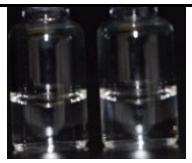	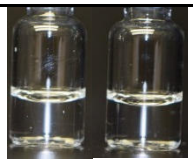	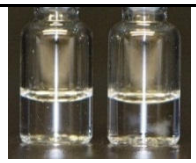
mAb PN 7.2		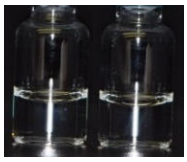	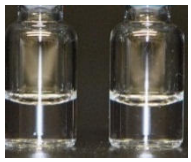
mAb Fl HS 6.5	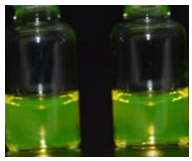		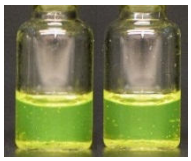
mAb Fl PN 7.2	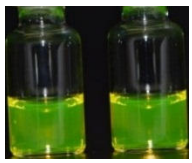	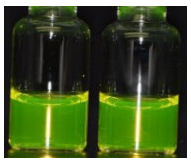	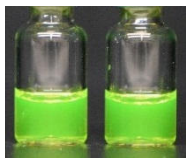
mAb DEAC HS 6.5	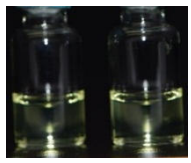	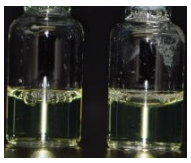	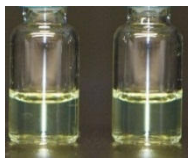
mAb DEAC PN 7.2	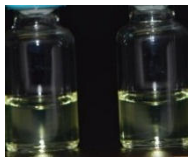		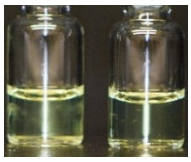
mAb Eo HS 6.5	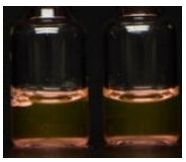	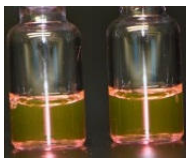	
mAb Eo PN 7.2		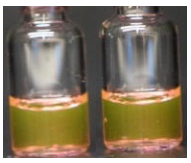	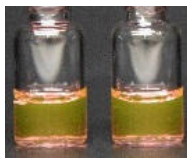
buffer HS 6.5		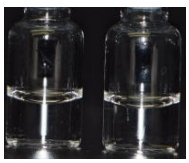	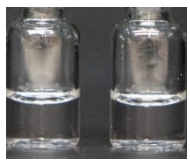
buffer PN 7.2	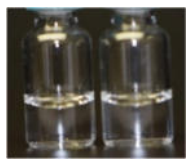	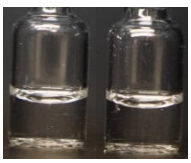	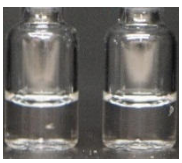

Figure SIII- 5: Photographs of the mAb samples after storage for 0, 3 and 6 months at 5 °C.

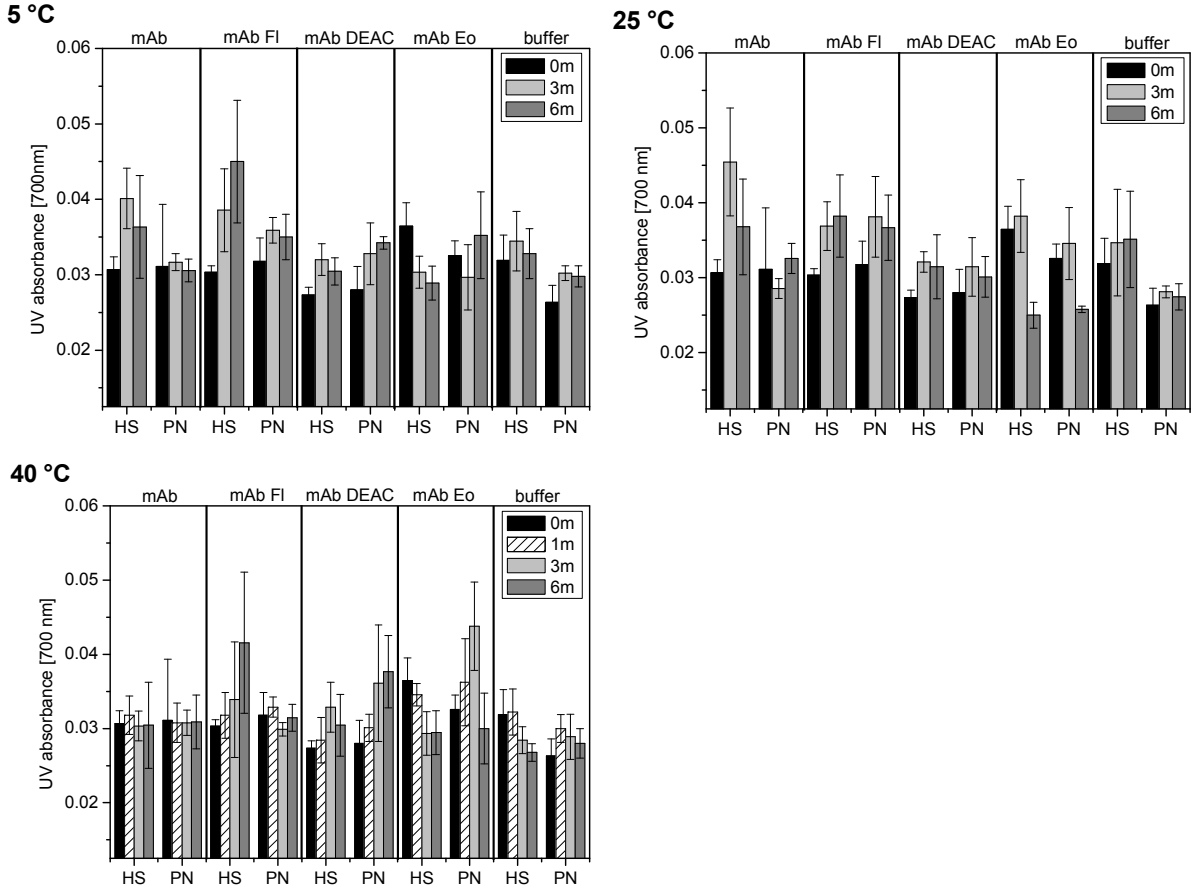

Figure SIII- 6: Turbidity values measured at 700 nm for mAb samples after 0, 1, 3 and 6 months.

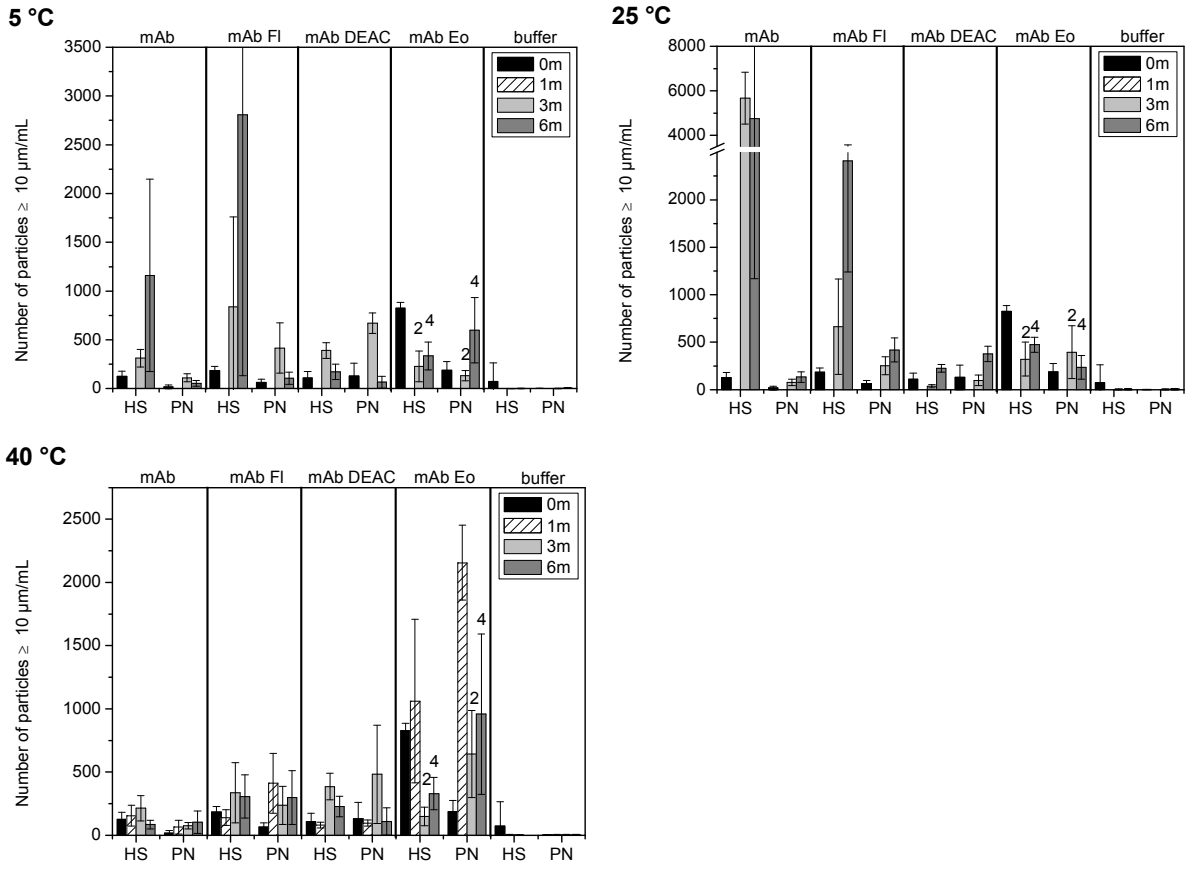

Figure SIII- 7: LO particle counts ≥ 10 µm/mL for naïve mAb and mAb conjugates stored for 0, 1, 3 and 6 months at 5, 25 and 40 °C.

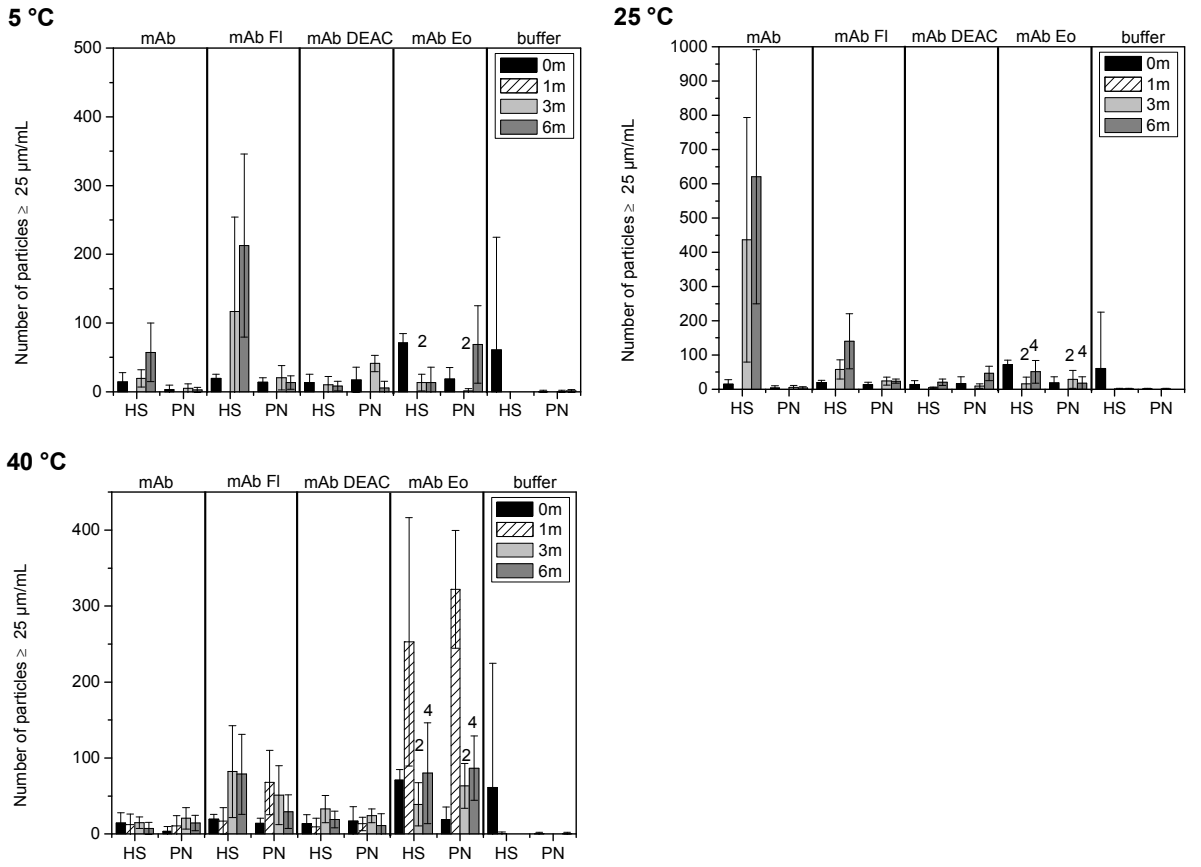

Figure SIII- 8: LO particle counts ≥ 25 µm/mL for naïve mAb and mAb conjugates stored for 0, 1, 3 and 6 months at 5, 25 and 40 °C.

Table SIII- 3: Total AUC of the mAb samples in HS and PN buffers for 0, 1, 3, 6 months (t0, t1, t3, t6) at 5, 25 and 40 °C, respectively. Total AUC values were set in relation to 100 % AUC for each sample at t0.

		t0		t1, 40°C		t3, 5°C		t3, 25°C		t3, 40°C		t6, 5°C		t6, 25°C		t6, 40°C	
mAb	HS 6.5	**100.00**	± 2.78	**99.42**	± 2.91	**101.67**	± 0.33	**105.91**	± 2.02	**97.60**	± 1.07	**100.40**	± 2.88	**111.47**	± 3.84	**100.58**	± 0.46
	PN 7.2	**100.00**	± 2.99	**90.32**	± 5.16	**98.54**	± 0.40	**97.69**	± 0.49	**86.36**	± 2.37	**100.96**	± 2.28	**102.42**	± 1.88	**83.75**	± 5.23
mAb Fl	HS 6.5	**100.00**	± 2.24	**100.88**	± 3.29	**91.92**	± 3.95	**101.88**	± 2.71	**106.74**	± 0.53	**94.49**	± 4.45	**102.19**	± 2.73	**98.55**	± 7.04
	PN 7.2	**100.00**	± 2.08	**92.51**	± 1.89	**99.15**	± 0.36	**98.64**	± 0.42	**97.91**	± 1.51	**103.65**	± 1.56	**98.62**	± 2.42	**88.56**	± 3.10
mAb DEAC	HS 6.5	**100.00**	± 3.46	**86.46**	± 3.08	**96.01**	± 3.96	**91.26**	± 3.72	**64.78**	± 19.62	**90.94**	± 6.99	**102.23**	± 1.81	**112.15**	± 9.58
	PN 7.2	**100.00**	± 1.86	**97.28**	± 0.39	**100.85**	± 0.70	**99.41**	± 0.64	**96.51**	± 2.59	**102.04**	± 1.54	**100.44**	± 1.81	**97.97**	± 0.76
mAb Eo	HS 6.5	**100.00**	± 1.50	**102.46**	± 0.41	**107.57**	± 5.55	**110.86**	± 2.51	**95.10**	± 3.02	**99.02**	± 3.55	**106.37**	± 0.43	**77.11**	± 1.13
	PN 7.2	**100.00**	± 1.24	**89.14**	± 3.94	**105.71**	± 0.61	**103.69**	± 1.51	**81.26**	± 1.17	**100.80**	± 1.37	**101.21**	± 1.84	**81.32**	± 0.59

		5 °C	25 °C	40 °C
mAb	HS 6.5	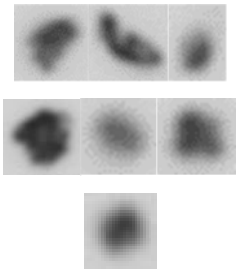	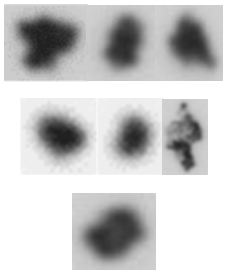	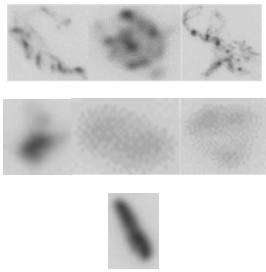
	PN 7.2	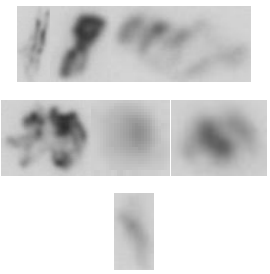	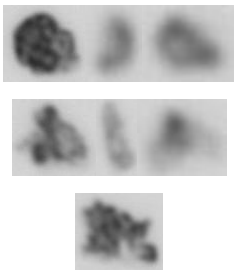	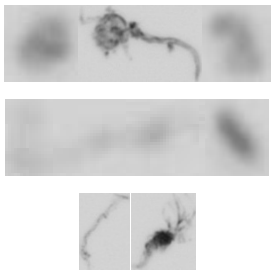
mAb Fl	HS 6.5	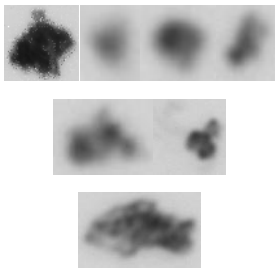	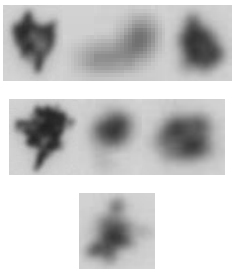	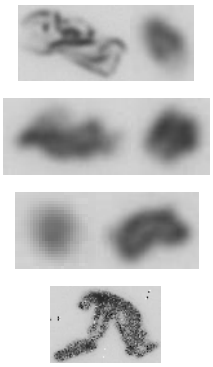
	PN 7.2	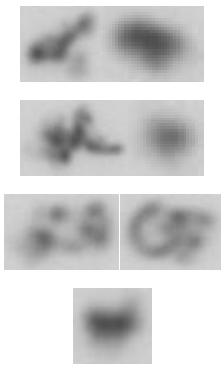	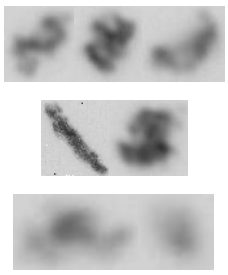	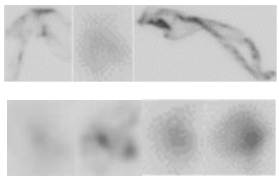

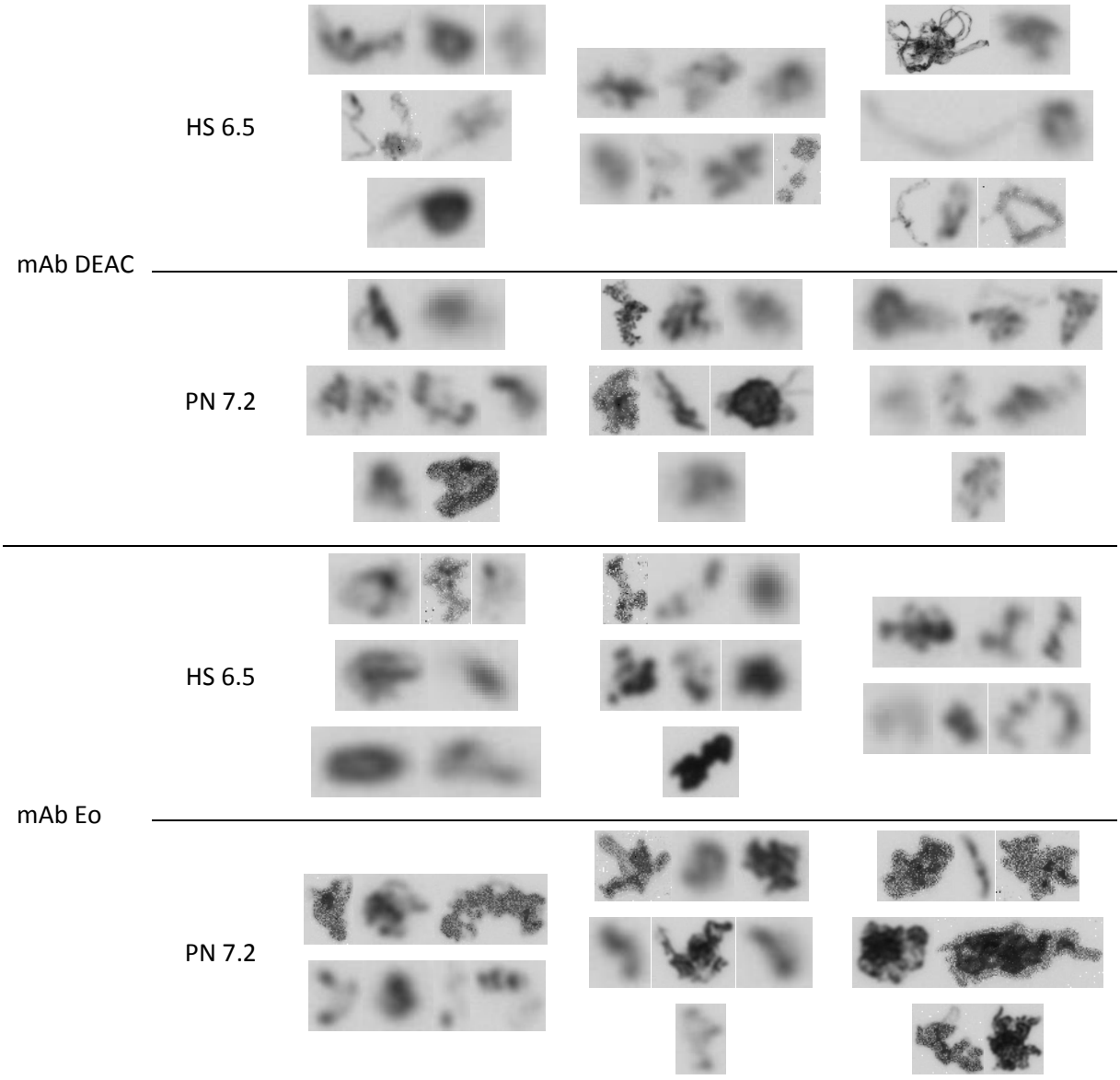

Figure SIII- 9: Representative particle images from MFI, scaled to the same height.

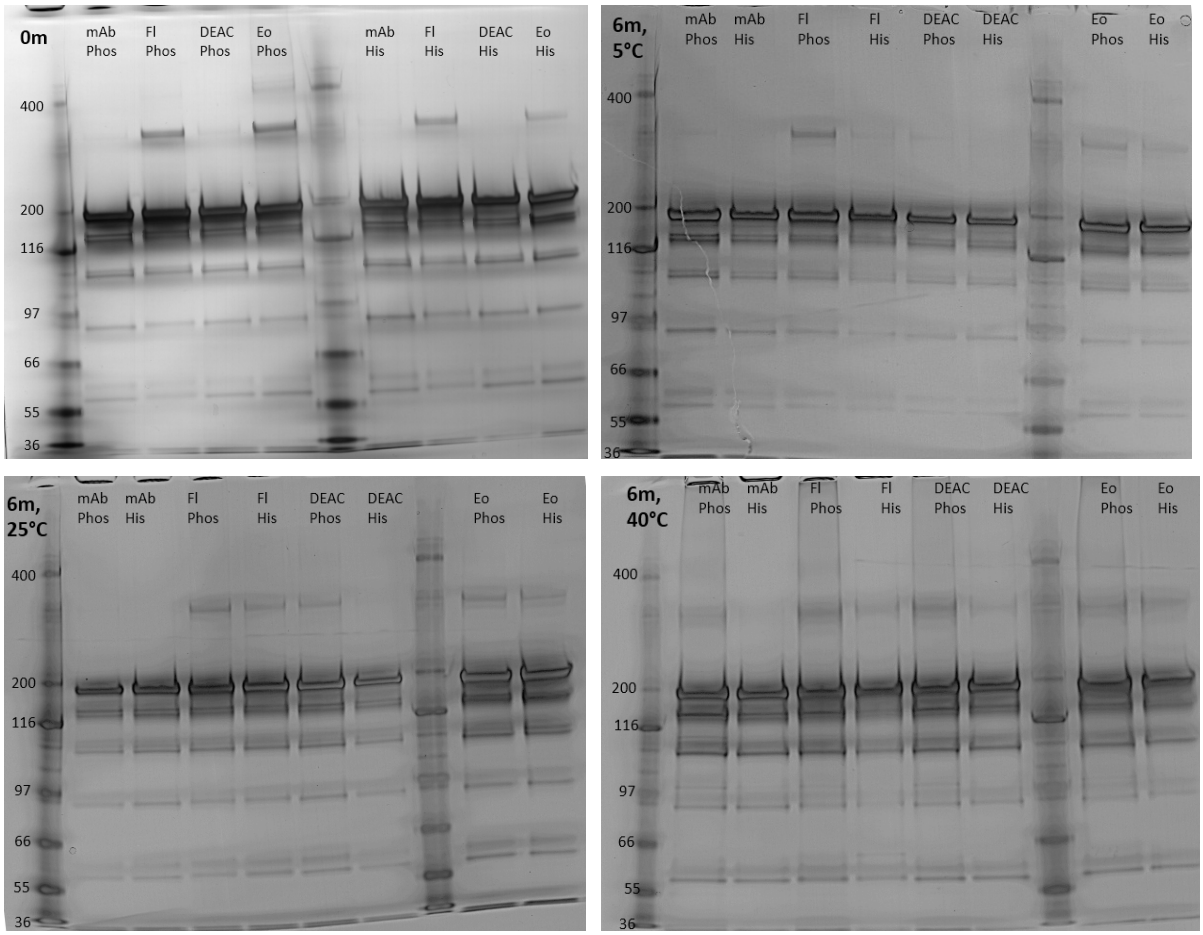

Figure SIII- 10: Decolorized scans of the non-reduced denatured SDS-Page gels after silver staining. The marker was applied on wells 1 and 5 for the gel after 0 m and on wells 1 and 8 for the gels after 6 months, respectively.

A)

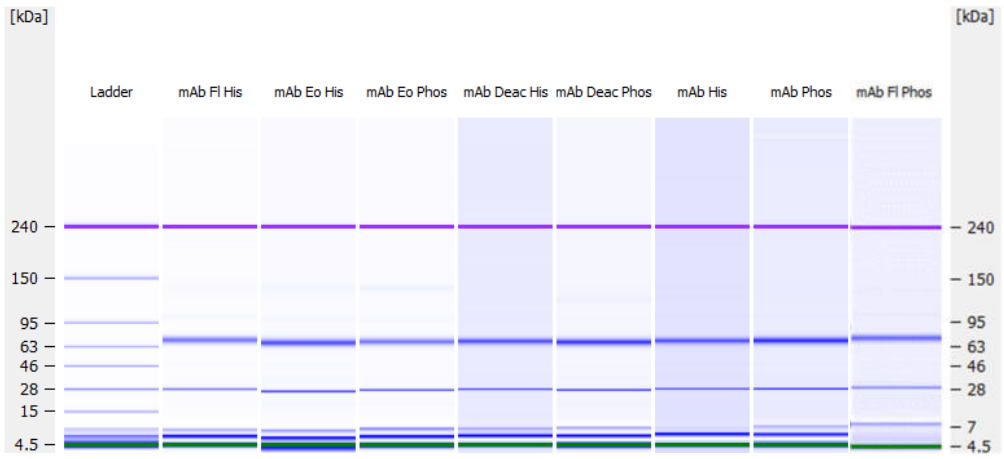

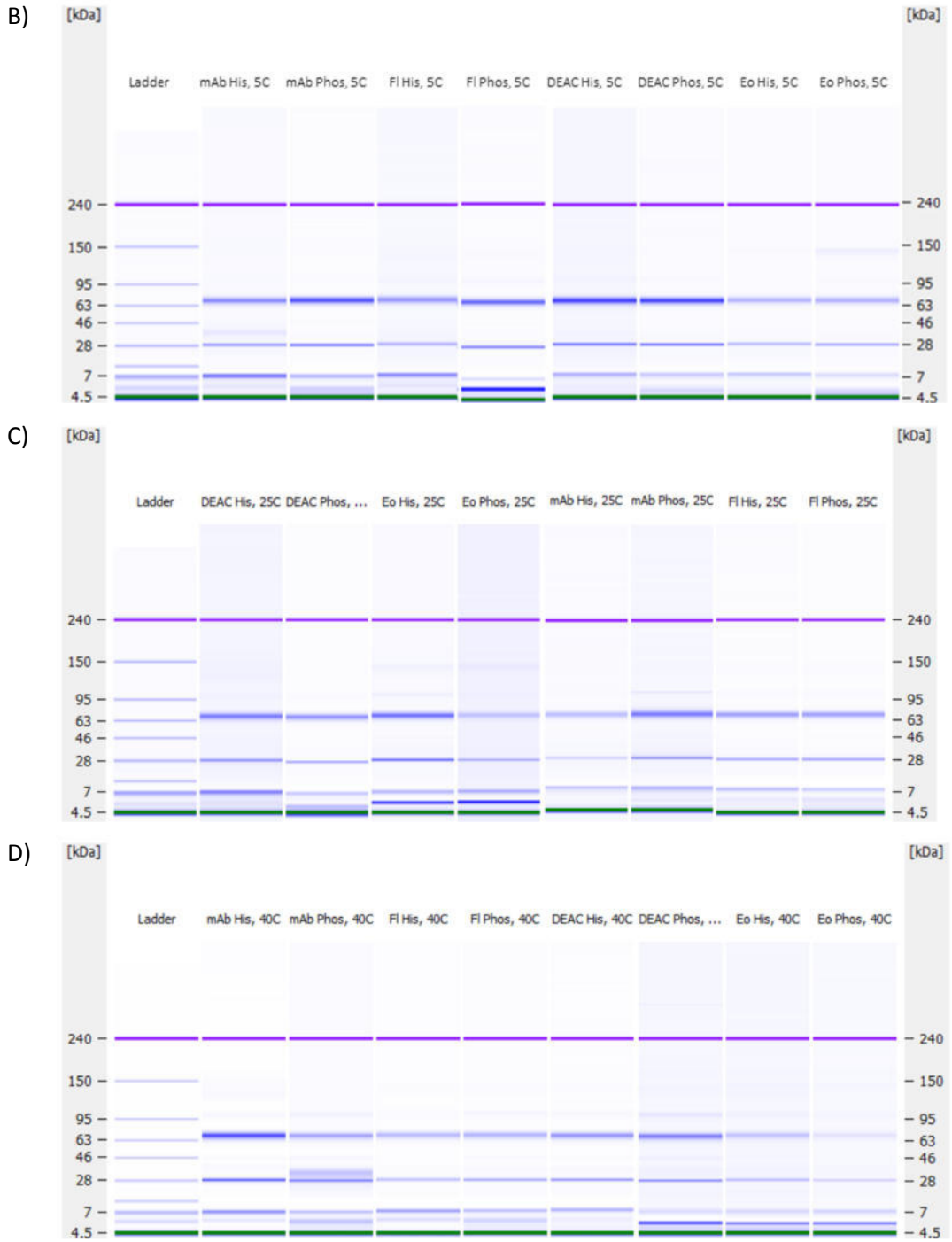

Figure SIII- 11: Reduced denatured CE-SDS gels after A) 0 m, B) 6 m 5 °C, C) 6 m 25 °C and D) 6 m 40 °C of mAb samples in His Suc and Phos NaCl buffers.

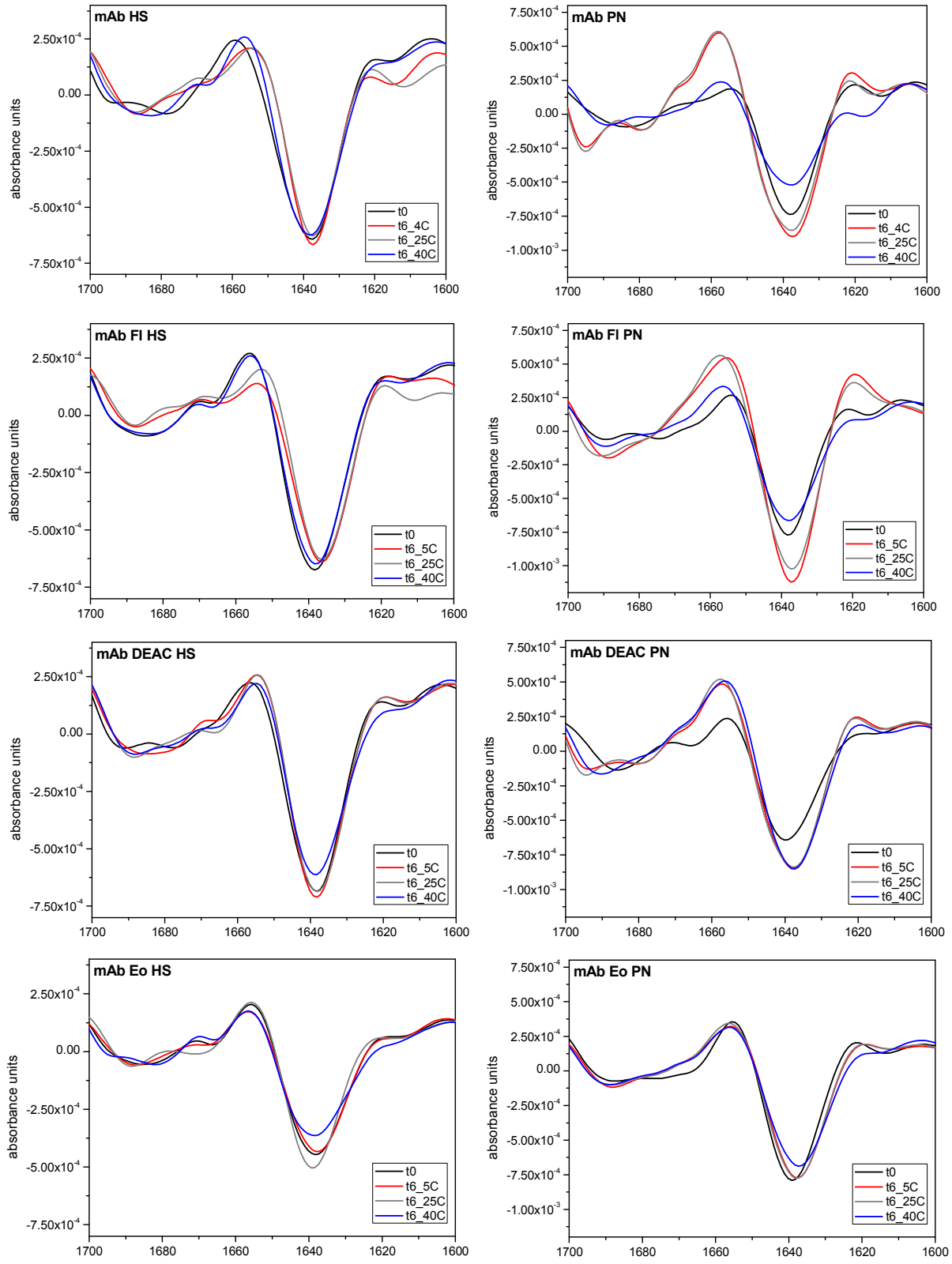

Figure SIII- 12: FT-IR spectra of mAb samples in stability study in HS 6.5 (HS) and PN 7.2 (PN) buffers.

CHAPTER IV:

ANTIBODY CONJUGATES – HOW DO THEY ADSORB AND INTERACT?

Abstract

The present work aims to investigate the stability of ADCs against mechanical stress. Three model antibody conjugates were generated through coupling of the hydrophobic fluorescent dyes fluorescein, eosin and coumarin to cetuximab. Agitation led to an increased number of subvisible particles for the mAb conjugates compared to the naïve mAb. The hydrophobic nature of the attached dyes may alter the adsorption behavior to the air-liquid and glass-liquid interfaces and in addition foster attractive protein-protein interactions, which could trigger aggregation. The most hydrophobic and negatively charged mAb conjugate, mAb Eosin, did not show increased adsorption to the air-liquid or the glass-liquid interface, but the highest particle formation and the most flexible, soft adsorbed film on glass. Moreover, for mAb Eosin, the attractive protein-protein interactions did not correlate with the increase in number of particles. In contrast, an increase in the air-liquid interaction and attractive protein-protein interactions were found for mAb DEAC. As mAb DEAC also displayed elevated particle numbers, but has a comparable pI as the naïve mAb, particle formation can be correlated to the added hydrophobicity for mAb DEAC. These results underline that the payload characteristics substantially contribute to the charge and hydrophobicity-based interactions of ADCs and affect the susceptibility to mechanical and interface related stress.

The following chapter is intended for publication.

1 INTRODUCTION

Antibody-drug conjugates (ADCs) are an emerging therapeutic possibility for the treatment of cancer, combining the target spectrum of monoclonal antibodies (mAbs) with cytotoxic payloads. This enhances the efficacy and selectivity for tumor cell killing [1-3]. Although ADCs have been mentioned in literature in the 1970s, first trials in the 1980s enjoyed limited success [4]. Only since the approval of Mylotarg® (Gemtuzumab ozogamicin) in 2000 and later Adcetris® (brentuximab vedotin), Kadcyla® (trastuzumab emtansine) and Besponsa® (inotuzumab ozogamicin), has research flourished [1, 4, 5]. Compared to unconjugated mAbs, the hydrophobic cytotoxic moiety of an ADC may induce aggregation and particle formation during manufacturing, transport or storage and thus reduce the product's shelf life [6-8].

During manufacturing and transportation, the product is exposed to mechanical or shear stresses and comes more extensively in contact with different interfaces [9-11]. Applying shaking stress is an established quick stability assessment for a mAb formulation [12]. Protein adsorption to the air-liquid interface in combination with compression and decompression of the protein film formed may lead to structural changes and aggregation [9, 12-16]. Moreover, cavitation, local thermal effects, bubble entrapment and transportation of the altered protein from the air-liquid or air-container interface into the solution are possible [13, 17-20]. Proteins are susceptible to adsorb to solid surfaces such as tubes, tanks and primary packaging material during production and storage [21].

The hydrophobic cytotoxic moiety may reduce the conformational and colloidal stability of the ADC compared to the parent mAb, which can increase its tendency to aggregate [22]. Storage at elevated temperatures has confirmed this hypothesis [6, 23]. However, only one study has recently been performed that focused on the interfacial stability of ADCs. Vortexing at 3600 rpm up to 60 min at room temperature showed that trastuzumab emtansine contained a slightly higher percentage of aggregates compared to the parent antibody [24]. However, an understanding of the behavior of ADCs at the air-liquid and air-container interface is lacking.

In this study, we examined the mechanical stability of mAb conjugates with a focus on particle formation. As model payloads for ADCs, we coupled three fluorescent dyes, NHS-Fluorescein (5/6-carboxyfluorescein, succinimidyl ester), DEAC-SE (7-diethylamino-coumarin-3 carboxylic acid, succinimidyl ester) and Eosin-ITC (Eosin-5-isothiocyanate) to the lysines of cetuximab. The three model ADCs had an average degree of labeling (DOL) of 4-5, resembling the optimal ratio of mAb to drug for ADCs of about 4 [25]. We studied the particle formation of the parent mAb and the mAb conjugates after agitation in glass vials. As interfacial adsorption phenomena may influence these results, we

analyzed the adsorption behavior to both the air-liquid and the glass-liquid interface. A reason for potentially enhanced particle formation could be stronger attractive protein-protein interactions.

2 MATERIALS AND METHODS

2.1 MAb as Model Protein

Erbitux® (Merck KGaA, Darmstadt, Germany) was purchased at the local pharmacy as a 5 mg/mL Cetuximab formulation in citrate buffer pH 5.5 with glycine, polysorbate 80 and sodium chloride (NaCl) as stabilizers. Prior to further use, the antibody was purified from polysorbate 80 using protein A affinity chromatography on an ÄKTApurifier® 10 (GE Healthcare, Little Chalfront, Buckinghamshire, UK) at a UV detection of 280 nm, as described by Tim Menzen [26]. The samples were then buffer exchanged to 10 mM phosphate, 145 mM NaCl PBS buffer pH 7.2 or 100 mM bicarbonate buffer pH 9.0 using a Minimate™ TFF Capsule with Omega™ 30 K Membrane (PALL Life Sciences, Port Washington, NY, USA). The concentration was determined using an ε_{280nm} of 1.49 mL g^{-1} cm^{-1}.

2.2 Preparation of Antibody Conjugates

The conjugation was performed as described in Chapter III. In brief, the fluorescent dyes were dissolved in DMSO (VWR International, Radnor, PA, USA) at 10 mg/mL and added to the mAb as described in Table IV- 1. DMSO was added to all mixtures to the same total percentage of 1.4 %. The mixtures were incubated at r.t. for 1 h and 20 rpm shaking.

Table IV- 1: Conjugation conditions of the fluorescent dyes to the mAb.

Fluorescent Dye	Supplier	Molar ratio dye to mAb	Conj. bufffer	Conj. Name
5/6-carboxyfluorescein succinimidyl ester	(Thermo Fisher Scientific, Waltham, MA, USA)	20 : 1	10 mM phosphate, 145 mM NaCl PBS pH 7.2	mAb Fl
7-diethylaminocoumarin-3-carboxylic acid succinimidyl ester	(Sigma-Aldrich, St. Louis, MO, USA)	10 : 1	10 mM phosphate, 145 mM NaCl PBS pH 7.2	mAb DEAC
Eosin-5-isothiocyanate	(ThermoFisher Scientific)	15 : 1	100 mM bicarbonate buffer pH 9.0	mAb Eo

All steps were performed under light protection. Separation of the unconjugated dye and organic solvents was performed using a Minimate™ TFF Capsule with Omega™ 30 K Membrane. Following a buffer exchange into 10 mM phosphate buffer pH 7.2, the samples were filtered with a 0.2 µm syringe filter (Pall, Port Washington, NY, USA). The naïve mAb was treated as the conjugate formulations but without addition of a dye. Concentration and degree of labeling (DOL) were measured with a Nanodrop 2000 spectrophotometer (Thermo Scientific, USA) and the concentration was calculated according to Equation IV-1. The antibody conjugates and the naïve mAb were stored under light protection at 2-8 °C. To achieve the target formulation buffer, the samples were dialyzed with Vivaspin 20 tubes with a 30 kDa molecular weight cutoff polyethersulfone membrane (Sartorius Stedim Biotech, Göttingen, Germany) into 10 mM phosphate or histidine at pH 6.5 and 7.2, with 145 mM sodium chloride or 7 % sucrose (Table IV- 2). The pH was adjusted with 1 M hydrogen chloride or sodium hydroxide standard volumetric solutions (AppliChem GmbH, Darmstadt, Germany), the samples were filtrated with 0.2 µm and the protein concentration was determined again.

Equation IV-1 Calculation of the protein concentration and degree of labeling [27].

$$Protein\ conc\ (M) = \frac{A_{280} - (A_{max,fl} * Correction\ factor)}{\varepsilon_{protein}}$$

$$Degree\ of\ labeling = \frac{A_{max,fl}}{\varepsilon_{fl} * protein\ conc\ (M)}$$

Table IV- 2. Buffers used.

buffer name	buffer type	excipient	pH
HS 6.5	10 mM histidine	7 % sucrose (m/V)	6.5
PN 6.5	10 mM phosphate	145 mM NaCl	6.5
PN 7.2	10 mM phosphate	145 mM NaCl	7.2

2.3 Mechanical Stability Testing

1.2 mL of the samples at 0.2 mg/mL were filled into 2R vials and were shaken at 500 rpm at 23 °C for 24 h. The samples were analyzed in triplicate.

2.3.1 Visual Inspection

Photographs of each sample were taken using the camera Nikon D3500 (Nikon Corporation, Tokyo, Japan) against a black background.

2.3.2 Light Obscuration (LO)

LO was measured with the PAMAS SVSS-35 instrument equipped with a HCB-LD-25/25 optical sensor (Partikelmess- und Analysesysteme GmbH, Rutesheim, Germany). The system was flushed with at least 10 mL highly purified water to obtain not more than 30 particles ≥ 1 µm/mL before analysis. Four measurements of 0.2 mL were executed with a pre-run volume of 0.2 mL at a fixed fill, emptying and rinse rate of 10 mL/min. The result of the first of the four measurements was discarded [28]. Particle concentrations were recorded by the PAMAS PMA V 2.1.2.0 software and the samples were analyzed in triplicate. Results of the particle counts were calculated as the mean value of the last three measurements for particles ≥ 1, ≥ 10 and ≥ 25 µm/mL.

2.4 Surface Pressure

The surface pressure was assessed with a Micro Trough X Langmuir film balance (Kibron Inc., Helsinki, Finland) using a Teflon multiwell plate. During all measurements, the temperature was set at 21 ± 0.5 °C with an external water bath. After calibrating the film balance with highly purified water, 800 µL of each sample was filled onto the plate and equilibrated for 0.5 h. The surface pressure (π) was recorded, which describes the difference of the surface tension of the solvent minus the surface tension of the solution [29]. Measurements of samples in the concentrations of 0.2, 1 and 2 mg/mL were performed at least in triplicates.

2.5 Adsorption on Silicon Dioxide Surfaces

The adsorption of the samples to a silicon dioxide (SiO_2) surface was analyzed on a quartz crystal microbalance (QCM) apparatus qCellT (3T Analytik GmbH & Co. KG; Tuttlingen, Germany) on SiO_2 coated quartz crystal chips (No. 711.05.Si, 3T Analytik GmbH & Co. KG) at 25 °C, using qGraph as software. An exemplary QCM run is shown in Figure SIV- 4. The chip was equilibrated in flow mode with the placebo buffer (10 mM phosphate 145 mM NaCl PBS buffer pH 7.2). Equilibration was considered to be complete when a stable baseline in frequency (±1 Hz within 10 minutes) and damping (±10 Hz within 10 minutes) was reached. 115 µL of 2 mg/mL mAb sample were added to the crystal and equilibrated statically for 2 h. This filling volume was calculated based on the active area of the chip (19.6 mm^2; 38.7 µL) in correlation to a filling volume of 1 mL in a vial with a surface of 5.06 cm^2. About 75 µL were required to compensate the dead volume of the tubing. The samples were analyzed in triplicates. The reversibility of protein adsorption was tested by flushing the chip with placebo buffer. Placebo buffer with 0.05 % SDS and deionized water were used for protein desorption. The system was connected to an Ismatec pump operating at 60 µL/min for placebo and protein samples and at 200 µL/min for desorption media. After each measurement, the SiO_2 chip was cleaned with

piranha solution (sulfuric acid (99 %): hydrogen peroxide (30 %) 3:1) [30] for 15 minutes using the cleaning device (3T Analytik). The chip was then rinsed with purified water and 50 % ethanol, ultrasonicated for 3 minutes, rinsed with purified water and dried with filtrated air.

The adsorption of protein to the quartz chip was calculated as adsorbed mass (Δm) via the frequency shift (ΔF), the QCM specific constant (C) and the active area of the chip (A). Therefore, the Sauerbrey equation was modified from [30] with the QCM specific constant from 3T Analytik GmbH & Co. KG [31] used to calculate the adsorbed mass, which is shown in Equation IV-2.

Equation IV-2: Modified Sauerbrey equation:

$$\Delta m = \frac{\Delta F \cdot C}{A}$$

QCM constant: $C = 0.86 \frac{ng}{Hz}$

Active area: $A = 19.6\ mm^2$

The viscoelastic properties of the adsorbed mass layer on the chip were calculated using Equation IV-3 to evaluate the quotient of damping (Γ) and frequency (f) shifts [32]. The indices 2 and 1 represent the damping and frequency values of the protein sample for the first buffer run and second buffer run, respectively.

Equation IV-3: Evaluation of viscoelastic properties with obtained damping signal Γ and frequency signal f:

$$\frac{\Delta \Gamma}{\Delta f} = \left| \frac{\Gamma_2 - \Gamma_1}{f_2 - f_1} \right|$$

2.6 Dynamic Light Scattering (DLS)

DLS measurements were performed in 96-well plates (Corning® Costar®, Corning Inc., Corning, NY, US) using a Zetasizer APS (Malvern Instruments, Malvern, UK). Each well was measured in triplicate with 20 acquisitions of 2 s per well. The temperature was ramped between 20 and 85 °C in 5 °C steps with a scan rate of about 60 °C/h and an equilibration time of 120 s. The refractive index and viscosity values used to calculate the diffusion coefficient and the derived hydrodynamic radius (r_h) via the Stokes-Einstein equation, are shown in Table IV- 3.

Table IV- 3: Refractive indices and viscosities for the buffers used for DLS temperature ramps.

	Refractive index	Viscosity [mPa*s]
Phos NaCl	1.333	1.051
Phos Suc	1.339	1.639
His NaCl	1.335	1.154
His Suc	1.342	1.354

Seven concentrations between 0.2 and 10 mg/mL were measured for each sample. The k_D and A_2^* values were calculated manually as described in Chapter III [33, 34]. Below 60 °C, outliers were removed. To analyze the colloidal stability at room temperature, only the results for 25 °C were used in this study.

3 RESULTS

3.1 Mechanical Stability of Antibody Conjugates

To investigate the susceptibility of the naïve mAb and mAb conjugate formulations to mechanical stress, these were shaken at 500 rpm for 24 h at 23 °C. The two pH values of 6.5 and 7.2 were selected to evaluate the samples at conditions relevant for protein formulations and to cover conditions at and close to the pI. The pI of the naïve mAb is at 7.6 - 8.0, mAb DEAC exhibits a pI of 7.0 - 8.0, in contrast to mAb Fl and mAb Eo with a broader pI distribution varying from 5.3 – 7.4 (Chapter III). Thus, whereas the naïve mAb and mAb DEAC are positively net charged at pH 6.5, mAb Fl and mAb Eo are slightly negatively net charged at pH 7.2. Visible particles were not noticed before and after mechanical stress, (Figure SIV- 1). The mAb Eo formulations were turbid after mechanical stress. Before the stress, the number of subvisible particles ≥ 1 µm/mL was similarly low for mAb and mAb conjugates (Figure IV- 1). Upon mechanical stress, the number of particles did not increase for the reference mAb. For the mAb conjugates, the number of subvisible particles ≥ 1 µm/mL increased, especially for mAb Eo.

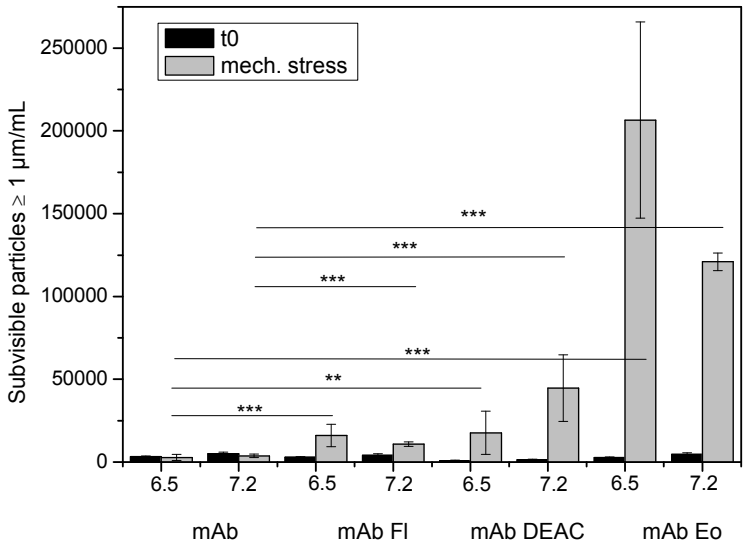

Figure IV- 1: Number of subvisible particles ≥ 1 µm/mL of mAb and mAb conjugates in PBS buffer pH 6.5 and 7.2 before (t0, black bars) and after 24 h of stressing at 500 rpm (mech. stress, grey bars) (* p ≤ 0.05, ** p ≤ 0.01, *** p ≤ 0.001).

The mAb conjugates can be ranked in the order of mAb Fl > mAb DEAC > mAb Eo in terms of stability against mechanical stress. The numbers of particles ≥ 10 and ≥ 25 µm/mL were comparable for all

samples before the stress and were not significantly increased after the stressing (Figure SIV- 2 and Figure SIV- 3). All particle numbers were well below the critical limits described in the Ph.Eur. [35].

3.2 Adsorption of MAb Conjugates to Silica Surfaces

QCM is a sensitive method to study protein adsorption and viscoelasticity at solid surfaces [36, 37]. SiO_2 chips imitate the glass vial surface [38]. An exemplary QCM run is displayed in Figure SIV- 4.

The frequency shifts of total adsorbed protein ranged from 130 Hz to 210 Hz (Table SIV- 1). Calculations with the Sauerbrey equation revealed that at pH 7.2, about 8 mg/m^2 of the naïve mAb adsorb to the SiO_2 surface (Figure IV- 2). For a homogenous IgG layer, this corresponds to a layer thickness of about 6 nm, applying a density of 1.35 g/cm^3 for IgG. 19 % of the adsorbed naïve mAb was desorbed upon rinsing with PBS buffer, indicating that this amount was reversibly adsorbed to the surface. Whereas less mAb Fl and mAb Eo adsorbed compared to the naïve mAb, the adsorbed mass was increased for mAb DEAC up to 9.1 mg/m^2. Approx. 13 % of mAb DEAC and mAb Eo were bound reversibly, whereas 17 % mAb Fl was bound reversibly.

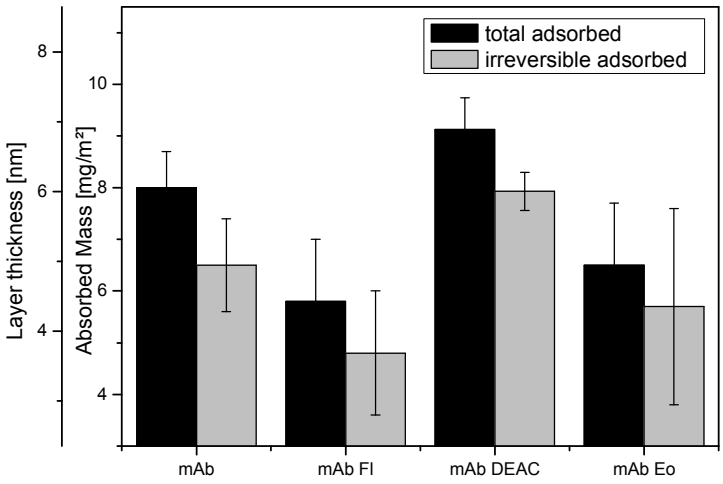

Figure IV- 2: Adsorbed mass and layer thickness of mAb and mAb conjugate formulations (in 10 mM phosphate with 145 mM NaCl PBS buffer pH 7.2) to SiO_2 chips.

As an indication for the viscoelastic behavior of antibodies, the rigidity of the adsorbed protein layers can be calculated by the quotient of damping and frequency shift. The higher the rigidity is, the more viscous is the adsorbed layer [32]. The rigidity quotient was 0.13 for the naïve mAb (Figure IV- 3). For the mAb conjugates, the rigidity was decreased to 0.10. For all samples, but mAb Eo, the rigidity

decreased upon desorption. Overall, all samples formed a rigid, elastic adsorbed layer on the hydrophilic SiO_2 surface.

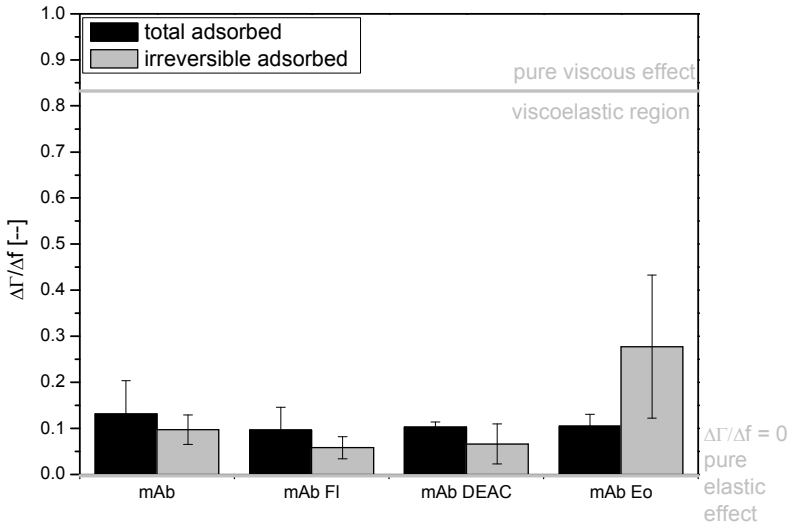

Figure IV- 3: Rigidity quotient (ΔΓ/Δf) of mAb and mAb conjugate formulations in 10 mM phosphate with 145 mM NaCl PBS buffer pH 7.2 on SiO_2 chip.

3.3 Surface Pressure of MAb Conjugates

The measurements indicate an increase of surface pressure at the air-liquid interface with increasing concentration (Figure IV- 4). Around 2 mg/mL a plateau is reached, which has been described previously [16]. For the naïve mAb at pH 6.5, the surface pressure was 10 mN/m at 0.2 mg/mL, which increased up to 16 mN/m for 2 mg/mL. MAb Eo and mAb Fl behaved overall similar to the naïve mAb. However, for mAb Eo at pH 6.5 the surface pressure was significantly lower. In contrast, the mAb DEAC samples exhibited higher surface pressure values compared to the naïve mAb.

Already at 0.2 mg/mL rather high surface pressure values of approx. 16 mN/m and 14 mN/M were found at pH 6.5 and 7.2, respectively. The equilibrium appears to be reached at lower concentration compared to the other molecules tested as at 1 and 2 mg/mL identical surface pressure values of approx. 20 mN/m and 16.5 mN/m were obtained for pH 6.5 and 7.2, respectively. The values at pH 6.5 of 20 mN/m reflect the highest of all samples.

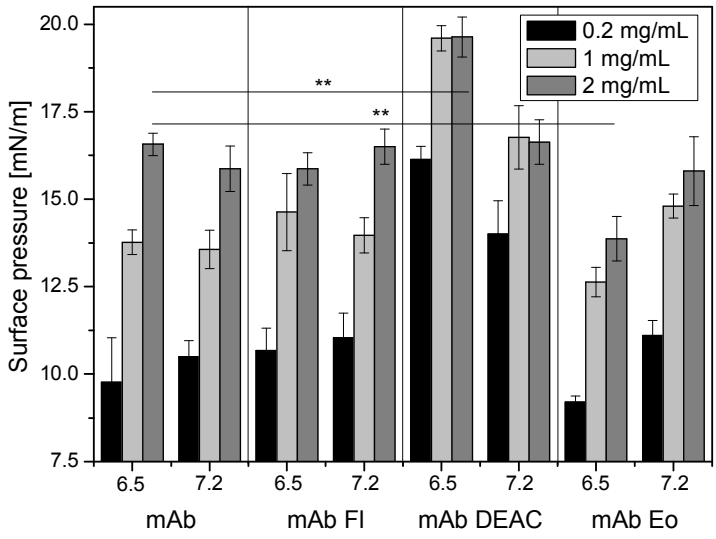

Figure IV- 4: Surface pressure of mAb and mAb conjugates in 10 mM phosphate with 145 mM NaCl PBS buffer pH 6.5 and 7.2 (* p ≤ 0.05, ** p ≤ 0.01, *** p ≤ 0.001).

3.4 Protein-Protein Interactions of MAb Conjugates

The A_2^* values at 25 °C are summarized in Figure IV- 5. Attractive protein-protein interactions are displayed by negative A_2^*, values and positive values reveal repulsive interactions [34, 39]. For the naïve mAb, A_2^* was slightly negative at pH 6.5 and showed slightly positive values for pH 7.2 but with a higher standard deviation. Negative values, and hence attractive net interactions were determined for mAb DEAC in both buffers. In contrast, mAb Fl and mAb Eo displayed negative values at pH 7.2 and positive ones for pH 6.5, implying repulsive protein interactions at the lower pH, at which they are closer to their pI.

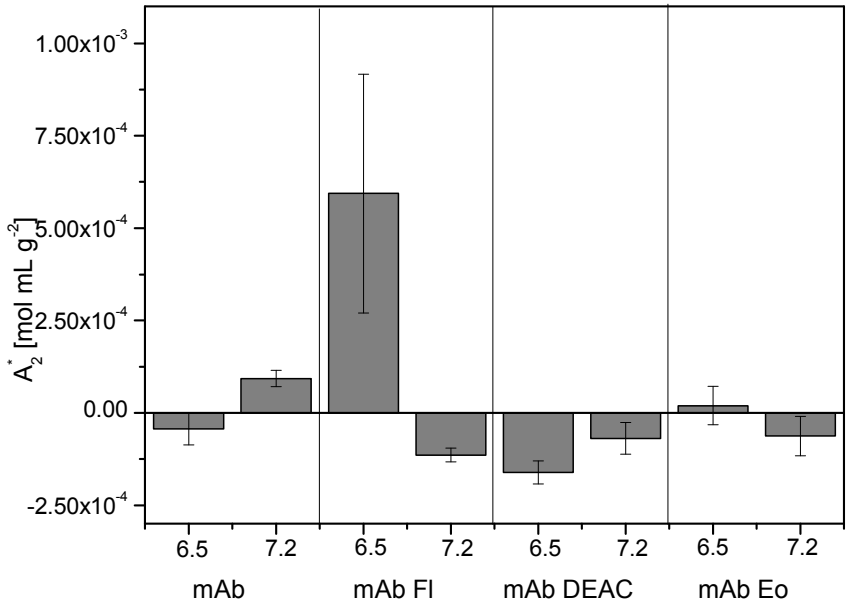

Figure IV- 5: Apparent osmotic second virial coefficient (A_2^*) at 25 °C for the naïve mAb (mAb), mAb Fluorescein (mAb Fl), mAb DEAC (mAb DEAC) and mAb Eosin (mAb Eo) at PBS buffer pH 6.5 and 7.2, respectively.

4 DISCUSSION

In this study, we demonstrate that the stability against shaking stress of mAb conjugates is significantly decreased compared to the naïve mAb. We analyzed the adsorption to silica as well as air and studied protein-protein-interactions to explain this behavior.

4.1 Mechanical Stability of Antibody Conjugates

The mechanical stress proteins encounter during manufacturing and shipment is known to primarily induce physical degradation [9, 40]. As previous reports demonstrated that agitation of an IgG leads mainly to the formation of insoluble aggregates [41, 42], this study focused on particle formation.

After the mechanical stress, visible particles were evident for mAb Eo formulations. Moreover, the number of subvisible particles for ≥ 1 µm/mL increased for the mAb conjugates. The stability of mAb conjugates against mechanical stress declined in the order mAb Fl > mAb DEAC > mAb Eo. Particle formation was similar at both pH 6.5 and 7.2 most likely because the NaCl present in the formulations shields the charges, which are essential for repulsive interactions. Fluorescein and Eosin are both triaryl methane dyes, of which Eosin is more hydrophobic. Fluorescein and DEAC exhibit a similar hydrophobicity, but DEAC is charged differently. Fluorescein and Eosin introduce negative charges upon conjugation at the pH values tested, whereas DEAC is neutrally charged and does not alter the pI significantly. Considering the charge shielding effect of the NaCl added, the highest susceptibility of the Eosin conjugate can be referred to the most pronounced increase in hydrophobicity. Particle formation has been observed after mechanical stress testing of cetuximab [43, 44]. Lahlou et al. claim that biexponential aggregation in the phosphate buffer occurred upon the exposure of the antibody to the air-liquid interface [44]. A surfactant may reduce the generation of particles notably [9, 41, 45, 46], but this was not the focus of this study.

Agitation may induce aggregation and particle formation through nucleation at the continuously regenerated air-water or air-container interface [9, 47-49]. Furthermore, protein-protein interactions in solution have been correlated with protein aggregation [50]. Another possibility are aggregation hot spots, which are described to be highly hydrophobic, lack charges and form beta sheets with adjacent strands [51].

4.2 Adsorption Behavior of MAb Conjugates

The higher particle numbers obtained for the mAb conjugates compared to the naïve mAb may result from an altered adsorption behavior. Antibodies are amphiphilic and hence adsorb to the air-liquid interface or to the container [15, 16, 49, 52-54]. The hydrophobic moiety of the mAb conjugates could

enhance the adsorption and lead to an increased number of aggregates. The adsorption to the air-liquid interface and SiO_2, the main component of the glass vial surface, were analyzed.

At pH 7.2, about 8 mg/m^2 of the naïve mAb absorb to the hydrophilic, markedly negatively charged SiO_2 surface [55-57]. MAb Fl and mAb Eo displayed slightly lower, mAb DEAC slightly higher adsorption values. Overall, the adsorbed amounts compare well to literature [53, 57, 58]. The rigidity quotient indicates that the protein film is mostly rigid and elastic in nature [32, 59]. MAb Eo formed a softer, more viscoelastic film after rinsing, pointing to increased hydration and possibly a higher tendency to unfolding [60]. Different charges of the absorbent and surface should increase adsorption [54, 57, 61]. At pH 7.2, the parent mAb and mAb DEAC are slightly positively charged, whereas mAb Fl and mAb Eo are at the upper end of their pI (5.3-7.4). Hence, mAb Fl and mAb Eo are neutrally to negatively charged at this pH, which may explain the lower amounts adsorbed to the negatively charged SiO_2 surface. As "soft" proteins, i.e. of low internal stability, mAbs may even adsorb at repelling surfaces due to an increased conformational entropy upon adsorption [53]. At the pI, adsorption is considered to be most pronounced due to reduced repulsion amongst the adsorbed molecules [21, 62]. Again, the effect of pH, surface and protein charge may be less important in our study due to the high ionic strength and charge shielding. As the naïve mAb and mAb DEAC carry close to no net charge, the adsorption may be more affected by hydrophobic interactions. Furthermore, SiO_2 is not entirely hydrophilic [57]. Thus, the addition of hydrophobic payloads may induce a different adsorption behavior to surfaces compared to the parent mAb.

Protein adsorption to the air-liquid interface in combination with compression, decompression and disruption is known to be the main contribution to protein instability upon shaking [9, 15, 49, 63, 64]. The surface pressure resulting from cetuximab adsorption is comparable to literature [63, 65]. No differences became evident between the naïve mAb and mAb Fl. The surface adsorption was only slightly decreased at pH 6.5 for mAb Eo, but increased for mAb DEAC. Thus, both the charge effect of the payloads as well as the hydrophobicity influence the adsorption behavior. Brych et al. suggested that particle formation upon agitation of IgG may occur due to reduced disulfide bond formation at the air-liquid interface [41], which fails to explain the differences between cetuximab and its conjugates.

4.3 Protein-Protein Interactions of MAb Conjugates

Recent studies indicate that the formation of particles upon shaking of mAb formulations is strongly related to the interaction parameter between protein molecules. As the compressed protein film at the air-liquid interface gets decompressed or disrupted, this region of highly concentrated clustered protein molecules can either dissolve to the monomeric state or particles may sustain and disperse in

the bulk [15]. Attractive protein-protein interactions hereby foster the formation of particles. Overall, the hydrophobic payload may contribute to stronger hydrophobic interactions. In addition, the high salt content of the formulation shields the electrostatic interactions. At 25 °C, the negative A_2^* values indicate net attraction for cetuximab at pH 6.5, mAb DEAC at both pH values and mAb Fl and mAb Eo at pH 7.2. For the sample with the most pronounced particle generation upon shaking, mAb Eo pH 6.5, slightly repulsive interactions were found. Moreover, the naïve mAb and mAb DEAC carry slightly positive net charges at pH 6.5, in contrast to mAb Fl and mAb Eo. One reason for the missing correlation between particle formation and A_2^* may be that the A_2^* determined at low concentration in the bulk does not adequately reflect the interactions in the highly concentrated interfacial film. Similarly, Ghazvini et al. found no correlation between colloidal stability and particle formation after mechanical stress [49].

5 CONCLUSION

Agitation of antibody conjugates led to significantly increased particle formation compared to the naïve mAb. For mAb DEAC, which carries the same charge as the naïve mAb, particle formation can be related to an increased adsorption at the interface. The hydrophobicity of the attached dyes was not indicative for adsorption to a surface or mechanical instability. Moreover, attractive protein-protein interactions did not directly correlate to particle formation. mAb Eosin displayed the most sub-visible and visible particles after mechanical stress and had the most flexible, soft adsorbed film on SiO_2. Thus, the effect a payload has on ADC stability is difficult to forecast as protein-protein interactions and behavior at the interfaces are altered and possibly aggregation hot-spots are formed during conjugation.

6 ACKNOWLEDGMENTS

We thank Coriolis Pharma (Martinsried, Germany) for the possibility to use the Zetasizer APS. Moreover, we are grateful for the excellently conducted experiments Nicole Popp and Ivonne Seifert have performed during their Master's projects.

7 REFERENCES

[1] R. V. Chari, M. L. Miller, and W. C. Widdison, "Antibody-drug conjugates: an emerging concept in cancer therapy," *Angew Chem Int Ed Engl,* vol. 53, no. 15, pp. 3796-827, 2014.

[2] A. M. Wu and P. D. Senter, "Arming antibodies: prospects and challenges for immunoconjugates," *Nat Biotechnol,* vol. 23, no. 9, pp. 1137-46, 2005.

[3] R. S. Zolot, S. Basu, and R. P. Million, "Antibody-drug conjugates," *Nat Rev Drug Discov,* vol. 12, no. 4, pp. 259-60, 2013.

[4] I. Sassoon and V. Blanc, "Antibody–Drug Conjugate (ADC) Clinical Pipeline: A Review," in *Antibody-Drug Conjugates*. vol. 1045, L. Ducry, Ed., ed: Humana Press, pp. 1-27, 2013.

[5] R. J. Ho and J. Chien, "Trends in translational medicine and drug targeting and delivery: new insights on an old concept-targeted drug delivery with antibody-drug conjugates for cancers," *J Pharm Sci,* vol. 103, no. 1, pp. 71-7, 2014.

[6] Y. T. Adem, K. A. Schwarz, E. Duenas, T. W. Patapoff, W. J. Galush, and O. Esue, "Auristatin antibody drug conjugate physical instability and the role of drug payload," *Bioconjug Chem,* vol. 25, no. 4, pp. 656-64, 2014.

[7] A. Wakankar, Y. Chen, Y. Gokarn, and F. S. Jacobson, "Analytical methods for physicochemical characterization of antibody drug conjugates," *mAbs,* vol. 3, no. 2, pp. 161-172, 2011.

[8] I. Hollander, A. Kunz, and P. R. Hamann, "Selection of Reaction Additives Used in the Preparation of Monomeric Antibody-Calicheamicin Conjugates," *Bioconjugate Chemistry,* vol. 19, no. 1, pp. 358-361, 2008.

[9] S. Kiese, A. Papppenberger, W. Friess, and H. C. Mahler, "Shaken, not stirred: mechanical stress testing of an IgG1 antibody," *J Pharm Sci,* vol. 97, no. 10, pp. 4347-66, 2008.

[10] H. C. Mahler, R. Muller, W. Friess, A. Delille, and S. Matheus, "Induction and analysis of aggregates in a liquid IgG1-antibody formulation," *Eur J Pharm Biopharm,* vol. 59, no. 3, pp. 407-17, 2005.

[11] T. W. Randolph, E. Schiltz, D. Sederstrom, D. Steinmann, O. Mozziconacci, C. Schoneich, et al. and C. S. Lengsfeld, "Do not drop: mechanical shock in vials causes cavitation, protein aggregation, and particle formation," *J Pharm Sci,* vol. 104, no. 2, pp. 602-11, 2015.

[12] A. Eppler, M. Weigandt, A. Hanefeld, and H. Bunjes, "Relevant shaking stress conditions for antibody preformulation development," *Eur J Pharm Biopharm,* vol. 74, no. 2, pp. 139-47, 2010.

[13] S. N. Telikepalli, O. S. Kumru, C. Kalonia, R. Esfandiary, S. B. Joshi, C. R. Middaugh, and D. B. Volkin, "Structural characterization of IgG1 mAb aggregates and particles generated under various stress conditions," *J Pharm Sci,* vol. 103, no. 3, pp. 796-809, 2014.

[14] Y.-F. Maa and C. C. Hsu, "Protein Denaturation by Combined Effect of Shear and Air-Liquid Interface," *Biotechnology and Bioengineering,* vol. 54, no. 6, pp. 503-512, 2000.

[15] E. Koepf, S. Eisele, R. Schroeder, G. Brezesinski, and W. Friess, "Notorious but not understood: How liquid-air interfacial stress triggers protein aggregation," *Int J Pharm,* vol. 537, no. 1-2, pp. 202-212, 2018.

[16] E. Koepf, R. Schroeder, G. Brezesinski, and W. Friess, "The film tells the story: Physical-chemical characteristics of IgG at the liquid-air interface," *Eur J Pharm Biopharm,* vol. 119, pp. 396-407, 2017.

[17] A. Hawe, M. Wiggenhorn, M. van de Weert, J. H. Garbe, H. C. Mahler, and W. Jiskoot, "Forced degradation of therapeutic proteins," *J Pharm Sci,* vol. 101, no. 3, pp. 895-913, 2012.

[18] J. S. Bee, J. L. Stevenson, B. Mehta, J. Svitel, J. Pollastrini, R. Platz, et al. and T. W. Randolph, "Response of a concentrated monoclonal antibody formulation to high shear," *Biotechnol Bioeng,* vol. 103, no. 5, pp. 936-43, 2009.

[19] M. K. Joubert, Q. Luo, Y. Nashed-Samuel, J. Wypych, and L. O. Narhi, "Classification and characterization of therapeutic antibody aggregates," *Journal of Biological Chemistry,* vol. 286, no. 28, pp. 25118-25133, 2011.

[20] I. Gulseren, D. Guzey, B. D. Bruce, and J. Weiss, "Structural and functional changes in ultrasonicated bovine serum albumin solutions," *Ultrason Sonochem,* vol. 14, no. 2, pp. 173-83, 2007.

[21] M. Rabe, D. Verdes, and S. Seeger, "Understanding protein adsorption phenomena at solid surfaces," *Adv Colloid Interface Sci,* vol. 162, no. 1-2, pp. 87-106, 2011.

[22] J. Guo, S. Kumar, A. Prashad, J. Starkey, and S. K. Singh, "Assessment of physical stability of an antibody drug conjugate by higher order structure analysis: impact of thiol- maleimide chemistry," *Pharm Res,* vol. 31, no. 7, pp. 1710-23, 2014.

[23] Aditya A. Wakankar, Maria B. Feeney, Javier Rivera, Yan Chen, Michael Kim, Vikas K. Sharma, and Y. J. Wang, "Physicochemical Stability of the Antibody-Drug Conjugate Trastuzumab-DM1: Changes due to Modification and Conjugation Processes," *Bioconjugate Chemistry,* vol. 21, no. 9, pp. 1588-1595, 2010.

[24] H. E. Mohamed, A. A. Mohamed, M. A. Al-Ghobashy, F. A. Fathalla, and S. S. Abbas, "Stabilty assessment of antibody-drug conjugate Trastuzumab emtansine in comparison to parent monoclonal antibody using orthogonal testing protocol," *Journal of Pharmaceutical and Biomedical Analysis,* vol. 150, pp. 268-277, 2018.

[25] P. D. S. Kevin J. Hamblett, Dana F. Chace, Michael M. C. Sun, Joel Lenox, Charles G. Cerveny, Kim M. Kissler, Starr X. Bernhardt, Anastasia K. Kopcha, Roger F. Zabinski, Damon L. Meyer, Joseph A. Francisco, "Effects of Drug Loading on the Antitumor Activity of a Monoclonal Antibody Drug Conjugate," *Clin Cancer Res,* vol. 10, no. 20, pp. 7063-7070, 2004.

[26] T. A. Menzen, "Temperature-Induced Unfolding, Aggregation, and Interaction of Therapeutic Monoclonal Antibodies," Fakultät für Chemie und Pharmazie, Ludwig-Maximilians-Universität München, Dissertation, 2014.

[27] Molecular probes by life technologies, "Amine-Reactive Probes," MAN0001774, MP00143, 2013.

[28] USP, "General Chapters: <787> Subvisible particulate matter in therapeutic protein injections," in *USP 37 - NF 32* vol. 28, ed: Pharmacopeial Forum, 2014.

[29] R. Maget-Dana, D. Lelièvre, and A. Brack, "Surface Active Properties of Amphiphilic Sequential Isopeptides: Comparison Between α-Helical and β-Sheet Conformations," *Biopolymers,* vol. 49, no. 5, pp. 415-423, 1999.

[30] N. Dixit, K. M. Maloney, and D. S. Kalonia, "Application of quartz crystal microbalance to study the impact of pH and ionic strength on protein-silicone oil interactions," *International Journal of Pharmaceutics,* vol. 412, no. 1-2, pp. 20-27, 2011.

[31] 3T Analytik GmbH & Co. KG, “Sensor Instrument for Surface Interction Analysis in Real Time - qCell / qCellT.”, 2013.

[32] V. Saller, "Interactions of formulation and disposables in biopharmaceutical drug product manufacturing " PhD, Deparment of Pharmaceutical Technology and Biopharmaceutics, LMU Munich, Dissertation, 2015.

[33] J. Rubin, L. Linden, W. M. Coco, A. S. Bommarius, and S. H. Behrens, "Salt-induced aggregation of a monoclonal human immunoglobulin G1," *J Pharm Sci,* vol. 102, no. 2, pp. 377-86, 2013.

[34] T. Menzen and W. Friess, "Temperature-Ramped Studies on the Aggregation, Unfolding, and Interaction of a Therapeutic Monoclonal Antibody," *Journal of Pharmaceutical Sciences,* vol. 103, no. 2, pp. 445-455, 2014.

[35] European Pharmacopoeia, "2.9.19 Partikelkontamination – Nicht sichtbare Partikeln," *European Directorate for the Quality of Medicine (EDQM),* vol. 8, pp. 438-441, 2014.

[36] E. Hartl, N. Dixit, A. Besheer, D. Kalonia, and G. Winter, "Weak antibody-cyclodextrin interactions determined by quartz crystal microbalance and dynamic/static light scattering," *Eur J Pharm Biopharm,* vol. 85, no. 3 Pt A, pp. 781-9, 2013.

[37] K. A. Marx, "Quartz Crystal Microbalance: A Useful Tool for Studying Thin Polymer Films and Complex Biomolecular Systems at the Solution-Surface Interface," *Biomacromolecules,* vol. 4, no. 5, pp. 1099-1120, 2003.

[38] R. Voigt, *Pharmazeutische Technologie - Für Studium und Beruf* vol. 11, 2010.

[39] S. Yadav, T. M. Scherer, S. J. Shire, and D. S. Kalonia, "Use of dynamic light scattering to determine second virial coefficient in a semidilute concentration regime," *Anal Biochem,* vol. 411, no. 2, pp. 292-6, 2011.

[40] E. Tamizi and A. Jouyban, "Forced degradation studies of biopharmaceuticals: Selection of stress conditions," *Eur J Pharm Biopharm,* vol. 98, pp. 26-46, 2016.

[41] S. R. Brych, Y. R. Gokarn, H. Hultgen, R. J. Stevenson, R. Rajan, and M. Matsumura, "Characterization of antibody aggregation: role of buried, unpaired cysteines in particle formation," *J Pharm Sci,* vol. 99, no. 2, pp. 764-81, 2010.

[42] M. Jayaraman, P. M. Buck, A. A. Ignatius, K. R. King, and W. Wang, "Agitation-induced aggregation and subvisible particulate formation in model proteins," *Eur J Pharm Biopharm,* vol. 87, no. 2, pp. 299-309, 2014.

[43] H. C. Mahler, R. Müller, W. Frieß, A. Delille, and S. Matheus, "Induction and analysis of aggregates in a liquid IgG1-antibody formulation," *European Journal of Pharmaceutics and Biopharmaceutics,* vol. 59, no. 3, pp. 407-417, 2005.

[44] A. Lahlou, B. Blanchet, M. Carvalho, M. Paul, and A. Astier, "Mechanically-induced aggregation of the monoclonal antibody cetuximab," *Annales Pharmaceutiques Francaises* vol. 67, no. 5, pp. 340-352, 2009.

[45] V. B. Fainerman, S. A. Zholob, M. Leser, M. Michel, and R. Miller, "Competitive adsorption from mixed nonionic surfactant/protein solutions," *J Colloid Interface Sci,* vol. 274, no. 2, pp. 496-501, 2004.

[46] A. Martos, W. Koch, W. Jiskoot, K. Wuchner, G. Winter, W. Friess, and A. Hawe, "Trends on Analytical Characterization of Polysorbates and Their Degradation Products in Biopharmaceutical Formulations," *J Pharm Sci,* vol. 106, no. 7, pp. 1722-1735, 2017.

[47] T. Torisu, T. Maruno, Y. Hamaji, T. Ohkubo, and S. Uchiyama, "Synergistic Effect of Cavitation and Agitation on Protein Aggregation," *J Pharm Sci,* vol. 106, no. 2, pp. 521-529, 2017.

[48] L. Liu, W. Qi, D. K. Schwartz, T. W. Randolph, and J. F. Carpenter, "The effects of excipients on protein aggregation during agitation: an interfacial shear rheology study," *J Pharm Sci,* vol. 102, no. 8, pp. 2460-70, 2013.

[49] S. Ghazvini, C. Kalonia, D. B. Volkin, and P. Dhar, "Evaluating the Role of the Air-Solution Interface on the Mechanism of Subvisible Particle Formation Caused by Mechanical Agitation for an IgG1 mAb," *J Pharm Sci,* vol. 105, no. 5, pp. 1643-56, 2016.

[50] B. Frka-Petesic, D. Zanchi, N. Martin, S. Carayon, S. Huille, and C. Tribet, "Aggregation of Antibody Drug Conjugates at Room Temperature: SAXS and Light Scattering Evidence for Colloidal Instability of a Specific Subpopulation," *Langmuir,* vol. 32, no. 19, pp. 4848-61, 2016.

[51] C. J. Roberts, "Therapeutic protein aggregation: mechanisms, design, and control," *Trends Biotechnol,* vol. 32, no. 7, pp. 372-80, 2014.

[52] N. Dixit, K. M. Maloney, and D. S. Kalonia, "Application of quartz crystal microbalance to study the impact of pH and ionic strength on protein-silicone oil interactions," *Int J Pharm,* vol. 412, no. 1-2, pp. 20-7, 2011.

[53] K. Nakanishi, T. Sakiyama, and K. Imamura, "On the adsorption of proteins on solid surfaces, a common but very complicated phenomenon," *Journal of Bioscience and Bioengineering* vol. 91, no. 3, pp. 233-244, 2001.

[54] T. Perevozchikova, H. Nanda, D. P. Nesta, and C. J. Roberts, "Protein adsorption, desorption, and aggregation mediated by solid-liquid interfaces," *J Pharm Sci,* vol. 104, no. 6, pp. 1946-59, 2015.

[55] R. G. Couston, M. W. Skoda, S. Uddin, and C. F. van der Walle, "Adsorption behavior of a human monoclonal antibody at hydrophilic and hydrophobic surfaces," *MAbs,* vol. 5, no. 1, pp. 126-39, 2013.

[56] S. H. Behrens and D. G. Grier, "The charge of glass and silica surfaces," *The Journal of Chemical Physics,* vol. 115, no. 14, pp. 6716-6721, 2001.

[57] J. Mathes and W. Friess, "Influence of pH and ionic strength on IgG adsorption to vials," *Eur J Pharm Biopharm,* vol. 78, no. 2, pp. 239-47, 2011.

[58] S. Funke, "Cartridge filling with biopharmaceuticals with focus on the optimization of the siliconization process," PhD, Deparment of Pharmaceutical Technology and Biopharmaceutics, LMU Munich, Dissertation, 2016.

[59] I. Reviakine, D. Johannsmann, and R. P. Richter, "Hearing what you cannot see and visualizing what you hear: interpreting quartz crystal microbalance data from solvated interfaces," *Anal Chem,* vol. 83, no. 23, pp. 8838-48, 2011.

[60] A. Oom, M. Poggi, J. Wikstrom, and M. Sukumar, "Surface interactions of monoclonal antibodies characterized by quartz crystal microbalance with dissipation: impact of hydrophobicity and protein self-interactions," *J Pharm Sci,* vol. 101, no. 2, pp. 519-29, 2012.

[61] M. G. E. G. Bremer, J. Duval, W. Norde, and J. Lyklema, "Electrostatic interactions between immunoglobulin (IgG) molecules and a charged sorbent," *Colloids and Surfaces A: Physicochemical and Engineering Aspects,* vol. 250, no. 1-3, pp. 29-42, 2004.

[62] J. Bujis, P. A. W. van den Berg, J. W. T. Lichtenbelt, W. Norde, and J. Lyklema, "Adsorption Dynamics of IgG and Its F (ab')2 and Fc Fragments Studied by Reflectometry," *Journal of Colloid and Interface Science,* vol. 178, no. 2, pp. 594-605, 1996.

[63] I. C. Shieh and A. R. Patel, "Predicting the Agitation-Induced Aggregation of Monoclonal Antibodies Using Surface Tensiometry," *Mol Pharm,* vol. 12, no. 9, pp. 3184-93, 2015.

[64] J. S. Bee, D. K. Schwartz, S. Trabelsi, E. Freund, J. L. Stevenson, J. F. Carpenter, and T. W. Randolph, "Production of particles of therapeutic proteins at the air–water interface during compression/dilation cycles," *Soft Matter,* vol. 8, no. 40, p. 10329, 2012.

[65] T. Serno, E. Hartl, A. Besheer, R. Miller, and G. Winter, "The role of polysorbate 80 and HPbetaCD at the air-water interface of IgG solutions," *Pharm Res,* vol. 30, no. 1, pp. 117-30, 2013.

8 SUPPLEMENTARY INFORMATION

sample	pH	t0	mech. stress
mAb	6.5		
	7.2		
mAb Fl	6.5		
	7.2		
mAb DEAC	6.5		
	7.2		

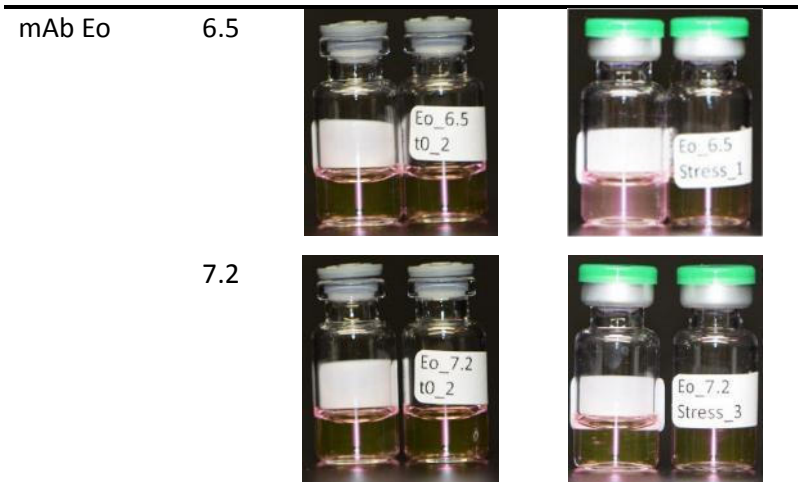

Figure SIV- 1: Photographs of the mAb samples in vials before (t0) and after mechanical stress (mech. stress) for 24 h, 500 rpm, 23 °C.

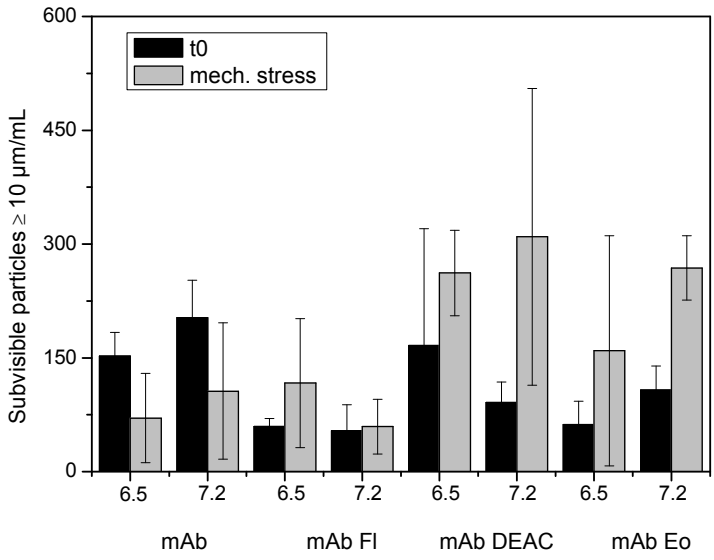

Figure SIV- 2: Number of subvisible particles ≥ 10 µm/mL of mAb and mAb conjugates in PBS buffer pH 6.5 and 7.2 before (t0, black bars) and after 24 h of stressing at 500 rpm (mech. stress, grey bars).

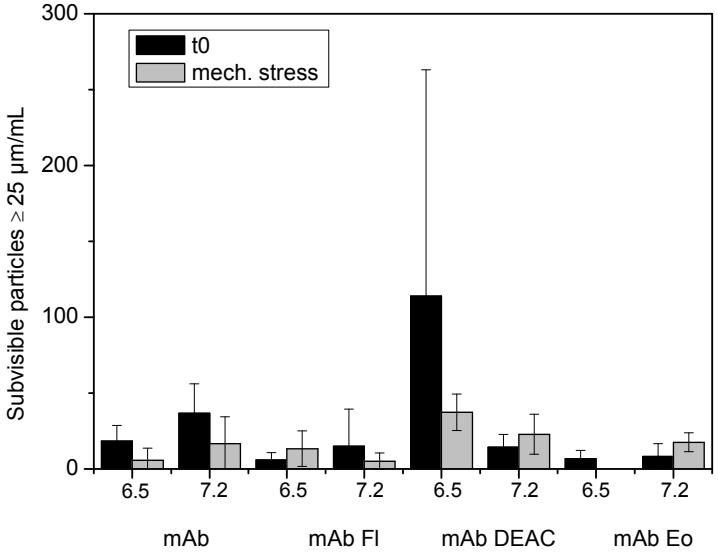

Figure SIV- 3: Number of subvisible particles ≥ 25 µm/mL of mAb and mAb conjugates in PBS buffer pH 6.5 and 7.2 before (t0, black bars) and after 24 h of stressing at 500 rpm (mech. stress, grey bars).

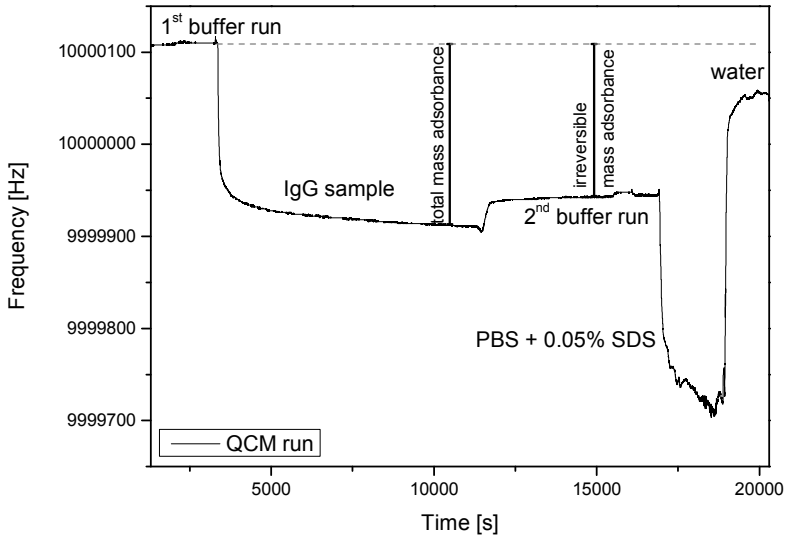

Figure SIV- 4: Representative QCM for mAb Eo on a SiO_2 chip.

Table SIV- 1: QCM frequency shifts upon adsorption of mAb samples in 10 mM phosphate with 145 mM NaCl PBS buffer pH 7.2 to SiO_2.

Sample	Frequency shift [Hz]	
	total adsorbed	irreversibly adsorbed
mAb	182.3 ± 15.7	148.0 ± 21.6
mAb Fl	132.0 ± 26.9	108.7 ± 28.3
mAb DEAC	208.0 ± 14.0	180.7± 8.3
mAb Eo	148.3 ± 27.0	129.2± 44.3

CHAPTER V:

INTERACTIONS OF MAB CONJUGATES WITH PLASMA

1 INTRODUCTION

Protein aggregates may be present in the drug product but may also form upon mixing with the physiological fluid in the patient's bloodstream after application of the drug [1-4]. This phenomenon is rarely studied for ADCs [5]. Tudor Arvinte et al. have described light microscopy as a method to probe the interaction of the drug product and the respective mAbs with human plasma [6]. We used this method to test whether the ADC model payloads NHS-Fluorescein (5/6-carboxyfluorescein, succinimidyl ester), DEAC-SE (7-diethylamino-coumarin-3 carboxylic acid, succinimidyl ester) and Eosin-ITC (Eosin-5-isothiocyanate) induce aggregation in human plasma.

2 MATERIALS AND METHODS

2.1 Preparation of Antibody Conjugates

The conjugation was performed as described in Chapter III. In brief, the fluorescent dyes were dissolved in DMSO (VWR International, Radnor, PA, USA) at 10 mg/mL and added to cetuximab as described in Table V - 1.

Table V - 1: Conjugation conditions of the fluorescent dyes to the mAb.

Fluorescent Dye	Supplier	Conj. Name
5/6-carboxyfluorescein succinimidyl ester	Thermo Fisher Scientific, Waltham, MA, USA	mAb Fl
7-diethylaminocoumarin-3-carboxylic acid succinimidyl ester	Sigma-Aldrich, St. Louis, MO, USA	mAb DEAC
Eosin-5-isothiocyanate	ThermoFisher Scientific	mAb Eo

The unconjugated dye and organic solvents were removed using a Minimate™ TFF Capsule with Omega™ 30 K Membrane. The antibody conjugates and the naïve mAb were stored under light

protection at 2-8 °C. To achieve the target formulation buffer, the samples were dialyzed with Vivaspin 20 tubes with a 30 kDa molecular weight cutoff polyethersulfone membrane (Sartorius Stedim Biotech, Göttingen, Germany) into the buffers indicated in Table V - 2.

Table V - 2: Buffers used.

Buffer	Excipient	pH
10 mM histidine	7 % sucrose (m/V)	6.5
10 mM phosphate	-	7.2
10 mM phosphate	145 mM NaCl	7.2

2.2 Interactions with Plasma

The mAb and mAb conjugate samples were tested in 10 mM histidine with 7 % sucrose (m/V) pH 6.5 and 10 mM phosphate with 145 mM PBS buffer pH 7.2. A 10 mg/mL stock solution in 10 mM phosphate pH 7.2 was diluted to 1 mg/mL with a dextrose solution to reach a final concentration of 5 % dextrose. 2.5 µL of 1 mg/mL of the naïve mAb or mAb conjugates were pipetted into a FastRead 102™ slide (Immune Systems) and 2.5 µL of fresh frozen human plasma, filtered through a 0.45 µm filter, were added [6]. The plasma was kindly donated by the Blutdepot of the LMU Klinikum. Interactions were monitored using the light microscope Keyence VHX-500F (Keyence GmbH, Neu-Isenburg, Germany) at 30x or 150x magnification. Herceptin® (Roche Registration Limited, Welwyn Garden City, United Kingdom) was purchased in a local pharmacy. After reconstitution, the solution contained 21 mg/mL trastuzumab, L-histidine hydrochloride, L-histidine, polysorbate 20 and α,α-trehalose dehydrate. Herceptin® was buffer exchanged with Protein A chromatography to remove polysorbate 20.

3 RESULTS AND DISCUSSION

Precipitation of mAbs upon parenteral application can be detected by analyzing mixtures of the samples with human plasma using a light microscope. The Herceptin® in 5 % dextrose control showed aggregation at the compact mixing region as described in literature [6] (Figure V - 1A). These aggregates were comprised of the mAb with plasma proteins, in particular with complement proteins. Hence, the aggregation of mAbs in plasma has been explained by the interaction of the mAb with the proteins of the plasma [7]. Typically for infusion settings, 5 % dextrose or 0.9 % NaCl are used, which was simulated in this study. PBS buffer pH 7.2 and 10 mM histidine 7 % sucrose pH 6.5 were used to symbolize injections. None of the mAb conjugates nor the naïve mAb showed aggregate formation upon mixing with human plasma (Figure V - 1 and Figure V - 2).

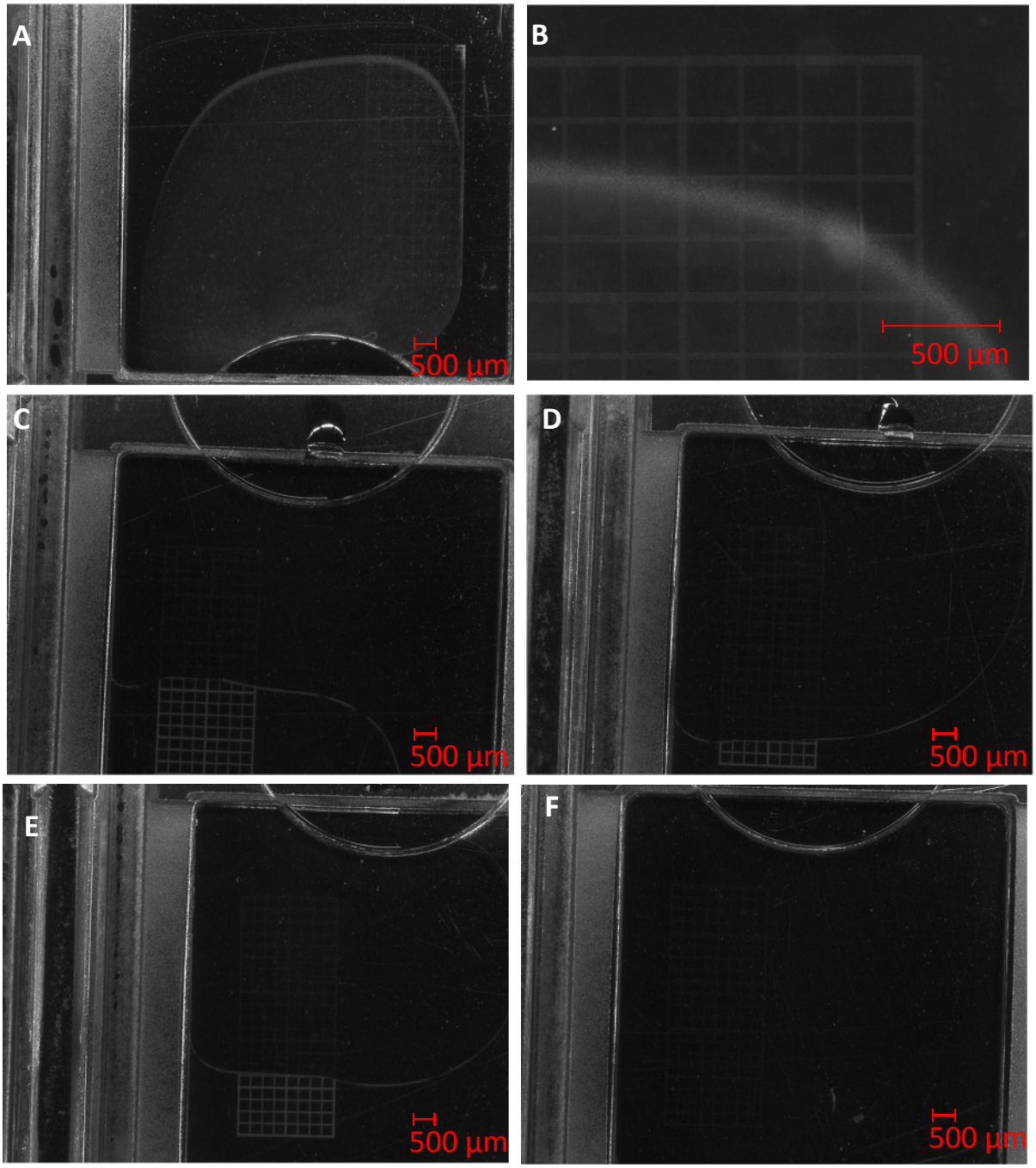

Figure V - 1: Decolorized light microscopy pictures of human plasma mixed with 5 % dextrose solutions of 1 mg/mL Herceptin® (A, B), naïve mAb (C), mAb Fl (D), mAb DEAC (E) and mAb Eo (F). One square has a size of 250 µm * 250 µm. Pictures are shown at 30x (A, C, D, E, F) or 150x (B) magnification.

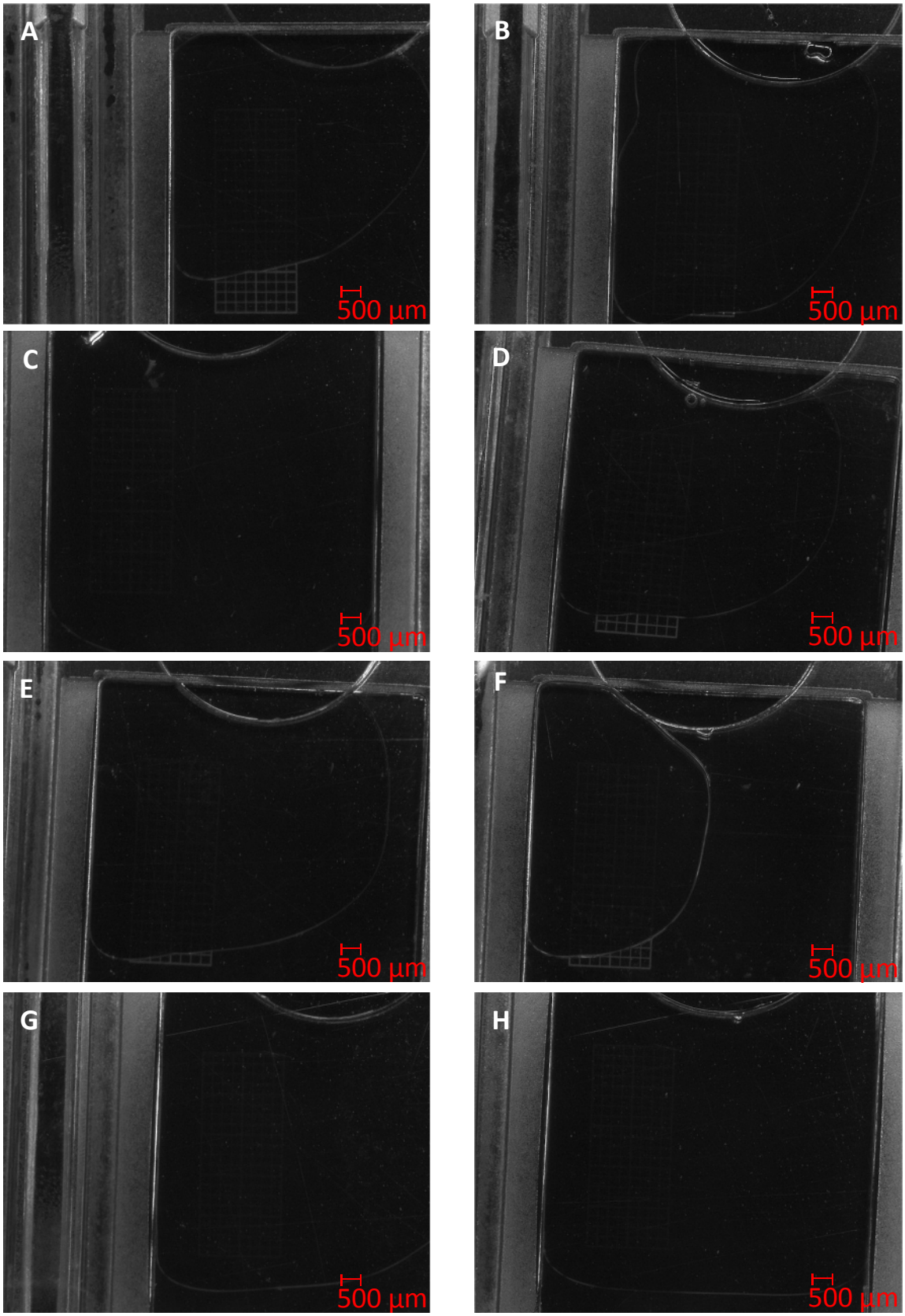

Figure V - 2: Decolorized light microscopy pictures of human plasma mixed with naïve mAb (A,B), mAb Fl (C,D), mAb DEAC (E,F) and mAb Eo (G,H) in PBS buffer pH 7.2 (left column) and 10 mM histidine 7 % sucrose pH 6.5 (right column), respectively. 1.0 mg/mL mAb solutions were mixed with human plasma. One square has a size of 250 µm * 250 µm. Pictures are shown at 30x magnification.

4 CONCLUSION

In this study we tested the interaction of human plasma with Herceptin® and our mAb conjugates in vitro. Cetuximab and the three model conjugates formulated in 5 % dextrose, PBS or histidine sucrose buffer did not display any aggregation with human plasma.

5 ACKNOWLEDGMENTS

We appreciate the kind donation of fresh frozen plasma by the Blutdepot of the LMU München, Klinikum Großhadern.

6 REFERENCES

[1] E. M. Moussa, J. P. Panchal, B. S. Moorthy, J. S. Blum, M. K. Joubert, L. O. Narhi, and E. M. Topp, "Immunogenicity of Therapeutic Protein Aggregates," *J Pharm Sci,* vol. 105, no. 2, pp. 417-30, 2016.

[2] M. Ahmadi, C. J. Bryson, E. A. Cloake, K. Welch, V. Filipe, S. Romeijn, et al. and M. H. Fogg, "Small amounts of sub-visible aggregates enhance the immunogenic potential of monoclonal antibody therapeutics," *Pharm Res,* vol. 32, no. 4, pp. 1383-94, 2015.

[3] H. C. Mahler, W. Friess, U. Grauschopf, and S. Kiese, "Protein aggregation: pathways, induction factors and analysis," *J Pharm Sci,* vol. 98, no. 9, pp. 2909-34, 2009.

[4] A. M. Fathallah, M. Chiang, A. Mishra, S. Kumar, L. Xue, R. Middaugh, and S. V. Balu-Iyer, "The Effect of Small Oligomeric Protein Aggregates on the Immunogenicity of Intravenous and Subcutaneous Administered Antibodies," *J Pharm Sci,* vol. 104, no. 11, pp. 3691-702, 2015.

[5] M. B. Hock, K. E. Thudium, M. Carrasco-Triguero, and N. F. Schwabe, "Immunogenicity of Antibody Drug Conjugates: Bioanalytical Methods and Monitoring Strategy for a Novel Therapeutic Modality," *AAPS J,* vol. 17, no. 1, pp. 35-43, 2014.

[6] T. Arvinte, C. Palais, E. Green-Trexler, S. Gregory, H. Mach, C. Narasimhan, and M. Shameem, "Aggregation of biopharmaceuticals in human plasma and human serum: implications for drug research and development," *MAbs,* vol. 5, no. 3, pp. 491-500, 2013.

[7] S. Luo and B. Zhang, "Dextrose-mediated aggregation of therapeutic monoclonal antibodies in human plasma: Implication of isoelectric precipitation of complement proteins," *MAbs,* vol. 7, no. 6, pp. 1094-103, 2015.

CHAPTER VI:

SUMMARY OF THIS THESIS

Antibody-drug conjugates (ADCs) combine the advantages of high target specificity and efficacious target cell destruction. This exciting possibility has led to a constant increase in the number of constructs in research and development. Linkage and hydrophobic payload induce more complexity beyond the already high challenges of the antibody molecule. The currently available information on ADC stability and formulation was presented in **Chapter 1**. The aim of this thesis was to analyze how the hydrophobic payload and its coupling to the antibody change the stability of the parent antibody.

Although four ADCs have reached market approval and stability studies for ADCs must be widely implemented in industry, the published knowledge is very limited or dealt as proprietary know-how. **Chapter 3** aims to shed some light on the conformational and colloidal stability of ADCs. Three different non-toxic fluorescent dyes with similar characteristics as an ADC payload were coupled via the lysine residues of a therapeutic IgG1 antibody at payload to antibody ratios between 0 and 4. Negative charges of two of the fluorescent dyes (Fluorescein and Eosin) strongly decreased the isoelectric point with 4 payload molecules coupled per antibody. The other fluorescent dye, DEAC, only slightly decreased the isoelectric point, carrying a neutral charge compared to the positive charge of the lysine at the formulation relevant pH conditions. All antibody conjugates exhibited a broad distribution in the number of isoforms. The conformational stability was slightly decreased for the antibody conjugates, especially for the conjugates with an additional negative charge. The formulation strongly influenced the colloidal stability in terms of aggregation temperatures and apparent osmotic second virial coefficient. The colloidal stability was significantly decreased for the conjugates. To correlate these parameters with long-term stability data, liquid samples were stored for 6 months at 2-8, 25 and 40 °C. Aggregation and to some extent particle formation were induced upon conjugation of the antibody. This confirmed that the degree of destabilization was more related to changes in charges than to hydrophobicity of the fluorescent dyes. Different to the parent mAb, antibody conjugates were more stable in histidine/sucrose buffer compared to phosphate/sodium chloride buffer. This accentuates the necessity to develop stable formulations based on the ADC not the parent mAb.

Proteins are not only destabilized by temperature, but also e.g. through mechanical stress or contact with surfaces. The instability of the model mAb conjugates compared to the naïve mAb was studied in **Chapter 4**. Agitation led to significantly increased particle numbers for the antibody conjugates

compared to the parent antibody. The most hydrophobic payload, Eosin, led to the greatest extent of particle formation. In contrast to the colloidal stability, the mechanical stability was decreased for the mAb DEAC conjugate as well. During agitation in a vial with headspace, the protein film at the air-liquid is constantly compressed, decompressed and regenerated. Protein adsorption to the interfaces was expected to be affected by the hydrophobic nature of the attached dyes. As an increase in adsorption to the air-liquid and the liquid-container interfaces was seen for mAb DEAC, particles formed after agitation can be related to the added hydrophobicity of the DEAC, a coumarin derivative. mAb Fluorescein and mAb Eosin did not show an increased adsorption to the air-liquid and liquid-container interfaces, but an increase in subvisible particles after agitation. At the pH values tested, Fluorescein and Eosin introduced negative charges and hydrophobicity to the mAb after coupling, which can both influence the adsorption on the charged interfaces. Hence, for the mAb conjugates, the negative charges had a more significant impact on adsorption behavior than hydrophobicity. On an SiO_2 surface, mAb Eosin showed an increased hydration and possibly a higher tendency to unfolding, which may explain the highest particle numbers. Attractive protein-protein interactions did not correlate with particle formation.

Finally, upon injection to the human body, the product will encounter human plasma. If aggregates form in the patient's bloodstream, immunogenic reactions may occur. **Chapter 5** showed that the antibody conjugates and the naïve antibody did not reveal any aggregation in human plasma.

In conclusion, this work provided useful insights into the physicochemical characteristics of ADCs, which are strongly dependent on the chosen payload. The use of three different model payloads demonstrated that hydrophobicity, as well as added charge, decreased the thermal and mechanical stability of the mAb conjugates compared to the parent mAb. In future investigations, the effect of the linker on ADC stability should also be considered. The knowledge on the effect of payloads on ADC stability obtained in this thesis can make a substantial contribution to develop stable drug products for the numerous upcoming ADCs.